

Università degli Studi di Bologna

Dottorato di Ricerca

-Scienze Chimiche-

XIX Ciclo - CHIM/02

Gianluca Accorsi

**Trivalent Lanthanide Ions:
Luminescence and Applications**

Coordinatore: *Prof. Vincenzo Balzani*

Relatore: *Prof. Alberto Juris*

Correlatore: *Dr. Nicola Armaroli*

2007

ABSTRACT

CONTENTS

1 General introduction	1
1.1 Historical notes	1
1.2 Abundance and resources	4
2 Spectroscopic properties	6
2.1 General	6
2.2 Non-radiative processes	10
2.3 Luminescence	14
3 Applications	17
3.1 Outline of this thesis	17
3.2 Overview on applications	17
3.3 Lighting	19
3.4 Bioassay	21
3.5 Telecommunications	23
3.6 Lasers	24
4 Results and discussion	26
4.1 Phenanthroline type complexes	26
4.2 Naphthalene and quinoline type complexes	35
4.3 <i>d-f</i> complexes	41
4.4 Ln(III) complexes doped Sol-gel glasses	51
4.5 Eu(III) complex adsorbed on single-walled carbon nanotubes sidewalls	56
5 Experimental Setup	65
6 Final remarks	67
Bibliography	69
Acknowledgments	82

1 GENERAL INTRODUCTION

1.1 Historical notes

The rare-earth elements (REE) are defined as a group of chemical elements composed of scandium, yttrium, and the lanthanides. The lanthanides are a group of 15 chemically similar elements with atomic numbers 57 through 71, inclusive. Although not a lanthanide, yttrium (atomic number 39), is included in the rare earths because it often occurs with them in nature, having similar chemical properties. Scandium (atomic number 21), is also included in the group, although it



Bastnasite

typically occurs in rare-earths ores only in minor amounts because of its smaller atomic and ionic size.¹

Rare-earths production is derived from the rare-earths ores bastnasite, monazite, xenotime, and ion-adsorption clay. Bastnasite is the world's principal source of rare earths and is found in China and the United States. Significant quantities of rare earths are also recovered from the mineral monazite. Xenotime and

ion-adsorption clays account for a much smaller part of the total production but are important sources of yttrium and other heavy-group rare earths.

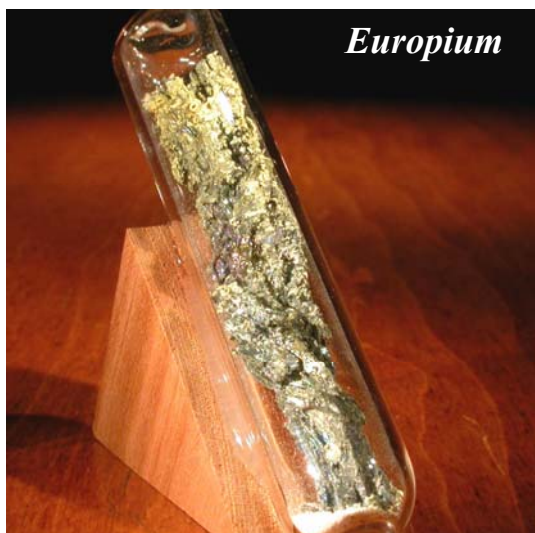
The discovery of the rare earths (in truth, during the past centuries, this term was applied to any unusual synthetic oxide), wheels around two fundamental facts. In 1794, the Swedish mineralogist F. Cronsted discovered a new mineral from which, independently, J. J. Berzelius and W. Hisinger isolated a new oxide which was named "ceric earth" (from the Latin *Ceres* = the creator).



Monazite

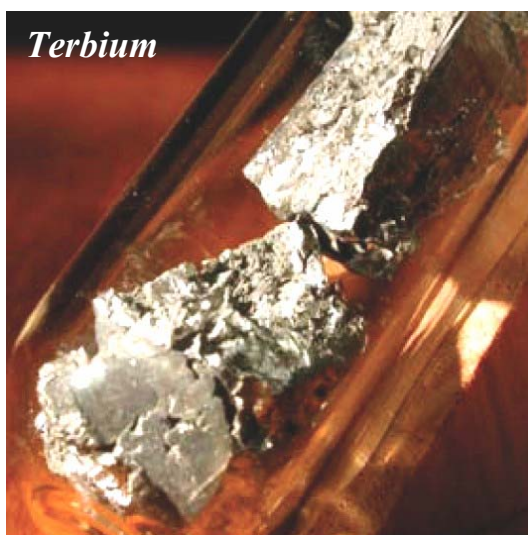
Meanwhile, the Finn chemist J. Gadolin, studying a new mineral extracted from a quarry close to Ytterby town in Sweden, obtained a new one he named "yttrica earth". During the following years,

it has been discovered that actually, the mentioned oxides were a mixture of several elements progressively isolated and identified. The history of the classification of the lanthanide elements ended in 1907 with the discovery of Lutetium.² Between 1839 and 1848, the Swedish chemist Carl



Gustav Mosander (1797-1858) obtained various lanthanides from ytterite. He claimed to have extracted an element from it, **lanthanum (La)**, but this was not prepared in pure form until 1923. In 1751, Swedish chemist Axel Crönstedt (1722-1765) described what he thought new form of tungsten, which he had found at the Bastnäs Mine near Riddarhyttan, Sweden. Later, German chemist Martin Heinrich Klaproth (1743-1817)

and Swedish chemist Wilhelm Hisinger (1766-1852) independently analyzed the material discovered by Crönstedt, and both concluded that this had to be a new element. It was named **cerium (Ce)** in honor of Ceres, an asteroid between Mars and Jupiter. Only in 1875 was cerium actually extracted from an ore. In 1885, C. F. Auer von Welsbach discovered two new elements, since he succeeded to separate the Didymium (once considered a unique new element; from the Greek *didymos* = twin) from double ammonium nitrates extracted from the “ceric earth”. The two new elements were called **praseodymium (Pr)** (from the Greek *praseos* = the yellow-green and *didymos*) and the **neodymium (Nd)** (from the Greek *neos* = new and *didymos*). The element with atomic number 61 escaped



for years to the searches of several laboratories. Around the 1925 the research groups of the Universities of Chicago and Florence, announced that a new element was isolated suggesting to call it Illinio (from the name of the State of the Illinois) and Florenzio (in honour of Florence). Actually,

following studies demonstrated that it was a mixture of rare-earths. Thanks to the development in the nuclear reaction field, between 1945 and 1947, J. A. Marinsky, L. And Glendenin and C. D. Coryell isolated and identified the element 61 as one of the products of the nuclear reactors. They called it **promethium (Pm)**, from the name of the mythological hero *Prometheus*. **Samarium (Sm)** was isolated in 1879 by L. de Boisbaudran as a mineral (Samaraskite, name from a Russian engineer) and obtained pure metallic form in 1901. During 1896, E. Demarcay isolated a new element called **europium (Eu)**, from the name of the continent, but its first pure compound was obtained almost ten years later by G. Urbain and H. Lacombe. In the 1880 J. C. G. Marignac obtained from the “Yttrica earth” a new impure element which the acronym 'Y' was assigned; later, he succeeded to obtain it in a purer form and in 1886 he proposed for the new element the name of **gadolinium (Gd)** in honour of the Finn chemist who discovered the “Yttrica earth”. Mosander was examining ytterite in 1843 when he identified three different "earths," all of which he also named after Ytterby: yttria, erbia, and terbia (the pure metallic form of **terbium (Tb)** was obtained by C. Urbain in 1905). Named for the Greek word *dysprositos*, or "hard to get at," **dysprosium (Dy)** was discovered by Boisbaudran while separating ytterite in 1886. **Holmium (Ho)** (from the latin *Holmia* of Stockholm) was discovered separately from J. C. Soert in Switzerland in 1878 and from P. T. Cleve in 1879 in Sweden. A pure **Erbium (Er)** oxide, following Mosander discovery in 1843 (above), was prepared in 1905 by French chemist Georges Urbain (1872-1938) and American chemist Charles James (1880-1928), but the pure metal itself was only obtained in 1934. **Thulium (Tm)** (from the Latin *Thule* meaning the very northern lands) was isolated by P. T. Cleve in the 1879 from the “yttrica earth”. The pure oxide was obtained in 1911 by C. James who had to make approximately 15.000 recrystallizations to get a pure thulium bromate. In 1878, J. C. G. Marignac found an oxide that he thought to be that of a pure element who called *neoytterbium*. Actually, in 1907 G. Urbain demonstrated that the Marignac compound contained two elements: **Ytterbium (Yb)** and **Lutetium (Lu)**. The two elements were originally called *Aldebaranium* (from the name of the Aldebaran star) and *Lutecium* (from the latin name of Paris *Lutetia*) respectively.

1.2 Abundance and resources

lanthanides are also known as rare earth because they are difficult to extract from compounds containing other substances, including other lanthanides.

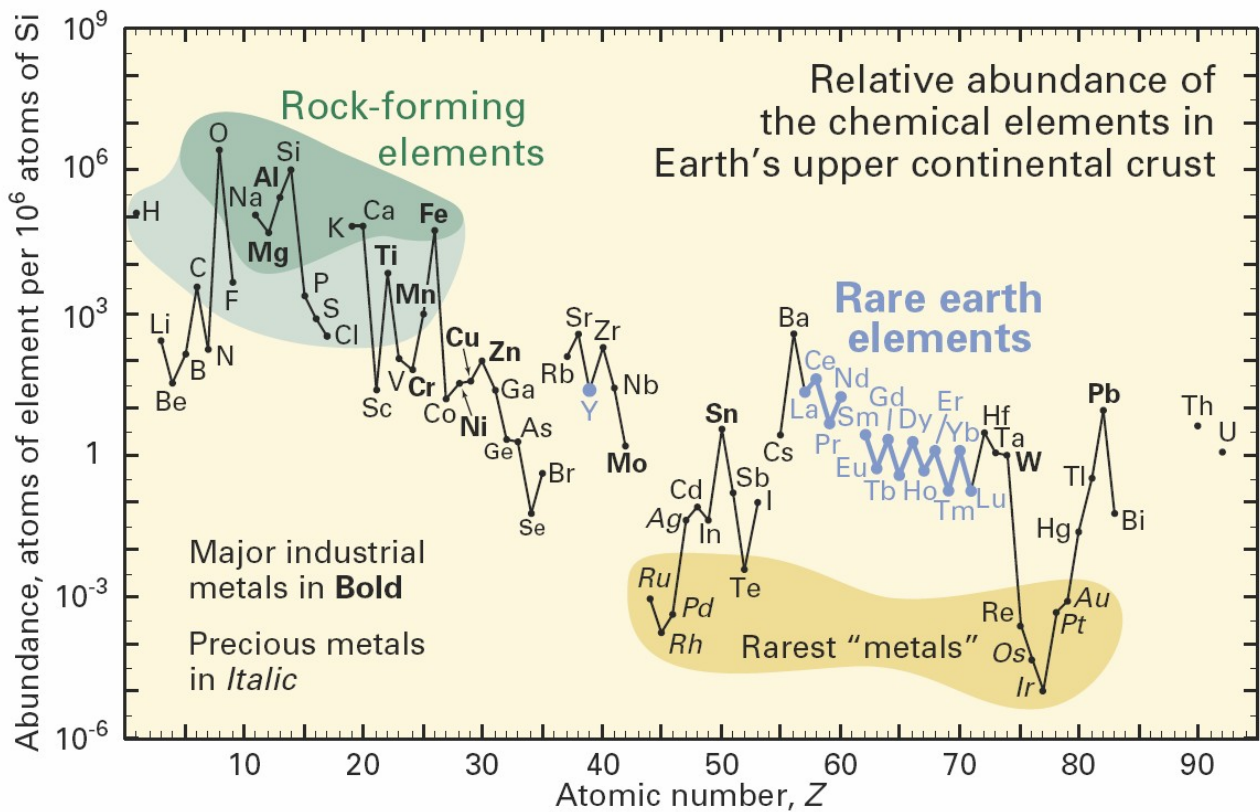


Fig.1.2.1 Abundance (atom fraction) of the chemical elements in Earth's upper continental crust as a function of atomic number.³

For instance, thulium and lutetium, the least abundant of the lanthanides, occur in the Earth's crust at higher concentrations than thallium, antimony, cadmium, bismuth and are nearly 200 times more common than gold (Fig. 1.2.1). In terms of parts per million (ppm), thulium has a presence in Earth's crust equivalent to 0.5 ppm. Cerium, the most abundant of the group, is more abundant than copper. Over decades, due to the increase of hi-tech and environmental applications the REE demand of has grown dramatically. Emerging countries, such as China, improved the REE extraction from their ores and became the main exporter of lanthanides around the world. Also the United States, once largely self-sufficient in these critical materials, over the past decade have

become dependent upon imports. In 1999 and 2000, more than 90% of REE required by U.S. industry came from deposits in China. (Fig. 1.2.2).³

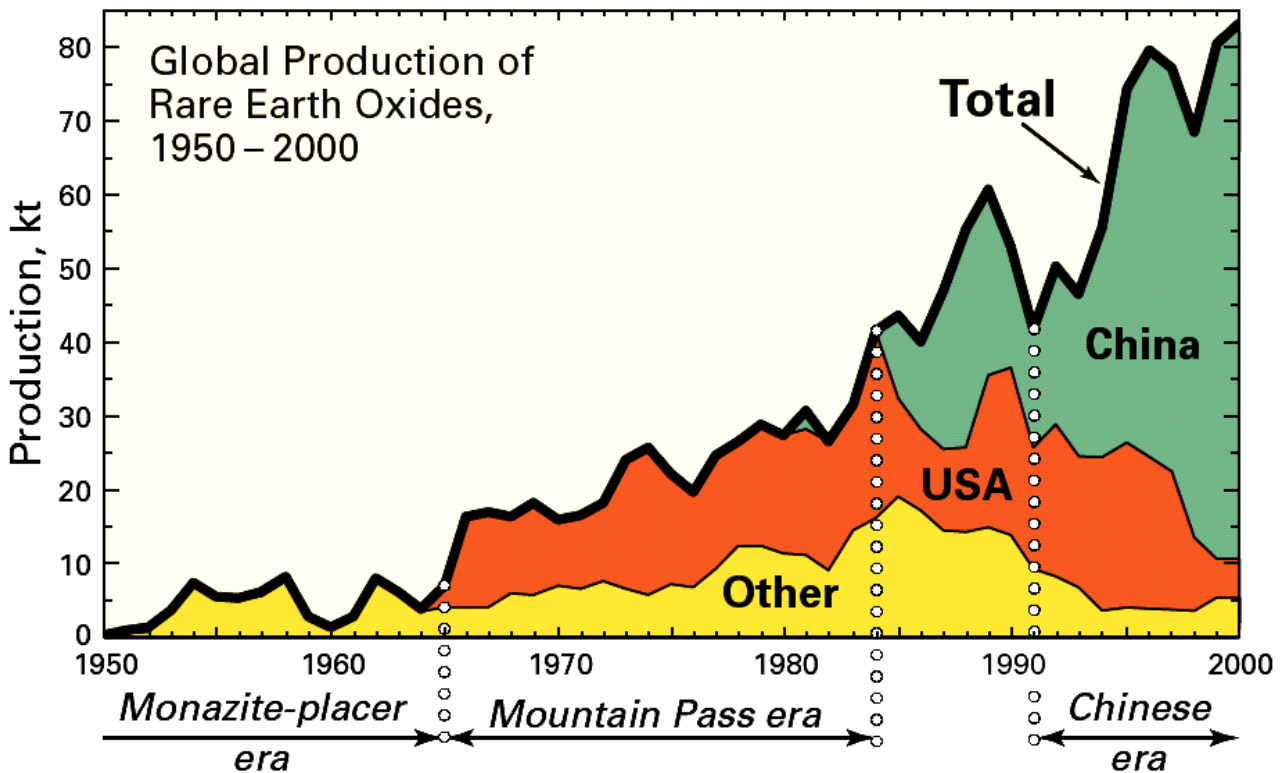


Fig. 1.2.2 Global rare earth element production (1 kt=106 kg) from 1950 through 2000, in four categories: United States, almost entirely from Mountain Pass, California; China, from several deposits; all other countries combined, largely from monazite-bearing placers; and global total. Four periods of production are evident: the monazite-placer era, starting in the late 1800s and ending abruptly in 1964; the Mountain Pass era, starting in 1965 and ending about 1984; a transitional period from about 1984 to 1991; and the Chinese era, beginning about 1991.³

Nowadays, China has the biggest world deposit of RE minerals discovered so far with more than 43 million (metric) tonnes, followed by Russia with 19 million tonnes, the United States with 13 million tonnes, and Malawi (Africa) with over 11 million tonnes.⁴ The overall production increased from 1000 tonnes per year at the beginning of the 20th century to 16 000 tonnes in 1966. At this time prices dropped significantly. At the end of the 20th century 80.000 tonnes are produced worldwide^{5, 6}

2 SPECTROSCOPIC PROPERTIES

2.1 General

Lanthanides are characterized by the progressive filling of the $4f$ orbitals with an electronic configuration $[\text{Xe}]4f^n 5d^n 6s^n$.^{7,8} The oxidation states are included between 2+ (Yb) and 4+ (Sm and Eu), but 3+ is by far the most common. Some general properties of the rare earth elements are shown in Table 2.1.1.⁹

Table 2.1.1. Selected physico-chemical properties of the RE elements.

		Z	ρ	T_{melt}	T_{boil}
Yttrium	Y	39	4.472	1799	3609
Lanthanum	La	57	6.146	1193	3743
Cerium	Ce	58	6.689	1068	3633
Praseodymium	Pr	59	6.640	1208	3563
Neodymium	Nd	60	6.800	1297	3373
Promethium	Pm	61	7.264	1373	3273
Samarium	Sm	62	7.353	1345	2076
Europium	Eu	63	5.244	1099	1800
Gadolinium	Gd	64	7.901	1585	3523
Terbium	Tb	65	8.219	1629	3503
Dysprosium	Dy	66	8.551	1680	2840
Holmium	Ho	67	8.795	1734	2993
Erbium	Er	68	9.066	1770	3141
Thulium	Tm	69	9.321	1818	2223
Ytterbium	Yb	70	6.570	1097	1469
Lutetium	Lu	71	9.841	1925	3675

Z = atomic number; ρ = density (g/cm³); T_{melt} and T_{boil} = melting and boiling point respectively (K).

The weak shielding of the f electrons provides a progressive increment of the *effective nuclear charge*⁸ leading to an atomic radii decrease (from 1.216 to 0.861). This trend is the so called *lanthanide contraction*.⁸ (Fig.2.1.1)

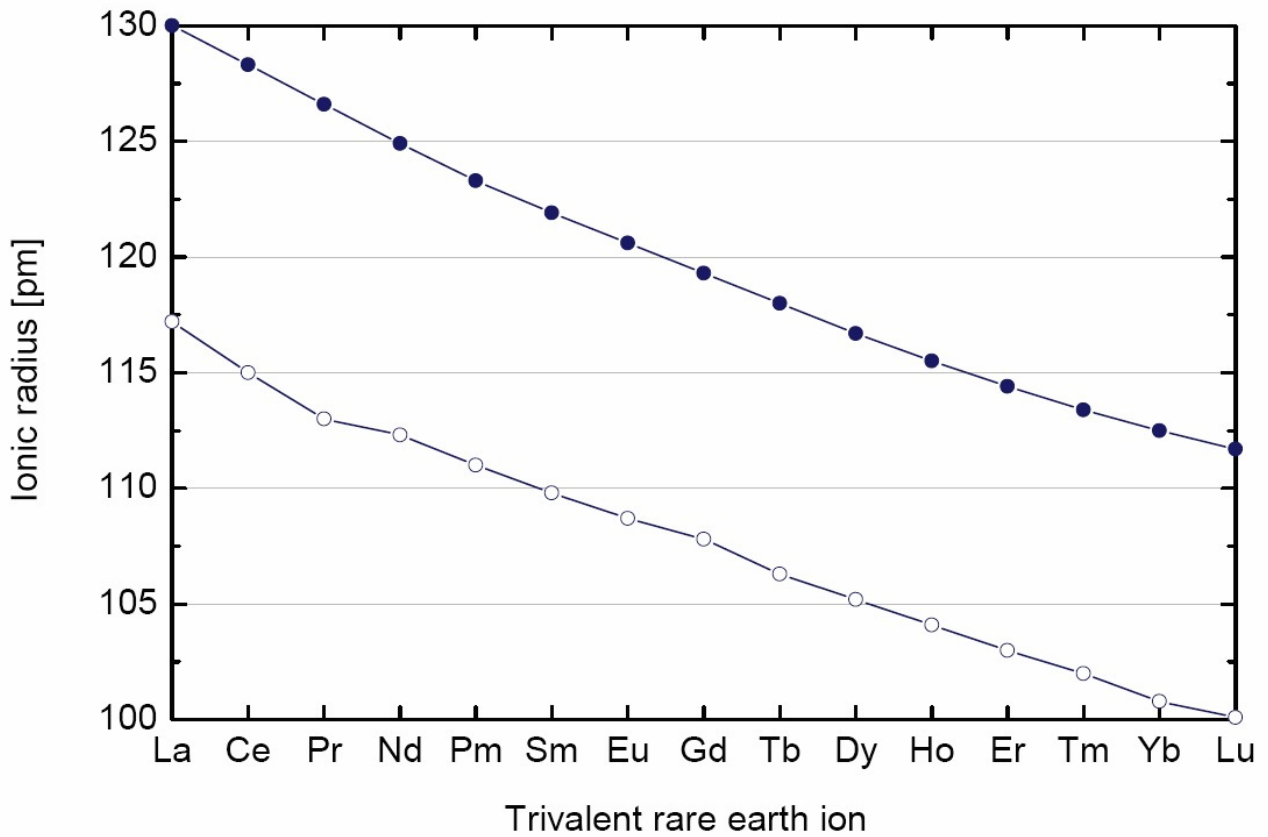


Fig. 2.1.1 Ionic radii of the trivalent lanthanide ions in eight- (•) and six-fold (○) coordination. The decrease of the size upon increasing the atomic number is referred to as lanthanide contraction.

The Russel-Saunders coupling allows the representation of the electronic states (Dieke diagram) as function of total angular moment (L), spin multiplicity (2S+1) and total angular quantum number (J) by the following expression:⁷ $^{(2S+1)}L_J$; where: $L = \sum_i l_i$, $S = \sum_i s_i$ and $J = |L - S|$. Given L = 1,2,3,4... the spectroscopic terms are S,P,D,F... respectively¹⁰ (Fig. 2.1.2).

Their electronic configuration $[\text{Xe}]4f^n$ is energetically split in spectroscopic terms, levels and states because of i) electronic repulsion ii) spin-orbit coupling and iii) ligand field (in a coordinating environment) as showed in Fig. 2.1.3

Excited configurations

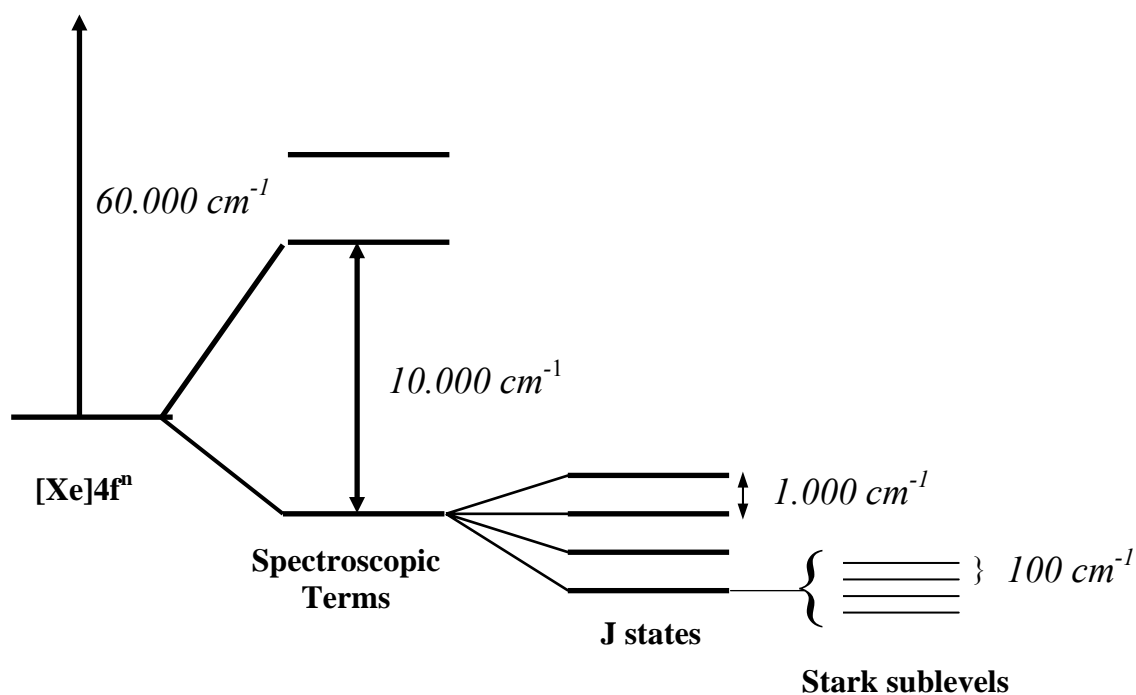


Fig. 2.1.3 Energetic splitting of the electronic configuration $4f^n$ for a generic Ln^{3+} ion.

Since the inner-shell $4f$ orbitals are well shielded by filled $5s$ and $5p$ valence orbitals, the interactions with the surrounding environment⁸ (ligands, solvent molecules, *etc*) are minimized, providing unique optical properties such as narrow (few nanometers) absorption and emission bands. The selection rules state that electronic transitions must involve the promotion of electrons without a change in their spin ($\Delta S = 0$) and with a variation of either the total angular momentum and the total angular quantum number of one unit at most ($\Delta L = \pm 1, 0$; $\Delta J = \pm 1, 0$). Relaxation of the rules can occur in the presence of heavy atoms (*heavy atom effect*) or ligands (*ligands field*) even though it must be remarked their scarce efficiency to lessen the prohibition, as confirmed by weak Ln(III) ions absorption coefficient ($1 < \epsilon < 10$) and long luminescence lifetime (micro- to

millisecond timescale).⁷ To enhance the absorption coefficients, the trivalent ions can be complexed with high absorbing ligand systems, which transfer energy to the central ion (antenna effect).¹¹ Strategies for building up lanthanide complexes involve a variety of classes of ligands like polyaminopolycarboxylates,^{12, 13} cryptands,^{14, 15} calixarenes,¹⁶ podands,¹⁷⁻¹⁹ and helicates^{20, 21} (further ligands are discussed in Chapter 4). Such complexed systems can feature a high solubility in a lot of common organic solvents like chloroform, benzene, toluene, etc.. allowing (in contrast to pure lanthanide salts) their use also in organic matrices (i.e. polymers).

2.2 Non-radiative processes

The mechanism of the indirect population of the Ln(III) emitting states, involves several processes.^{11, 22, 23} As schematized in Fig. 2.1.4, in the case of Ln(III) complex photoluminescence, the population of the lowest singlet excited state of the ligand (¹LC) is followed by i) intersystem crossing (ISC, transition between states of different spin multiplicity) to the lower triplet excited state (³LC) ii) energy transfer process to the metal centered (MC) emitting states iii) deactivation of the MC levels to the ground state(s). Systems involving direct energy transfer between ¹LC and MC emitting levels have been also reported.²⁴⁻²⁸ The rate of the ISC depends on intrinsic characteristics of the system. Besides, a (total or partial) rule relaxation occurs in presence of heavy atoms such as lanthanides. Concerning the non-radiative energy transfer process, two different mechanisms have been proposed by Förster²⁹ and Dexter³⁰ involving coulombic and exchange interactions, respectively.

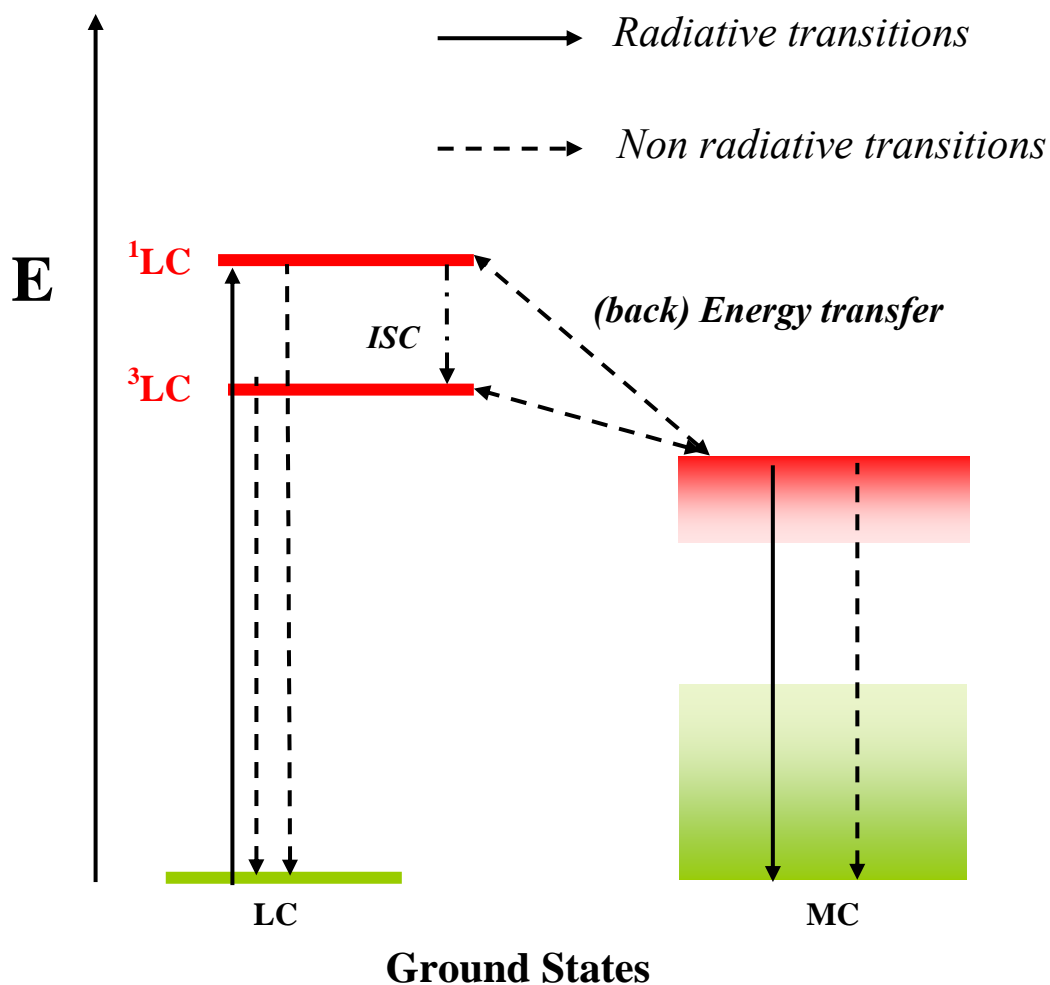


Fig.2.1.4 Photoinduced processes involved in Ln(III) complexes after ligand centred excitation. Both LC and MC excited (red) and ground (green) states are depicted.

Columbic energy transfer (Fig. 2.1.5 b) is dominated by long-range dipole-dipole interactions which cause perturbations of the energy donor (D) and acceptor (A). This mechanism does not imply electrons jumping between D* and A and can take place at large intermolecular distance (up to the order of 100 Å). In contrast, electron-exchange energy transfer (Fig. 2.1.5 a) requires closer contact between energy donor and acceptor since it involves a double electron transfer mechanism. The excited electron on D* moves to the lowest unoccupied molecular orbital (LUMO) of A. At the same time, an unexcited electron on A moves to HOMO of D. The two units must be sufficiently close to allow orbital overlapping.

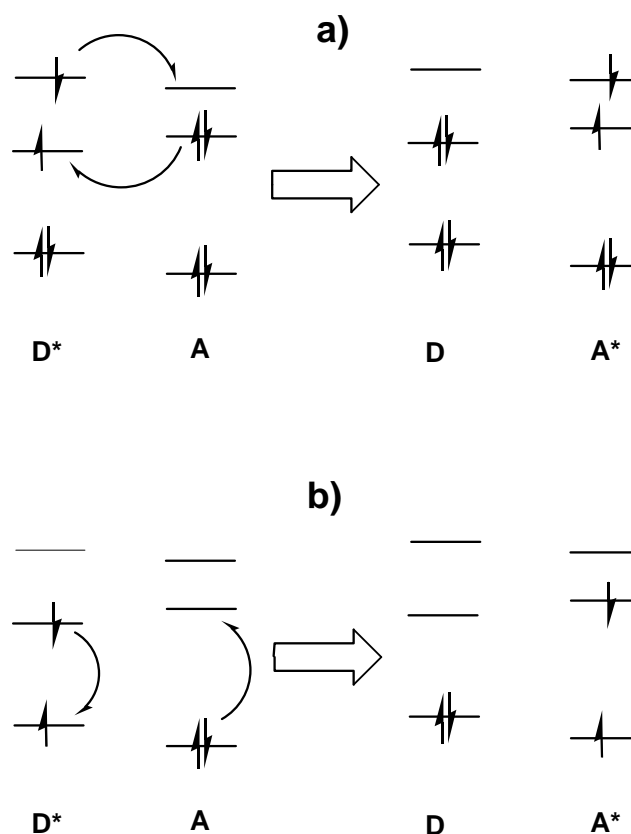


Fig. 2.1.5 Schematic representation of a) electron-exchange and b) columbic energy transfer mechanism steps.

The excited states of Ln(III) ions can be non radiatively deactivated by solvent molecules and coordinating ligands through vibronic coupling with -OH, -NH and -CH groups. The yield of the vibronic quenching process depends on i) the number of the oscillators close to the first coordination sphere, ii) the R parameter:⁷

$$eq. 2.2.1 \quad R = \Delta E / \hbar\omega = (\Delta E / \hbar) \sqrt{\mu/\kappa}$$

where ΔE = Energy gap between the metal emitting state and the higher energy J state of the ground multiplet, $\hbar\omega$ = oscillator vibrational quantum, μ = oscillator reduced mass and κ = oscillator force constant. In other words, R represents the number of vibrational quanta between ΔE ; the lower the number of the vibrational quanta the higher the rate of the vibronic coupling process. The most

efficient vibronic quencher for Ln(III) ions is the –OH group. By replacing the hydrogen atom with that of heavier deuterium (for instance by using deuterated solvents), the vibrational quantum of the oscillator decrease from nearly 4000 to 2000 cm^{-1} with the consequence of a substantial reduction of the luminescence quenching (*isotopic effect*, Fig. 2.1.6).³¹

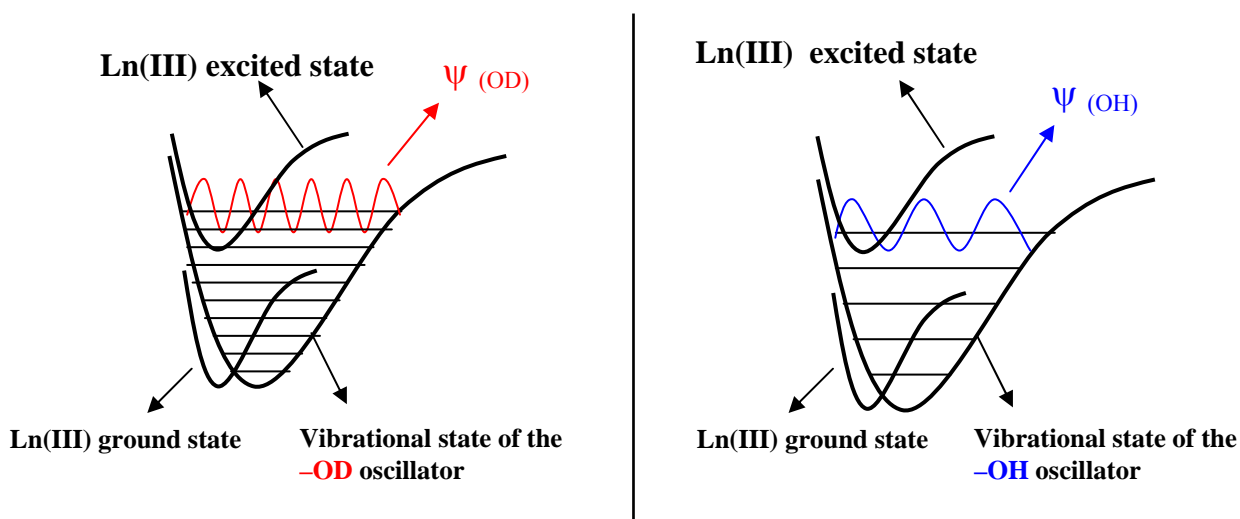


Fig. 2.1.6 Schematic representation of the vibrational states of –OD (left) and –OH (right) oscillators for pertinent electronic potential energy curves.

For ions with low reduction potentials, such as Eu(III) ($\text{Eu}^{3+}aq / \text{Eu}^{2+}aq = -0.38 \text{ eV}$, vs NHE, normal hydrogen electrode), a photoinduced electron transfer can occur in the presence of oxidants. The Eu^{2+} complexes have completely different photoluminescence (PL) properties relative to triple charged ones.

A further potential origin for the non-radiative deactivation of the Ln(III) ion excited states is the back-energy-transfer process (as in the case of Tb(III) where the emitting level lies at $\sim 20.500 \text{ cm}^{-1}$). It can take place between ^3LC and the ion emitting level(s) pointing out, once again, the central role of the antenna unit(s) choice.

2.3 Luminescence

Luminescence from Ln(III) ions covers a wide spectral range throughout the visible (Vis) and near-infrared (NIR) region. The emission intensities are strictly related to the antenna efficiency although, basically, visible-light emitting ions show stronger signals, relatively to NIR emitting ones, because of the *energy gap law*.³²

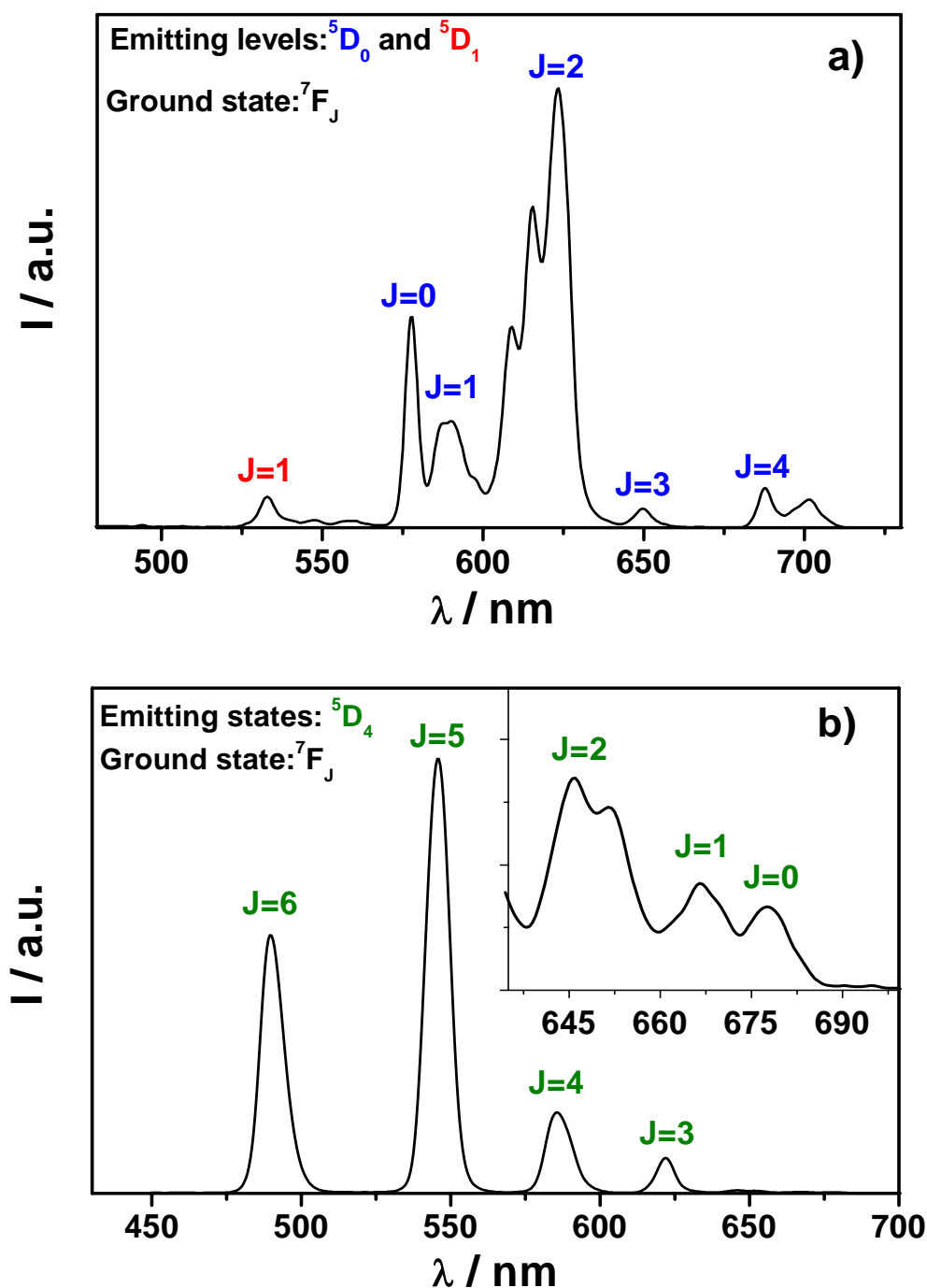


Fig. 2.3.1 Typical emission bands of a) Eu(III) and b) Tb(III) ions.

For instance, for a given electronic transition, the larger is the energy difference between the initial and the final states, the higher is the probability that radiative deactivations occurs. Since the discovery of their emission properties, the most popular and studied ions became europium and terbium, due to their strong red and green luminescence, respectively. The purity of the emitted

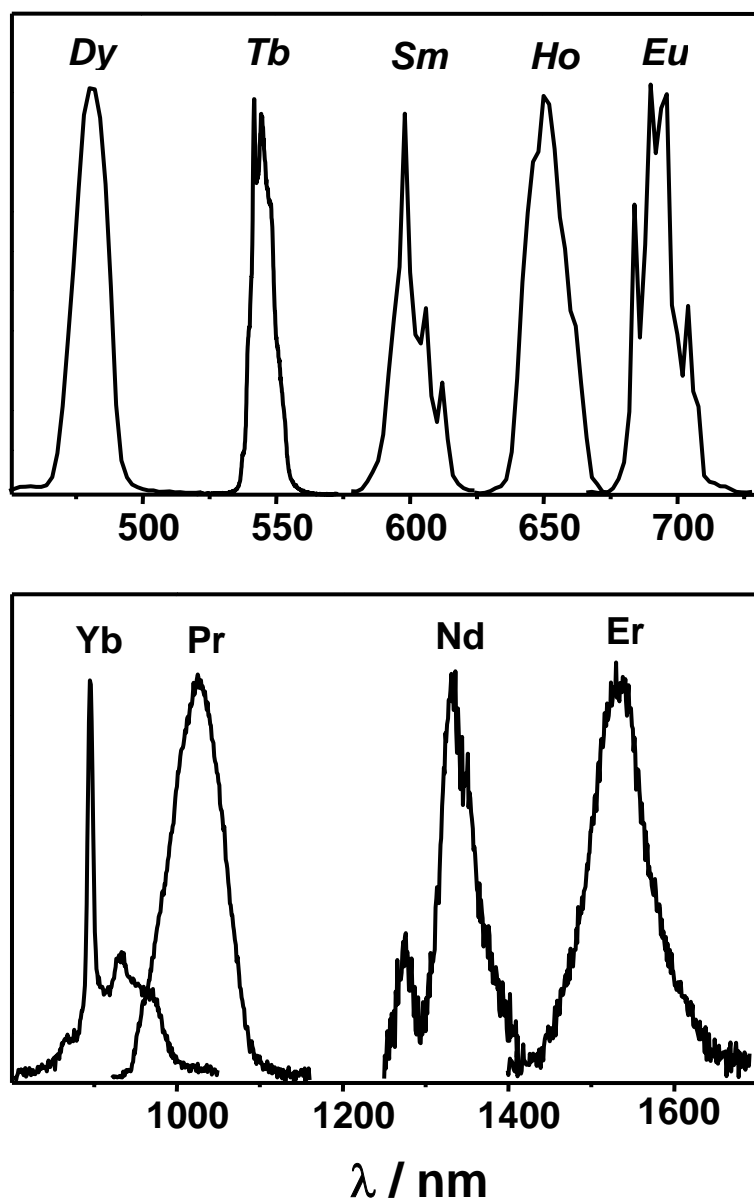


Fig.2.3.2 Selected emission bands of several Ln(III) ions.

Tm(III) shows a weak blue luminescence at 480 nm due to the $^1G_4 \rightarrow ^3H_6$ transition³⁵. Also Ce(III), when encapsulated in inorganic environment, shows purple to blue photoluminescence.³⁶ Selected emission profiles of several Ln(III) ions are reported in Fig. 2.3.2.

colours, conferred by line-like bands, are most widely exploited in lighting technologies. Fig. 2.3.1 shows the emission bands for both ions and the corresponding $J^* \rightarrow J$ transitions. Trivalent Nd, Yb and Er ions are pure NIR-emitters. Three emission bands are generally detectable for Nd(III) at 880, 1060, and 1330 nm ($^4F_{3/2} \rightarrow ^4I_{13/2}$, $^4I_{11/2}$ and $^4I_{9/2}$ respectively), one for Yb(III) (980 nm $^2F_{5/2} \rightarrow ^2F_{7/2}$), and one for Er(III) (1535 nm $^4I_{3/2} \rightarrow ^4I_{15/2}$) respectively.^{33, 34}

Differently, the emission of Ho, Dy, Pr and Sm trivalent ions includes the visible spectral range. Emissive levels are 5F_5 , $^4F_{9/2}$, 3P_0 - 1D_2 , and $^4G_{5/2}$, respectively.³³

Remaining lanthanides are of negligible interest as far as their luminescence properties are concerned. The Gd(III) lowest excited state lies at $\sim 32.000 \text{ cm}^{-1}$.³⁷ This rules out the metal ion sensitization process by most common organic antenna ligands (section 2.1 and Chapter 4) whose energy levels lie at lower energy, i.e. typically below 30.000 cm^{-1} . Therefore, the (ligand centred) luminescence of the Gd(III) complexes is normally investigated to estimate the energy of the lowest singlet and triplet excited states of the ligand via fluorescence and phosphorescence spectra acquisition.

3 APPLICATIONS

3.1 Outline of this thesis

This doctoral work focused on the study of the photoluminescence properties of several Ln(III) complexes emitting in the visible and near-infrared spectral window. The investigations have been carried out in both liquid and solid state, by using either well-known matrices (organic polymer and Sol-Gel glasses) or completely novel medium such as carbon nanotubes. As widely reported in literature, (i) lighting,^{35, 38-48} (ii) bioassay,⁴⁹⁻⁵¹ (iii) telecommunications⁵²⁻⁶¹ and (iv) lasers,^{62, 63} which well fit with the present experimental work, represent the most common applications involving lanthanides. Furthermore, rare-earth elements are of particular interest in many other areas which are now briefly described.

3.2 Overview on applications

High-technology and environmental applications of rare earth elements have grown dramatically in diversity and importance over the past four decades³. As many of these applications are highly specific, they have acquired a level of great technological significance, and demand for several of the less abundant REE has increased dramatically. Permanent magnet technology has been revolutionized by alloys containing Nd, Sm, Gd, Dy, or Pr ions. Small, lightweight, high-strength REE magnets have allowed miniaturization of numerous electrical and electronic components used in appliances, audio and video equipment, computers, automobiles, communications systems, and military gear. Many recent technological innovations (for example, miniaturized multi-gigabyte portable disk drives and DVD drives) would not be possible without REE magnets. Cerium, the most abundant and least expensive REE, has dozens of applications, some highly specific. For example, Ce oxide is uniquely suited as a polishing agent for glass. The polishing action of CeO₂ depends on both its physical and chemical properties, including the two

accessible oxidation states of cerium, Ce(III) and Ce(IV), in aqueous solution. Virtually all polished glass products, from ordinary mirrors and eyeglasses to precision lenses, are finished with CeO₂.

Environmental applications of REE have clearly increased over the past three decades. This trend will certainly continue, because of the growing alarms about global warming and energy efficiency.⁶⁴ Several REE are essential constituents of both petroleum fluid cracking catalysts and automotive pollution-control catalytic converters. Employ of REE magnets reduces the weight of automobiles. Large-scale application of magnetic-refrigeration technology (described below) also could significantly reduce energy consumption and CO₂ emissions.

In many applications, REE are advantageous because of their relatively low toxicity. For example, the most common types of rechargeable batteries contain either cadmium (Cd) or lead (Pb). Rechargeable lanthanum-nickel-hydride (La-Ni-H) batteries are gradually replacing Ni-Cd batteries in computer and communications applications and could eventually replace lead-acid batteries in automobiles. Although more expensive, La-Ni-H batteries offer greater energy density, better charge-discharge characteristics, and less environmental problems upon disposal or recycling. As another example, red and red-orange pigments made with La or Ce are superseding traditional commercial pigments containing Cd or other toxic heavy metals.

The next high-technology application of the REE is expected to be magnetic refrigeration. The six Ln(III) ions from Gd(III) through Tm(III) have unusually large magnetic moments, thanks to the many unpaired electrons. A recently developed alloy, Gd₅(Si₂Ge₂), with a “giant magnetocaloric effect” near room temperature will allow magnetic refrigeration to become competitive with conventional gas-compression refrigeration. This new technology could be employed in refrigerators, freezers, and residential, commercial, and automotive air conditioners. Magnetic refrigeration is considerably more efficient than gas-compression refrigeration and does not require refrigerants that are flammable or toxic, deplete the Earth’s ozone layer, or contribute to global warming.⁶⁴

3.3 Lighting

Interest on lighting has increased in the last decades because of growing demand and related consumption of electricity. For instance, by using a traditional tungsten lamp, we withdraw from a power station 100 units of primary energy, simply wasting 99 units as heat in the electricity production and in the bulb itself. Extensive adoption of more efficient light sources, such as light emitting diodes

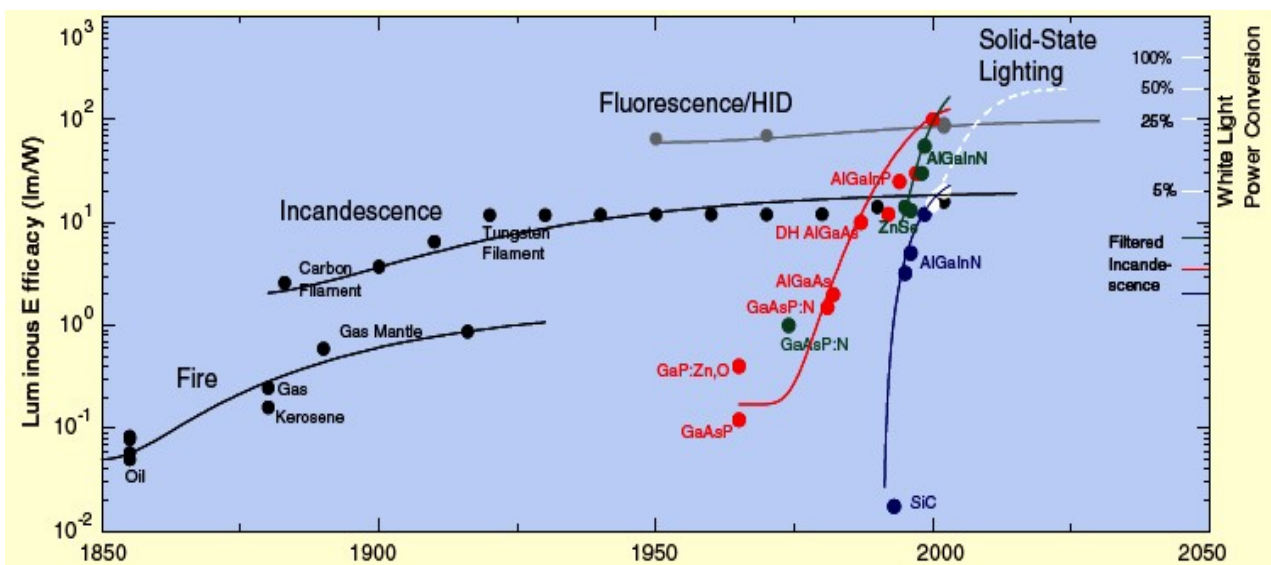


Fig. 3.3.1 Light source efficiencies between 1850 and 2050 (previsions).

(LED), organic light emitting diodes (OLED) and efficient fluorescent lamps, reduces the energy demand/waste and potentially achieve significant reductions in carbon dioxide emissions (equivalent to removing one-third of the automobiles currently on the road). Furthermore, old-fashioned Cathode Ray Tubes (CRT, consisting of a screen with red, green, and blue phosphor pixels excited by fast electrons), commonly used in computer monitors and television devices, being gradually replaced by much more high quality and efficient Liquid Crystal Displays (LCD) and Plasma Display Panels (PDP), which may bring significant electricity savings. LCD are non-organic, non-emissive devices that require an external light source or a back lighting system; self-

emissive alternatives are under development. PDP consist of a matrix of plasma discharge cells that works by applying a voltage between two transparent display electrodes on the front glass plate of the display, each cell generates a Xenon discharge with subsequent emission of red, green, or blue light. For instance, colour cathode-ray tubes and liquid-crystal displays used in computer monitors and televisions employ europium as the red phosphor and no substitute is known. OLED are the last frontier of lighting technology. They are

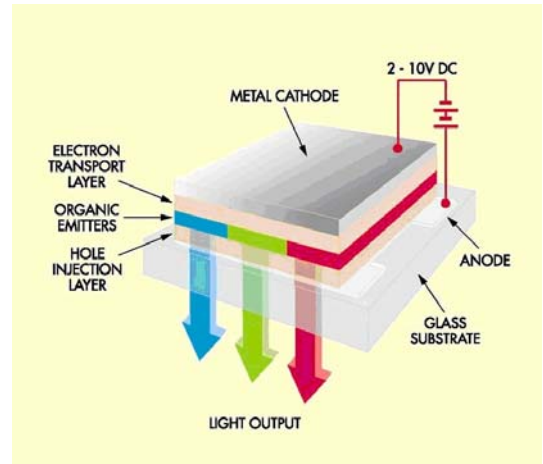


Fig 3.3.2. A typical OLED device structure. The number of layers can vary depending on used material and deposition technique

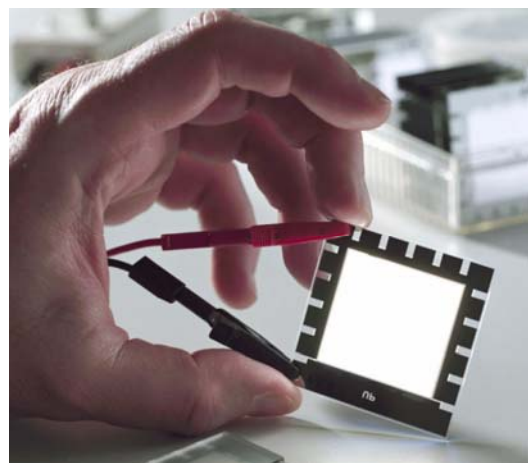


Fig. 3.3.3 WOLED (White OLED) device

thin-film multi-layer devices consisting of i) electrodes ii) active materials iii) electron and hole injectors. All layers are between protective barriers layer. At least one of the electrodes must be transparent to light (generally ITO: Indium Tin Oxide). When a voltage is applied, the generated electric field supports injection of charges through the electrodes / active layer interfaces. Holes (injected from

the anode) and electrons (injected from the cathode) migrate towards each other in the opposite directions, and finally meet. The charge recombination generates the excited states (or excitons) of the active materials which deactivate emitting light. It is clearly desirable that all deactivations involve photon output (light).

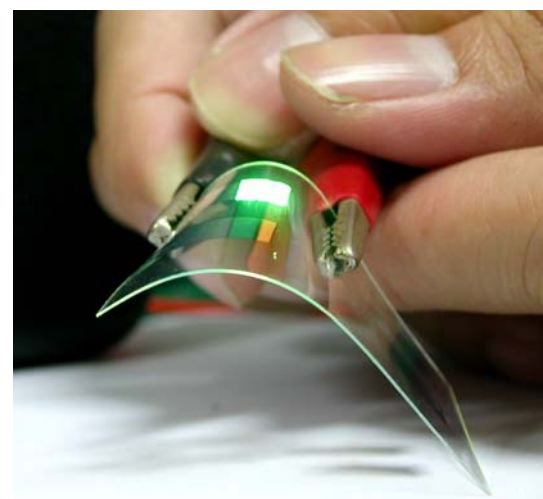


Fig. 3.3.4 Flexible OLED device

3.4 Bioassay

In the areas of life science, biotechnology and clinical diagnostics, several bio-labelling reagents, including radio-isotopes, enzymes, fluorescence dyes, and chemiluminescent compounds, have been developed and widely used for the detection of biological molecules.^{49, 50} Among these reagents, due to the high sensitivity and easy operation of luminescence detection, fluorescent dyes have occupied the most important position in today's biotechnology, being used in fluoroimmunoassay and medical-imaging^{65, 66}. Basically, fluoroimmunology determines the concentration of an antigen in a biological matrix taking advantage from the interaction antibody-

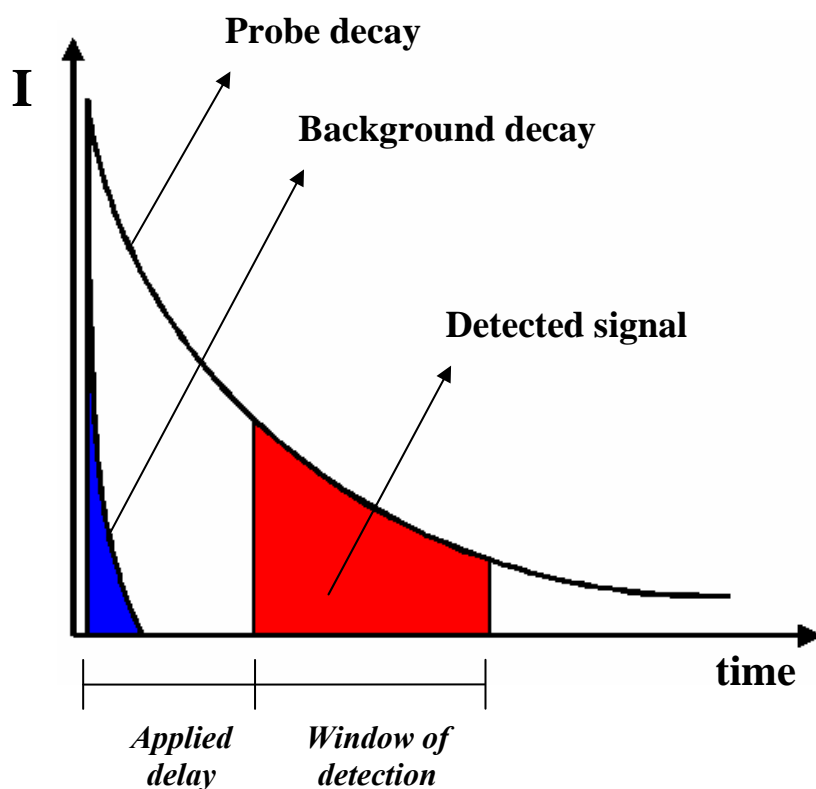


Fig. 3.4.1 Principle of time-resolved fluorometric measurements

luminescent probe through three basic steps: i) antibody-probe bonding ii) antibody-probe-antigen bonding iii) determination of the luminescence of the immunocomplex (as the only emitting species in the matrix). However, the conventional fluorescence bioassay has the problem that the fluorescence detection is easily affected by the background noises

caused by biological sample and analysis instrument. The use of Ln(III) complexes remarkably improves the sensibility of such diagnostic techniques. Because of their long-lived (micro-millisecond timescale) emission decays, the signal can be detected by applying a suitable delay (usually a few hundreds of nanoseconds) which cut off the undesired background noise (Fig. 3.4.1).

To this purpose, Vis and NIR emitting Ln(III) complexes can be employed due to their strong luminescence efficiency and relative transparency of human tissue, respectively.^{65, 67, 68}

On the other hand, the non-emissive Gd(III) ion represents the relaxation agent of choice because of its high magnetic moment and long electronic relaxation times. In fact, the ability of the gadolinium complexes to efficiently catalyse the proton relaxation of the water molecules is

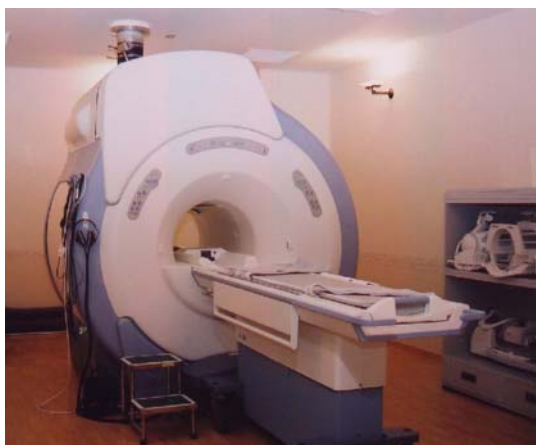


Fig. 3.4.2. MRI diagnostic apparatus

exploited in the contrast-enhanced magnetic resonance imaging technique⁶⁹ (MRI, Figs. 3.4.2 and 3.4.3).⁷⁰ This ability is described in terms of the relaxivity (r_{1p}), i.e. the enhancement in the solvent nuclei relaxation rate measured in a millimolar solution of the paramagnetic complex, at a given temperature and magnetic field strength (typically 25°C and 0.47 T). The proton relaxivity depends on several structural and dynamic

parameters that provides useful information on the metal complex. The most relevant are: (i) the number, q , of water molecules present in the inner coordination sphere of the Gd^{3+} ion; (ii) the distance, r , between the metal centre and the proton nuclei of the coordinated solvent molecules; (iii) the mean residence lifetime, τ_M , of these water molecules; (iv) the molecular reorientational correlation time, τ_R , related to the size of the complex; (v) the electronic relaxation time of Gd^{3+} described in terms of the parameters Δ^2 and τ_V , where Δ is the trace of the zero field splitting (ZFS) tensor and τ_V the correlation time for the modulation of the transient ZFS. The value of the relaxation parameters can be assessed by measuring the relaxivity as a function of the magnetic field strength and by fitting the experimental data (nuclear magnetic relaxation dispersion, NMRD, profile) to the proper set of equations

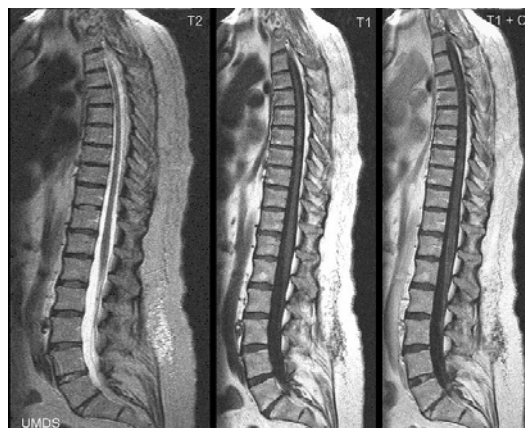
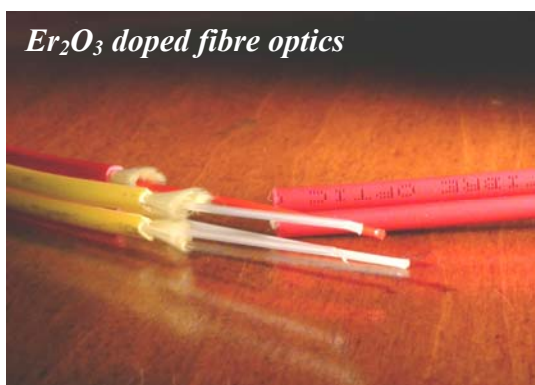


Fig. 3.4.3 T2 sample images from the sagittal, T1 weighted and T1+C weighed gadolinium enhanced MRI sequences of human tissue

describing the paramagnetic relaxation.^{71, 72} Furthermore, additional information on the possible occurrence of coordination equilibria, structural changes, hydrolysis and formation of hydroxo species, variation of the hydration number q , etc. can be obtained by investigating the dependence of r_{1p} from pH (and temperature).

3.5 Telecommunications

Telecommunication plays a vital role in modern society. Information handling is one of the peculiar features of the current century and increasing phenomena such as network accessibility for



more and more people (“global wiring”) need further technological implementation. By the way, internet makes use of only a small part of total bandwidth available.⁷³ Other services (HDTV – High Definition Television, Video-On-Demand, interactive television, voice traffic etc..) and applications which process a huge

amount of data (multimedia applications, video conferencing etc..) are supposed to be available to more and more people in the next future. Copper wires cannot satisfy the need for high volume data transfer because of low transmission speed and small signal bandwidth.

Information transmission by using optical cables, which transport pulses of light instead of electricity (Fig. 3.5.1), increases bandwidth massively.⁷⁴ Currently, the telecommunication systems installed work at 40 Gbit/s but the speed limit serviceable with all optical components has been foreseen to be up to 1 Tbit/s. Anyway, for long distance communication it is necessary to compensate the losses in the fibre by regenerating the signal typically every 50 –150 km (depending on the data rate). This is currently done by optical amplifiers. An amplifying medium contains a material capable of luminescence at the signal beam wavelength. The luminescent material needs to be pumped with a laser, a signal beam travelling through the amplifying medium will stimulate the

emission of light, which is of the same wavelength and phase. For amplification of an $1.55\ \mu\text{m}$ – signal, erbium doped fibre amplifiers (EDFA's) are used due to the ${}^4I_{13/2} \rightarrow {}^4I_{15/2}$ transition (see Fig. 2.3.2). The core of the fibre is doped with erbium ions during fibre fabrication. The amplifier is pumped at either $1.48\ \mu\text{m}$ or $0.98\ \mu\text{m}$ with a commercially available semiconductor diode laser coupled into the amplifier with a wavelength multiplexer. For creation of an optical transmission system totally made of organic compounds new materials are needed, which are transparent at certain wavelengths and can be optically and electrically activated only. Erbium, currently used in the laser repeaters despite its high cost, possesses the required optical properties.

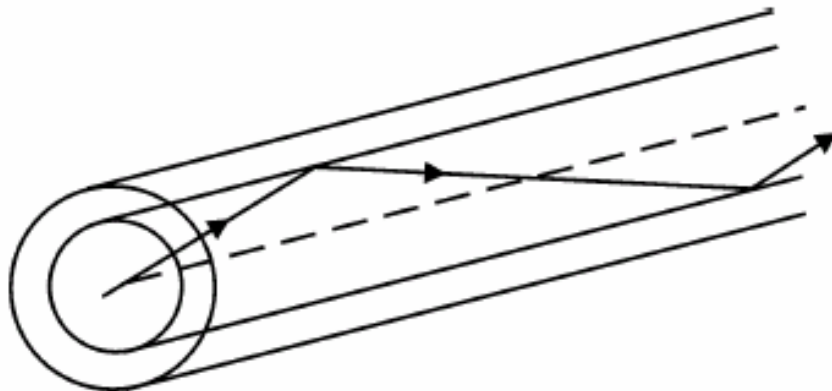


Fig. 3.5.1 Schematic representation of a (fiber-)waveguide, consisting of a core material embedded in a cladding material with lower refractive index. Basically waveguiding is the phenomenon of total internal reflection of a light beam in a material that is embedded in another material with a lower refractive index that confines and guides the light beam through the core of the fiber

3.6 Lasers

Rare earth ions doped into various crystals are well-known to exhibit laser operation as active elements, usually emitting in the IR spectral region. In combination with other rare earth or transition metal ions a variety of lasers has been manufactured. Recently, a comprehensive overview of transition metal and rare earth ion doped crystals for application as tunable solid-state lasers has been reported,⁶³ detailing the laser operation in the spectral range between $270\ \text{nm}$ and

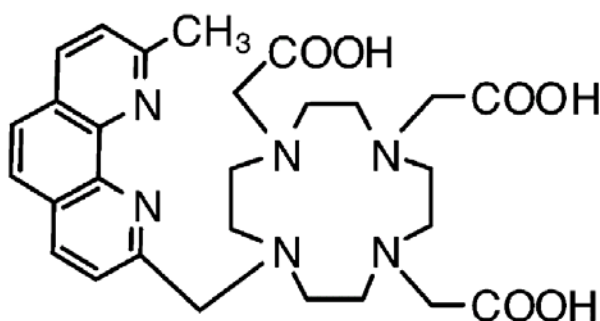
4500 nm, based on $3d \leftrightarrow 3d$ and $4f \leftrightarrow 5d$ transitions. Also, upconversion laser processes of crystals doped with rare earth ions have been reviewed extensively.⁷⁵

Neodymium, because of its emission line at 1064 nm, is the most common lanthanide used as laser source.⁶² Known laser crystals include Tm^{3+} doped YAlO_3 , $\text{Y}_3\text{Al}_5\text{O}_{12}$ (YAG).⁷⁶ After Yb^{3+} -sensitized materials were originally investigated for infrared quantum counters,⁷⁷ co-doping with rare earths such as Tm^{3+} proved to show efficient upconversion laser operation in several crystals. Recently, an orange and red upconversion laser has been presented, based on an avalanche pumping mechanism of Pr^{3+} , Yb^{3+} in BaY_2F_8 (BYF).⁷⁸⁻⁸⁰ Efficient tunable laser operation has been observed in diode-pumped Yb , $\text{Tm}:\text{KY}(\text{WO}_4)_2$ around 1.9 μm . BYF with Tm^{3+} concentrations ranging from 2 to 18 at.% varies its emission wavelength from 1927 nm up to 2030 nm, while the nature of the transition changes from purely electronic to vibronic. Besides laser applications of IR-visible upconversion materials, one should also mention three-dimensional displays,⁸¹ visualization of IR light, and security marking of official documents. Solid state lasers based on Tm^{3+} and Ho^{3+} have many applications in remote sensing, medical, and military technologies. Tm^{3+} , Ho^{3+} , Er^{3+} in $\text{Y}_3\text{Al}_5\text{O}_{12}$ (YAG) has been demonstrated to lase at room temperature.⁸² A high-power laser based on Cr^{3+} , Tm^{3+} , Ho^{3+} (CTH) in YAG has been conceived soon afterwards. Q-switched $\text{Cr},\text{Tm}:\text{YAG}$ and $\text{CTH}:\text{YAG}$ laser operation emitting at 2 μm wavelength has been achieved with maximum pulse energy of 0.7 and 0.5 J, respectively, and corresponding pulse widths of 140 ns and 165 ns. The extraordinary high efficiency is due to the Cr^{3+} to Tm^{3+} energy transfer having high quantum efficiency. These characteristics generate large interest for a wide range of applications, e.g. in the medical field. Recently, improved laser operation of $\text{LiCAF}:\text{Ce}^{3+}$ and $\text{LiLuF}_4:\text{Ce}^{3+}$ was observed at output energies of 60 mJ and 27 mJ, respectively.⁸³

4 RESULTS AND DISCUSSION

4.1 Phenanthroline type complexes

Luminescence properties in D₂O solution of Eu(III) and Er(III) complexes have been studied. The dipartite ligand **1**, (Scheme 4.1.1) includes (i) a 1,4,7,10-tetraazacyclododecane-1,4,7-triacetic acid (DO3A) unit serving as hosting site for the metal center; and (ii) a phenanthroline unit which plays the role of light antenna for the sensitization process of the metal centred luminescence.



Scheme 4.1.1. Chemical structure of the ligand 1

The ISC step for phenanthroline takes place with $\phi_{ISC} \gg 0.85$ (actually, not far from unit) within the complex,²² and the rate constant for the energy transfer step is $k_{EnT} \approx 10^7 \text{ s}^{-1}$, which compared to a deactivation rate constant $k_T \sim 3 \times 10^4 \text{ s}^{-1}$ for the T (Triplet) level results in $\phi_{EnT} \sim$ unit. X-ray and ¹H NMR results are consistent

with full saturation of the nine coordination sites within the Ln(III) complexes.²³ The luminescence results are consistent with both an effective intersystem crossing (ISC) at the light absorbing phenanthroline unit ($\lambda_{exc} = 278 \text{ nm}$) and an effective energy transfer process from the phenanthroline donor to the cation acceptor (with unit or close to unit efficiency for both steps).

In D₂O, the emission quantum yield, Φ_{se} , is 0.3 and 5×10^{-6} , for **Eu•1** (main luminescence peaks at 585, 612, 699 nm) and **Er•1** (luminescence peak at 1530 nm), respectively (Fig. 4.1.1).

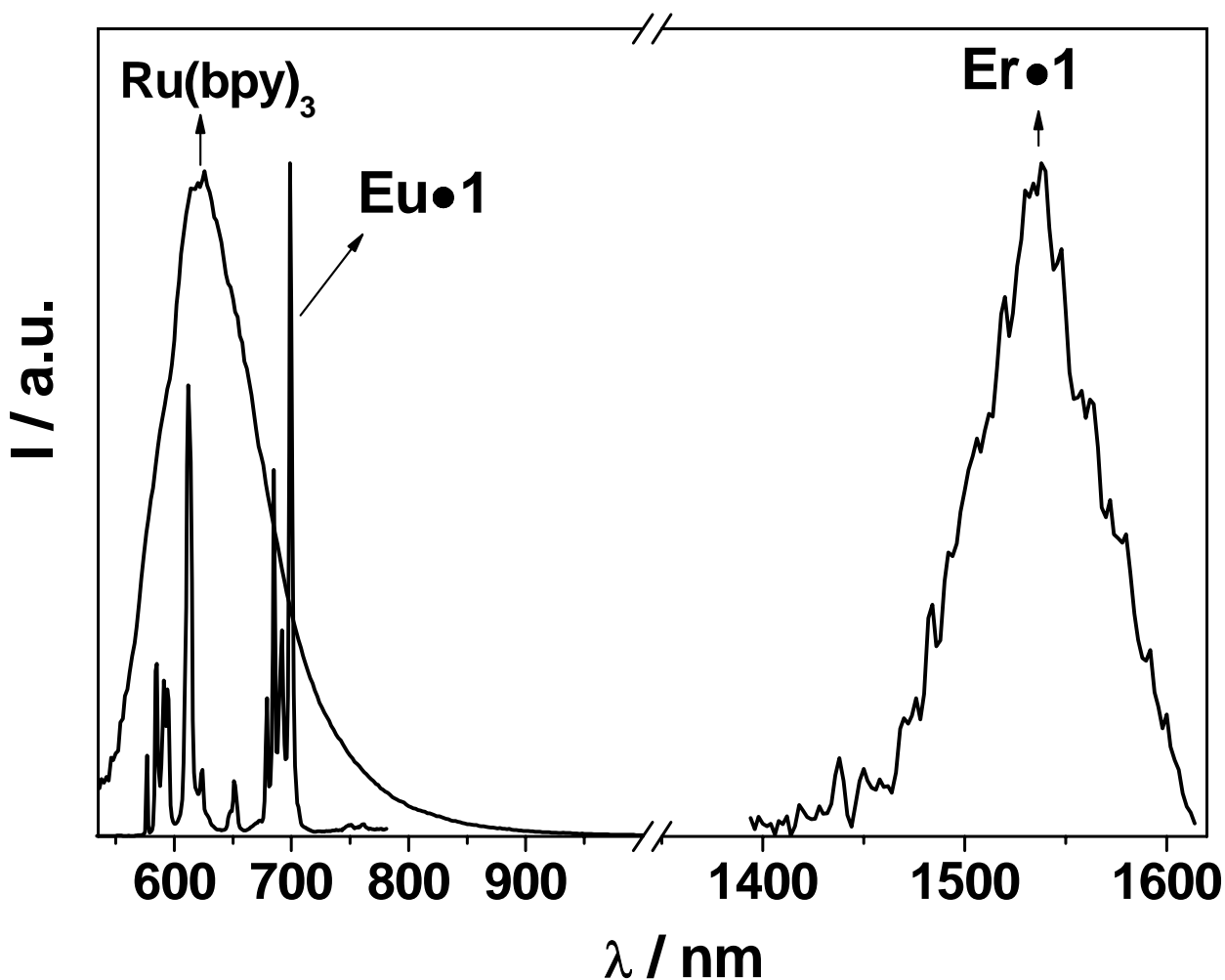
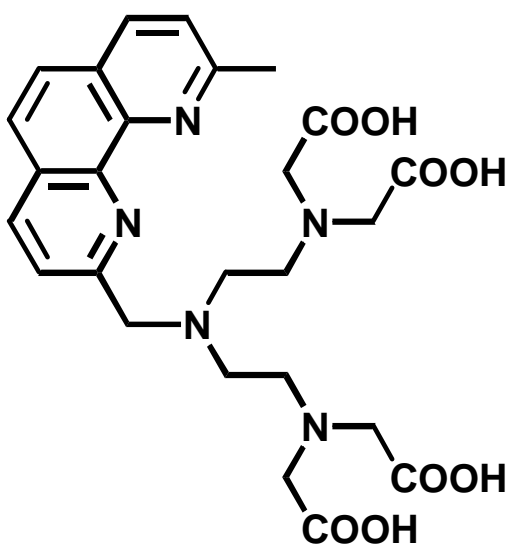


Fig. 4.1.1 Luminescence spectra of **Eu•1**, **Er•1**, and $[Ru(bpy)_3]^{2+}$ complexes H_2O ; excitation of isoabsorbing samples was performed at 278 nm.

It is worth noticing the low erbium luminescence quantum yield appears one,⁸⁴ or two,⁸⁵ orders of magnitude lower than what is found in other Er^{3+} complexes. It should be stressed however that most literature data regarding $Er(III)$ luminescence has been drawn relying on a comparison between observed and radiative lifetimes, according to $\Phi_{Er} = \tau_{obs}/\tau_{rad}$.^{86 87}

Our approach has been to proceed to a direct comparison of calculated areas for the luminescence profiles as obtained from corrected emission spectra and by using isoabsorbing solutions at the selected excitation wavelength, 278 nm. A largely employed luminophore, $[Ru(bpy)_3]^{2+}$ ($\Phi = 0.028$ in aerated water),²² has been selected as a standard.

Along this line, the synthesis of a new ligand (**2**), containing a single phenanthroline (phen) chromophore and a flexibly connected diethylenetriamine tetracarboxylic acid unit (DTTA) as a lanthanide coordination site, has been carried out [**2** is 4-[(9-Methyl-1,10-phenantrol-2-yl)methyl]-1,4,7-triazaheptane-1,1,7,7-tetracetic acid]. The open coordinating DTTA unit is expected to



Scheme 4.1.2: Chemical structure of the ligand 2

provide highly stable and more protected complexes relative to N-ring (DO3A) due to its increased flexibility, which results in a better coordination ability especially for cations with high coordination site number such as lanthanides. Using the ligand **2**, an extended series of water soluble lanthanide complexes was obtained (Ln = Eu(III), Tb(III), Gd(III), Sm(III), Dy(III), Pr(III), Ho(III), Yb(III), Nd(III), and Er(III)). The stoichiometry for the association was found 1:1, with an association constant $K_A \geq 10^7 \text{ s}^{-1}$ as determined by luminescence spectroscopy. The luminescence and photophysical properties of the series of lanthanide

complexes were investigated in both H₂O and D₂O solutions. High efficiencies for the sensitized emission, Φ_{se} , in air equilibrated water were observed for both Eu(III) and Tb(III) in the visible region and of Sm(III), Dy(III), Pr(III), Ho(III), Yb(III), Nd(III), and Er(III) in the Vis and/or near-Infrared region. For **Eu•2** and **Tb•2**, luminescence data for water and deuterated water allowed to estimate that no solvent molecules (q) are bound to the ion centers (q = 0). Luminescence quenching by oxygen was investigated in selected cases. Lanthanide complex solutions were obtained upon addition of one equivalent of Ln(Cl)₆•6H₂O to a water solution of **2** in which were previously added four equivalents of TBA (Tetrabutylammonium hydroxide) in order to deprotonate the carboxylic groups of the chelating ligand. The stoichiometry of the association between **2** and the lanthanide ions was 1:1, as evaluated by emission intensity titration experiments.

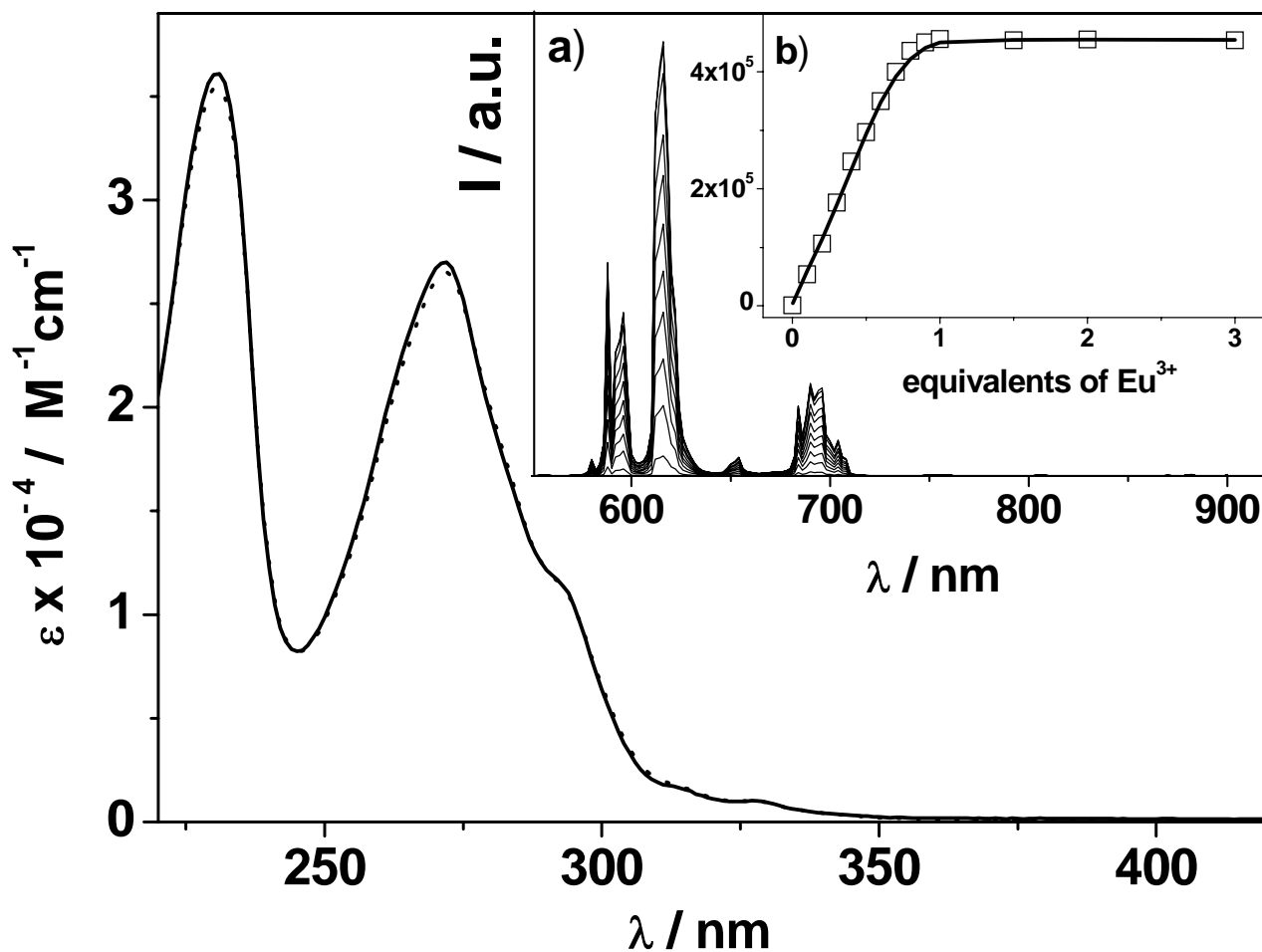


Fig. 4.1.2 Absorption spectra of **2** (solid line) and **Eu•2** (dashed line) in H_2O solutions. Inset a), luminescence titration of **2** in water solution upon addition of aliquots of $EuCl_3(H_2O)_6$; $\lambda_{exc} = 279$ nm. Inset b), luminescence intensity changes detected at $\lambda_{em} = 616$ nm; the full line results from the fitting procedure.

The experiments were performed for 2×10^{-5} M water solution of the ligand by using concentrated solution ($\approx 10^{-3}$ M) of lanthanide salts. For illustration purposes, insets a) and b) of Fig. 4.1.2 show results for the case of **Eu•2**; in the insets, I is luminescence intensity observed at 616 nm (corresponding to the ${}^5D_0 \rightarrow {}^7F_2$ transition, which appears as the strongest luminescent band⁸⁸ when no phototube correction for the fluorimeter is taken into account). Inset b) provides evidence for the 1:1 association and the full line results from a fitting procedure in accord with eq.4.1.1,^{89, 90}

$$eq.4.1.1 \quad I = I_0 + \frac{\Delta I}{2S_0} \left[K_{diss} + X + S_0 - \sqrt{(K_{diss} + X + S_0)^2 - 4XS_0} \right]$$

where I_0 and ΔI are the initial luminescence intensity and the its final increase, respectively, as observed at 616 nm, $K_{\text{diss}} = 1/K_{\text{ML}}$ (K_{ML} is the association constant), and, X and S_0 are the titrant and ligand concentrations respectively. Results of titration experiments always indicated that the 1:1 association takes place with $K_{\text{ML}} \geq 10^7 \text{ M}^{-1}$. Similar results were obtained for other Ln(III) complexes in the series.

The absorption spectra of **2** and **Eu•2** in water solution are shown in Fig. 4.1.2. Their spectral shapes remarkably overlap and the two peaks in UV region at 230 and 279 nm are ascribed to the phenanthroline centred transition. Similar results were obtained for the other Ln(III) complexes investigated. This is an uncommon outcome, because the presence of triply charged ions incorporated within a complex is usually signalled by a change of the absorption profile of the close chromophore^{17, 22}. Thus, apparently the coordination of the phenanthroline moiety at Eu(III) ion does not actually imply a strong electronic interaction between these two centers. What is relevant, however, is that efficient sensitization of the MC luminescence takes place, as revealed by the intense luminescence observed for all studied complexes. The (supposedly) weak electronic interaction between the light absorbing phen and the light emitting Ln(III) subunits is however sufficient to promote the occurrence of ligand-to-metal energy transfer. To our knowledge, a similar case is only reported in the literature for a system with appended a single acetophenone unit.⁹¹

Ligand centred emission. The absorption bands of lanthanide complexes are due to ligand-centered ¹LC transitions. The luminescence study of **Gd•2** allows to evaluate the energy levels of the lowest-lying singlet (S_1) and triplet (T) excited states in the presence of a heavy and triply charged center. Luminescence results for **Gd•2** were obtained at room temperature (fluorescence) and at 77 K (phosphorescence). With regard to the room temperature results as monitored at the fluorescence band for **2** ($\phi = 3.5 \times 10^{-3}$ and $\tau = 0.9 \text{ ns}$) and for **Gd•2** ($\phi = 7.4 \times 10^{-4}$ and $\tau < 0.5 \text{ ns}$) one draws the indication that the metal center causes an improved intersystem crossing within the complex, with respect to what happens for the phen ligand $\phi_{\text{ISC}} = 0.85^{22, 92}$, suggesting that for **2** ϕ_{ISC}

~ 1. As for the 77 K results, from the highest energy peak of the phosphorescence profile, the E_T level of phenanthroline origin can be estimated to lie at 21640 cm^{-1} for both **2** and **Gd•2**.

Metal Centred emission. The normalized luminescence spectra for complexes **Eu•2**, **Tb•2**, **Sm•2**, **Dy•2**, **Pr•2**, **Ho•2**, **Yb•2**, **Nd•2**, and **Er•2** are shown in Fig. 4.1.3, as arranged according to their predominant emission region, from Vis to NIR. Luminescence quantum yields and lifetimes in H_2O and D_2O solutions were obtained and are collected in Table 4.1.1. Experiments were also carried out in degassed water solution; only **Tb•2** exhibited oxygen sensitivity.

Coordination features. **Eu•2** and **Tb•2** showed a remarkably intense and long-lived luminescence in both H_2O and D_2O solutions. Comparison of luminescence results for water and deuterated water provides an assessment of solvent binding at the Eu(III) and Tb(III) centers. This is done by using the following equations,^{93, 94}

$$\text{eq. 4.1.2} \quad q^{\text{Eu}} = 1.2 (1/\tau_{\text{H}_2\text{O}} - 1/\tau_{\text{D}_2\text{O}} - 0.25)$$

$$\text{eq. 4.1.3} \quad q^{\text{Tb}} = 4.2 (1/\tau_{\text{H}_2\text{O}} - 1/\tau_{\text{D}_2\text{O}} - 0.06)$$

where q (uncertainty ± 0.5) is the number of coordinated solvent molecules and lifetimes are in ms.

For **Eu•2**, use of eq.4.1.2 provides $q^{\text{Eu}} = 0.02$. For **Tb•2**, $q^{\text{Tb}} = 0.01$, eq. 4.1.3.

These results indicate that the coordination shell of ligand effectively prevents water from binding at the metal centers. Of course, this is the basic reason for the high luminescence performances of complexes **Eu•2** and **Tb•2** in water, in agreement with the fact that OH oscillators are kept far from the metal centers and cannot act as quenchers (see Chapter 2).⁹³ It is interesting to notice that a potential cause of luminescence attenuation for NIR lanthanide emitters in water could be re-absorption of the emitted light due to the fact that the near-IR emitters exhibit luminescence profiles that nicely overlap with water absorption regions. For instance, Er(III)-containing

complexes undergo complete quenching in water, and their emission can only be detected in deuterated water.⁹⁵ On the other hand, complexes whose luminescence does not overlap with the

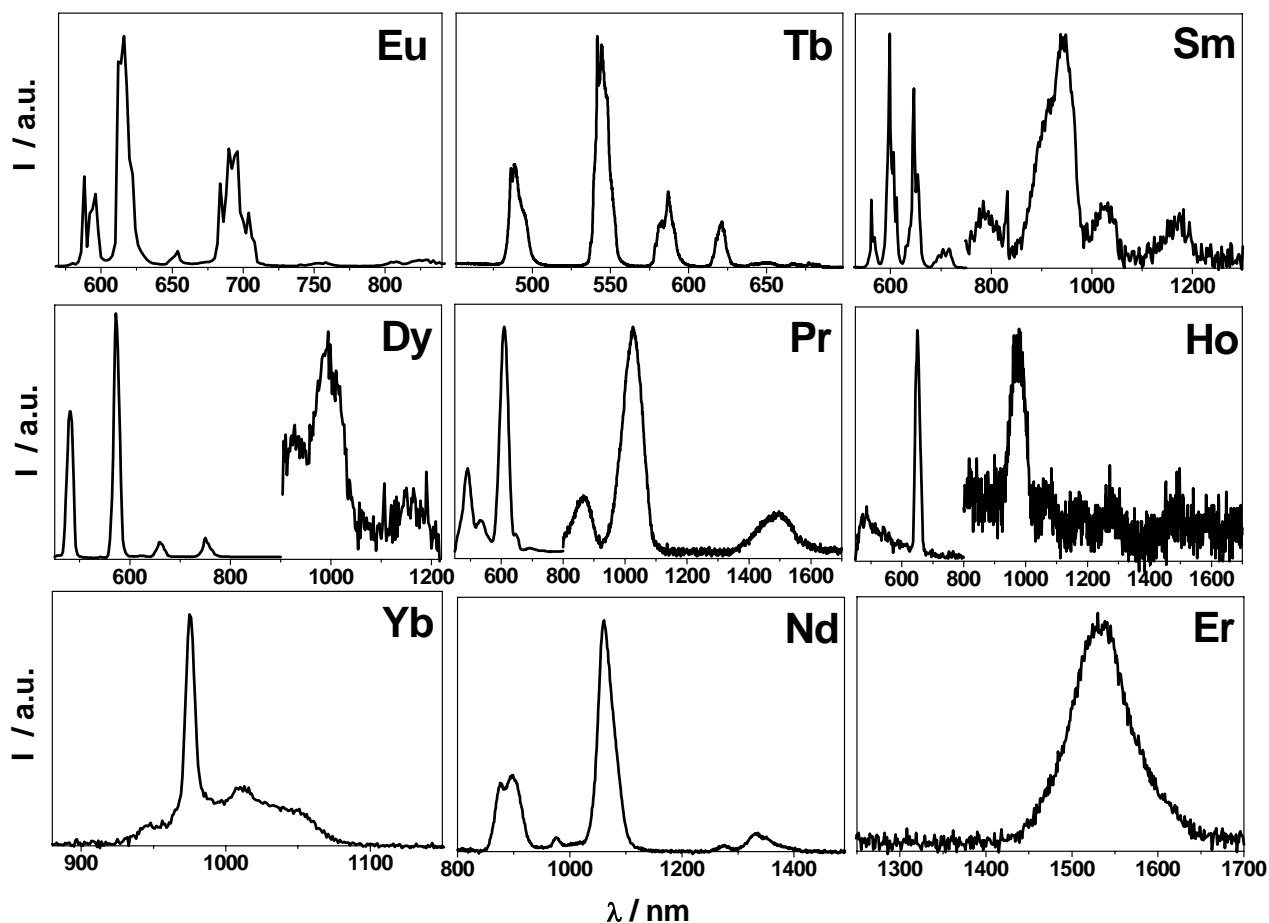


Fig.4.1.3 Room temperature uncorrected emission spectra for the complexes of the indicated lanthanide cations, in air-equilibrated D_2O solvent; $OD = 0.20$ at the employed $\lambda_{exc} = 279$ nm. For each complex, intensities from Vis and NIR regions are normalized.

water absorption (i.e., **Ho•2** and **Dy•2**) show practically unchanged emission features in both solvents. Regarding the coordination features of the **Sm•2**, **Dy•2**, **Pr•2**, **Ho•2**, **Yb•2**, **Nd•2**, and **Er•2** complexes, we assume that also in these cases no solvent molecules ($q = 0$) are present within the first coordination sphere.

Table 4.1.1. Metal centred luminescence properties in H₂O and D₂O solutions.^a

	H ₂ O			D ₂ O		
	λ_{\max}^b (nm)	ϕ_{se}	τ (μ s)	λ_{\max}^b (nm)	ϕ_{se}	τ (μ s)
Eu•2	616	0.24	1250	616	0.30	1880
Tb•2	544	0.15 0.45 ^c	780 2.3 ^c	544	0.14	820
Sm•2	598	2.5×10^{-3}	13.0	598	2.5×10^{-3}	34.0
Dy•2	478	5×10^{-4}	1.2	478	5×10^{-4}	1.1
Pr•2	608	3×10^{-5}	d	608	2×10^{-4}	d
Ho•2	650	2×10^{-5}	d	650	2×10^{-5}	d
Yb•2	980	2×10^{-4}	2.5	980	1×10^{-3}	10.0
Nd•2	1064	4×10^{-5}	< 0.2	1064	2×10^{-4}	0.4
Er•2	1530	d	d	1530	4×10^{-5}	1.2

^a Room temperature, excitation at 279 nm; the list is arranged according to the predominant Vis/NIR emission region. ^b Highest intensity line or band. ^c Degassed solution. ^d Not detected due to weakness of the signal.

Oxygen effect. Luminescence intensity and lifetime data in air-equilibrated and degassed water solutions of **Eu•2** and **Tb•2** were compared. For **Eu•2**, no relevant changes were noticed. By contrast, a three-fold increase of both parameters for **Tb•2** in degassed solution was found indicating the occurrence of a quenching by oxygen molecules. As it is known for complexes incorporating the phen chromophore,²² this effect is due a small energy gap between ligand-centred E_T levels and MC levels, so that both forward (ligand-to-metal) and backward (metal-to-ligand) energy transfer processes take place. This allows deactivation of the ligand E_T level through non-radiative quenching pathways by oxygen molecules. We have modeled the room temperature equilibrium between the E_T level of phenanthroline origin and the MC luminescent level of Tb(III)

by employing the following parameters. (i) The energy gap (ΔE) between the two levels was estimated from the luminescence profiles, (ii) the rate constant for the E_T decay was $k_p = 1/(35\mu s)$,⁹² and (iii) the rate constant for diffusional quenching by oxygen was $k_qO_2 = 2.0 \times 10^6 s^{-1}$, as evaluated from $k_{diff} \times [O_2]$, with $k_{diff} = 7 \times 10^9 M^{-1} s^{-1}$, and $[O_2] = 0.29 \times 10^{-3} M$.⁴ The three-fold changes of the luminescence features for **Tb•2** could be reproduced for $k_{12} \approx 5 \times k_qO_2$ [with the backward energy transfer $k_{21} = k_{12} \exp(-\Delta E/RT)$]. Accordingly, the phenanthroline→Tb(III) energy transfer step was evaluated to be $k_{en} \approx 1 \times 10^7 s^{-1}$.

For all complexes, except **Tb•2**, no changes of luminescence properties were appreciated for air-equilibrated and degassed samples. This behaviour can be understood mainly in terms of the energetic factor, i.e, because the energy gap between ligand and metal centred levels is $\Delta E \gg 1500 cm^{-1}$, i.e. too high to allow any effective back energy transfer. A distinctive reason for the lack of oxygen effect is met for the case of **Dy•2**, because the energy level of Dy(III) ($^4F_{9/2} \rightarrow ^6H_{15/2}$,³³ $\sim 21100 cm^{-1}$), is close-lying to that of Tb(III) ($\sim 20600 cm^{-1}$); however the two complexes exhibit opposite performances. In fact, for **Dy•2**, the shorter luminescence decay ($\sim 1 \mu s$) respect to that of **Tb•2** ($\sim 800 \mu s$) does not allow the establishment of an equilibrium between ligand (E_T) and Dy(III) centered levels. For the phen → Dy(III) energy transfer step, results of model calculations are consistent with a forward rate of $k_{12} \approx 1 \times 10^7 s^{-1}$, as for the case of **Tb•2**.

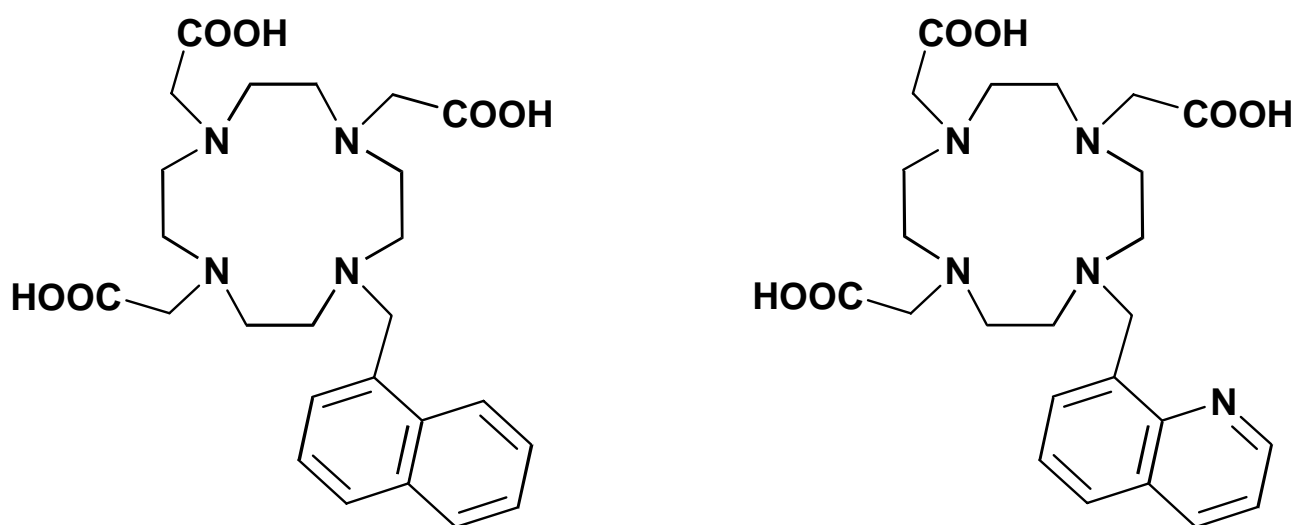
Near-Infrared emitters and solvent. As shown in Fig. 4.1.3, **Yb•2**, **Nd•2** and **Er•2** are real NIR emitting lanthanide complexes and their emission intensities appear to strongly depend on solvent, likely due to water reabsorption effects. Instead, the emission range for **Ho•2**, **Dy•2**, **Pr•2** and **Sm•2** includes visible spectral portion and such solvent effects are not registered, which might be explained by the fact that their luminescence profiles fall out of water absorption regions. In case of **Pr•2**, a relevant emission portion in the NIR region significantly contributes to the total luminescence. This likely explains why, on passing from D_2O to H_2O , a remarkable quenching

factor (one order of magnitude) is detected. One can conclude that for the full series of complexes the observed luminescence properties strongly depend on the solvent absorption regions.

Nature of the energy transfer step. As seen above, efficient phen \rightarrow Ln(III) energy transfer takes place for all investigated complexes; actually on the basis of the observed or derived parameters, a $\phi_{ISC} \times \phi_{en} \approx 1$ can be drawn. This result is consistent with results from ^1H NMR spectroscopy³⁷, indicating that the two nitrogen atoms of phen are involved in the coordination of the metal cation. On the other hand, it is remarkable that the absorption profile for the ligand **2** does not change upon inclusion of the trivalent Ln cations as it happens usually.^{17, 22} Furthermore, a dipole-dipole (Förster-type)²⁹ mechanism for energy transfer seems unlikely, given that the energy transfer step involves a triplet level for the phen donor (as clearly shown by comparison of results from air-equilibrated and degassed solutions of **Tb•2**, see above). All of these observations could likely be reconciled on the basis of the notion that a very small electronic interaction is enough to permit the occurrence of Dexter-Type energy transfer;³⁰ such a type of interaction might be mediated by the intervening sequence of bonds separating the phen chromophore and the DTTA site hosting the Ln(III) centers.

4.2 Naphthalene and quinoline type complexes

The two-component ligand systems **3** and **4** which contain 1,4,7,10-tetraazacyclododecane-1,4,7-triacetic acid (DO3A) as the hosting unit for the lanthanide cations, and naphthalene (which is devoid of any chelating ability) or quinoline units, respectively, have been studied in aqueous solution as chromophores complexed with Gd^{3+} , Eu^{3+} and Tb^{3+} in a 1:1 molar ratio. (Scheme 4.2.1) Tables 4.2.1 and 4.2.2 summarise luminescence and photophysical results and quantum efficiencies obtained for the various steps, that we shall examine in detail in the following. In particular, for the complexes of Eu^{3+} and Tb^{3+} we have determined the efficiency of the L-to-Ln energy transfer step, ϕ_{EnT} (Table 4.2.2).



Scheme 4.2.1: Chemical structures of the ligand 3(left) and 4(right)

ISC step. Regarding the ISC process occurring within the naphthalene and quinoline chromophores, we first notice that Φ_{ISC} can be taken close to unit for the investigated complexes. In fact, the pristine naphthalene chromophore exhibits a fluorescence lifetime $\tau_s = 96$ ns (fluorescence emission band maximum at $\lambda = 310$ nm, oxygen-free solution), with $\Phi_{ISC} = 0.75$.⁹⁶ For **3** and **Gd•3**, we found $\tau_s = 8.6$ and 2.4 ns, respectively, with identical results obtained for **Tb•3** and **Eu•3**. This is consistent with strongly enhanced ISC for the complexes of **3**, with $\phi_{ISC} \gg 0.75$. In principle, one should consider that for the case of Eu^{3+} complexes, quenching of the singlet level of the chromophore by photoinduced electron transfer might take place, leading to Eu^{2+} (the standard $\text{Eu}^{3+/2+}$ electrochemical potential is -0.35 V for the free aqua ion).⁹⁷ Actually, for naphthalene, the oxidation potential is $+1.7$ V (vs SCE) and the singlet excited level is at 3.99 eV.⁹⁶

Table 4.2.1 Luminescence and photophysical data at room temperature^a

	Φ_{EM} (H ₂ O)	τ_{H_2O} (ms)	Φ_{EM} (D ₂ O)	τ_{D_2O} (ms)	q	k_r (s ⁻¹)	$\Sigma k_{nr}^{OH, b}$ (s ⁻¹)	$\Sigma k_{nr}^{OD, b}$ (s ⁻¹)
Eu•3	3.2×10^{-3}	0.390	0.013	1.71	2.1 ^c	240 ^d	2.3×10^3	345
Eu•4	7.4×10^{-3}	0.500	0.026	1.79	1.4 ^[c]	190 ^d	1.8×10^3	370
Tb•3 ^[e]	5.6×10^{-3}	0.048	7.9×10^{-3}	0.050		360 ^f	2.1×10^4	2.0×10^4
Tb•4	2.4×10^{-3}	0.076	2.2×10^{-3}	0.075		360 ^f	1.3×10^4	1.3×10^4
Tb•4 ^g	0.013	0.337	0.015	0.450		360 ^f	2.6×10^3	1.9×10^3

^aAir-equilibrated samples unless otherwise indicated; photophysical results for **Gd•3** and **Gd•4** are reported and discussed throughout the text. ^b $\Sigma k_{nr} = 1/\tau - k_r$. ^cEstimated from $q^{Eu} = 1.2 (1/\tau_{H_2O} - 1/\tau_{D_2O} - 0.25)$.^[14] ^dCalculated from the MC emission profile, see text. ^eO₂-free samples, estimated Σk_{nr} values are affected by large uncertainties; in air-equilibrated samples no sensitised luminescence is observed. ^fFrom²². ^gO₂-free samples; in air-equilibrated samples sensitised luminescence intensity reduces to ca. 20%.

On these bases, the $S_{Nh} \rightarrow Eu^{3+}$ electron transfer step, which is evaluated to be strongly exothermic, would be in competition with the $S_{Nh} \rightarrow T$ intersystem crossing. On the other hand, for the excited **Gd•3**, no such electron transfer step is allowed (the standard $Gd^{3+/2+}$ electrochemical potential is -2.28 V for the free aqua ion),⁹⁷ and the fact that for both **Eu•3** and **Gd•3** the same singlet lifetime is observed, $\tau_S = 2.4$ ns, suggests that also for **Eu•3** the ISC step is the predominant one for singlet level deactivation at ligand **3**. Thus, the electron transfer step involving S_{Nh} and Eu^{3+} seems not to be competitive against the ISC step. Reasons for this behaviour might include (i) a relatively small intercentre electronic coupling for the $S_{Nh} \rightarrow Eu^{3+}$ electron transfer, and (ii) the fact that it should occur in “inverted region” conditions ($\Delta G^0 \sim -2$ eV), necessarily resulting in a remarkable slowing down.⁹⁸ As to the case of ligand **4**, the pristine quinoline chromophore is isostructural to naphthalene but contains a heteroatom, which is known to result in enhanced ISC processes,⁹⁹ consistent with the found $\tau_S = 7.7$ ns and < 0.1 ns for **4** and **Gd•4** (with nearly complete

disappearance of the fluorescence band, expected at 310 nm; identical results were obtained for **Tb•4** and **Eu•4**). On this basis, also for the complexes of **4**, ϕ_{ISC} is expected close to unit.

Table 4.2.2 Efficiency of intrinsic MC luminescence, of L-to-Ln energy transfer and oxygen effect ^a

	ΔE (cm ⁻¹)	$\Phi_{Lum}^{MC\ b}$		Φ_{EnT}	
		H ₂ O	D ₂ O	H ₂ O	D ₂ O
Eu•3	3380	0.094	0.034	0.41	0.032
Eu•4	4040	0.095	0.078	0.34	0.076
Tb•3 ^c	190	<i>e</i>	<i>e</i>	<i>e</i>	<i>e</i>
Tb•4 ^d	850	0.12	0.11	0.16	0.094

^aAir-equilibrated samples unless otherwise indicated. ^b $\Phi_{Lum}^{MC} = k_r/(k_r + k_{nr}^{MC})$, see Table 4.2.1 and text. ^c O₂-free samples; in air equilibrated samples, no sensitisation is observed. ^d O₂-free samples; in air-equilibrated samples the sensitisation luminescence is reduced to ca. 20%. ^e Not reported owing to too large uncertainties.

Ligand-to-Metal energy transfer. The energy transfer step takes place from the triplet energy level, E_T, of the ligand. The luminescence spectra (77 K) of water solutions of **Gd•3** and **Gd•4** allow determination of E_T, see Figure 4.2.1. In fact, the lowest-lying MC excited level (⁶P_{7/2}) of Gd³⁺ is at 32150 cm⁻¹, and the well-resolved luminescence spectra are to be ascribed to the phosphorescence of the chromophores. From the spectral profiles depicted in this Figure, E_T is evaluated 21320 and 21740 cm⁻¹, for **3** and **4**, respectively; τ_p^{77K} was 1.8 ms and 0.26 s, respectively. From these results, the energy gap, ΔE , between the higher-lying ligand E_T and the MC luminescent levels is estimated 3380 and 4040 cm⁻¹ for **Eu•3** and **Eu•4**, respectively, and 190 and 850 cm⁻¹ for **Tb•3** and **Tb•4**, respectively.^{88, 100} It should be noticed that in air-equilibrated samples, no emission was detected for **Tb•3**, due to the easily occurring Tb→L back energy transfer, consistent with $\Delta E = 190$ cm⁻¹, and concomitant quenching of the ligand-centred E_T level by oxygen.²²

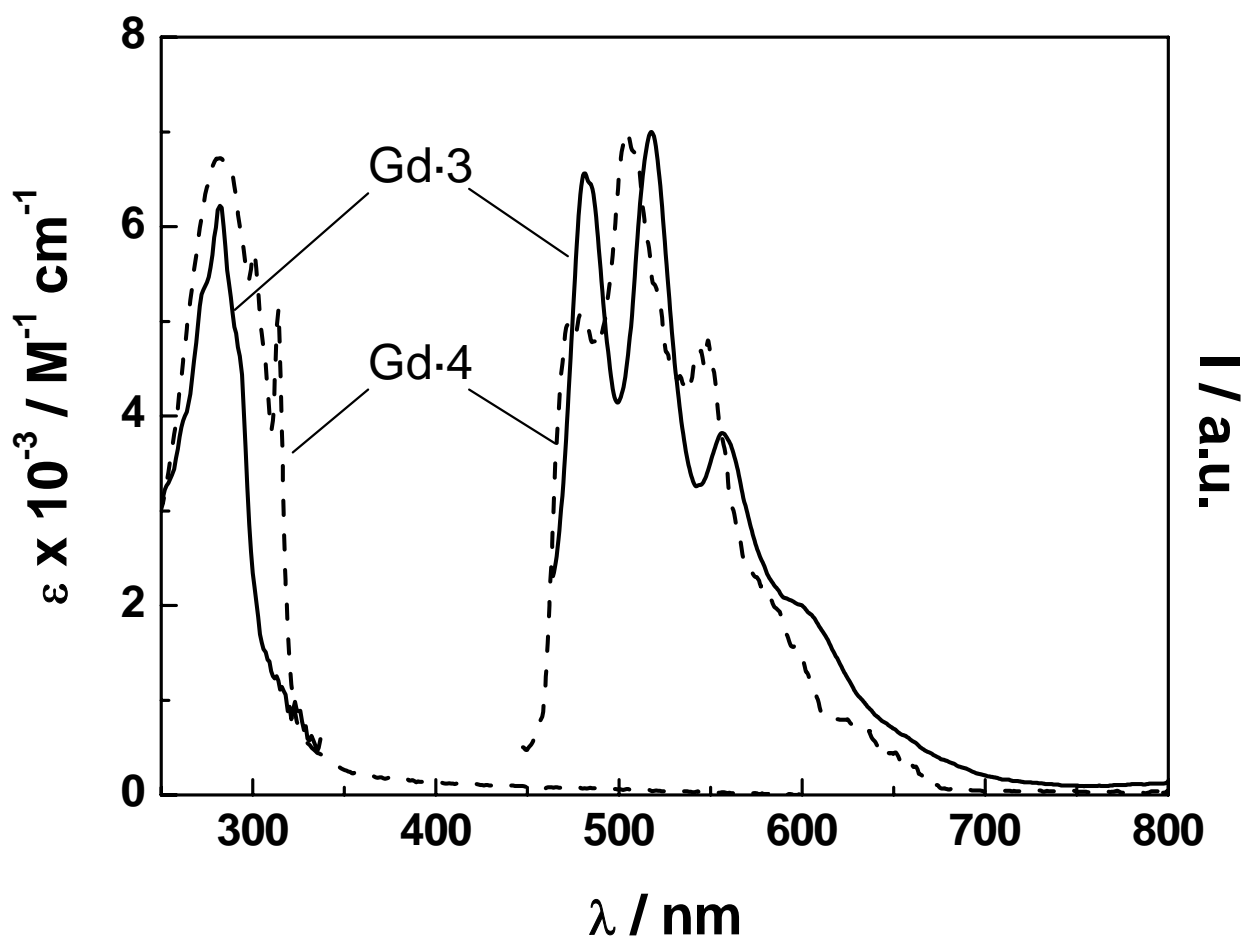


Fig. 4.2.1 Room temperature absorption spectra (left) and 77 K phosphorescence (right) for **Gd-3** (full line) and **Gd-4** (dashed line); water solvent, $\lambda_{exc} = 283$ nm.

Results for overall luminescence efficiencies, Φ_{EM} , and lifetimes, τ , obtained at room temperature water and deuterated water, from air-equilibrated and O_2 -free solutions, are listed in Table 4.2.1. The DO3A hosting unit fulfils seven coordination sites²² and for Eu^{3+} complexes, the number of water molecules of the coordination sphere, q , can be evaluated by using values for the lifetimes in water and deuterated water and according to *eq. 4.1.2*.⁹³ This provides $q \sim 2.1$ and 1.4 (uncertainty is ± 0.5) for the cases of naphthalene and quinoline antennae, respectively. On this basis, direct coordination of the chromophore is excluded for the case of **Eu-3**. Regarding **Eu-4**, the drawn indication seems less certain, because a fractional value for q might be related to the presence of coordination isomers differing in the hydration state. This is also consistent with results

from molecular modelling,¹⁰¹ for instance, for **Eu•3**, the metal-naphthalene closest separation distance is found to be in the range 4-6 Å.

For the case of the Tb³⁺ complexes, the use of the same equation for determining q, eq. 4.1.3,⁹³ yielded less reliable results because the detected metal-centred τ values are affected by the establishment of a thermal equilibrium between E_T and MC levels. Nevertheless, also based on the relaxometric results obtained with **Gd•3** and **Gd•4** (see above) we assume the same coordination properties for both the Tb³⁺ and Eu³⁺ examined complexes.

MC emission. In Table 4.2.1 are listed values for the k_r and Σk_{nr} rate constants, as obtained from the photophysical parameters and available literature sources.^{22, 100} Estimates of the pure radiative lifetime for Eu³⁺ complexes (τ_r = 1/k_r) were obtained according to an approach which compares the intensity of the ⁵D₀→⁷F₁ band (593 nm, insensitive to the coordination environment) to the overall shape of the emission spectrum, eq. 4.2.1.^{91, 102}

$$eq. 4.2.1 \quad k_r = A(0,1) \frac{I_{tot}}{I(0,1)}$$

In this equation, A(0,1) is the spontaneous emission probability of the ⁵D₀→⁷F₁ transition that is evaluated 32.4 s⁻¹ in water^{91, 103} and [I_{tot}/I(0,1)] is the ratio of the total integrated intensity of the Eu³⁺ emission spectrum to the portion of the profile for the ⁵D₀→⁷F₁ band.

To notice that MC non-radiative processes can include both intrinsic and back energy transfer contributions, $\sum k_{nr} = k_{nr}^{MC} + k_{nr}^{ben}$. The former are related to the presence of OH oscillators,^{88, 93, 100} and are therefore strongly depressed in D₂O for the cases of **Eu•3** and **Eu•4**, where competition from Ln→L back energy transfer is not effective, see Tables 4.2.1 and 4.2.2. On the contrary, for **Tb•3** and **Tb•4**, the energy gap ΔE between the ligand E_T level and the emissive MC level is very small (Table 4.2.2) and Tb→L back energy transfer is by far the major

contribution to the non-radiative deactivation. Values for the intrinsic MC luminescence quantum yield, $\Phi_{\text{lum}}^{\text{MC}} = k_r / (k_r + k_{\text{nr}}^{\text{MC}})$, are listed in Table 4.2.2.

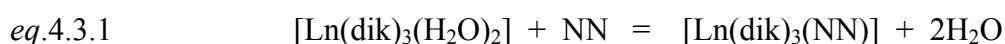
The L-to-Ln energy transfer efficiencies, Φ_{EnT} , for both water and deuterated water cases, were obtained from the experimentally determined values for Φ_{EM} and the evaluated values for Φ_{ISC} and $\Phi_{\text{Lum}}^{\text{MC}}$. A few relevant issues are noticed. (i) Owing to the partly unfilled coordination environment at the metal centres ($q = 2$ and 1.4), $\Phi_{\text{Lum}}^{\text{MC}}$ reaches the highest values in D_2O solvent, Table 4.2.1. (ii) For **Eu•3** and **Eu•4**, energy transfer efficiencies of ca. 3 and 8%, respectively, are observed. (iii) For **Tb•3** and **Tb•4**, the luminescence is very sensitive to the presence of oxygen, which is consistent with the establishment of an equilibrium between ligand-centred and metal-centred excited levels and the oxygen effect;²² for **Tb•3**, in air-equilibrated samples no luminescence is detected.

4.3 *d-f* complexes

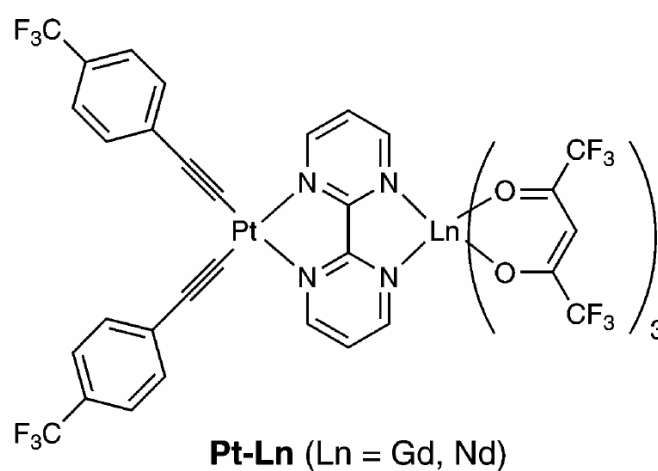
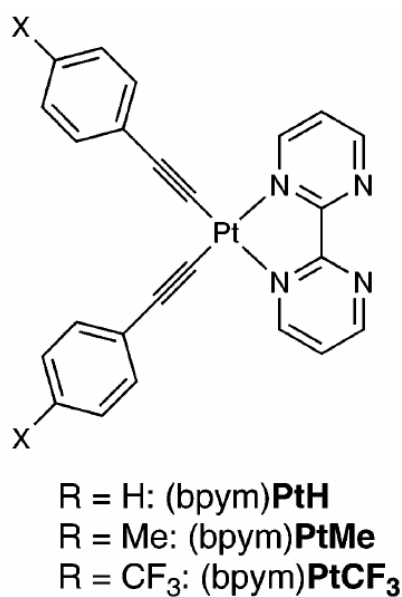
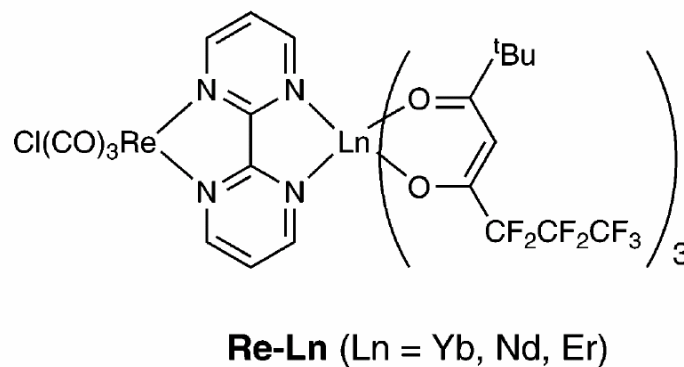
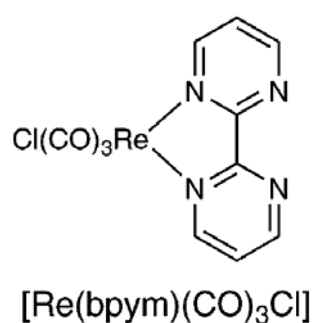
A different approach for the sensitization of the Ln(III) emitting levels is represented by the use of *d*-block metal fragments. The first examples of sensitised near-IR emission from lanthanide complexes using a covalently-attached *d*-block complex unit as sensitiser were described only a few years ago, from the groups of van Veggel and Parker, using $[\text{Ru}(\text{bipy})_3]^{2+}$ or ferrocenyl units¹⁰⁴ and Pd-porphyrin¹⁰⁵ as energy-donors, respectively. More recently, Cr(III) chromophores have been used as energy-donors to luminescent lanthanides in heterodinuclear helicate complexes,¹⁰⁶ and in oxalate-bridged dinuclear complexes.¹⁰⁷ Other heterodinuclear assemblies incorporating a metal polypyridyl unit connected to a lanthanide, which show $d \rightarrow f$ energy-transfer and subsequent NIR luminescence from the lanthanide, have been described by the groups of Faulkner and Coe,^{108, 109} Yanagida,¹¹⁰ Pikramenou,¹¹¹ and Beer.¹¹²

On our side, we investigated samples based on the two series of *d-f* complexes shown in Scheme 4.3.1: one based on a $[\text{Re}(\text{CO})_3\text{Cl}(\text{dimine})]$ unit and the other based on a Pt-diimine-bis(acetylide) unit both acting as energy donors.

In the two series, 2,2'-bipyrimidine is used as the bridging ligand connecting the two metal sites in order to keep the metal-metal separation short and facilitate energy-transfer. Their photophysical properties, in particular the occurrence of d→f energy-transfer, leading to quenching of the luminescence from the d-block unit and sensitised NIR luminescence from the lanthanide unit. Binding of a [Ln(dik)₃(H₂O)₂] units [dik = fod (*t*BuC(O)CH₂C(O)CF₂CF₂CF₃), or hfa (CF₃C(O)CH₂C(O)CF₃) or tta (2-thenoyltrifluoroacetone)] to diimines (NN), according to *eq. 4.3.1*, to give the 8-coordinate diimine adduct with liberation of two molecules of water is known to be a reversible process, with equilibrium constants of up to 10⁷ M⁻¹ for NN = 2,2'-bipyridine or 1,10-phenanthroline in hydrocarbon solvents.^{113, 114}



With less basic NN ligands the equilibrium constant is correspondingly reduced. For example, we recently observed binding constants of the order of 10⁴ M⁻¹ in CH₂Cl₂ for association of [Ln(dik)₃(H₂O)₂] to the vacant NN site of complexes such as [Cl₂Pt(dppz)] [dppz = 2,3-di(2-pyridyl)pyrazine] in which one of the vacant N donors is a pyrazine rather than a pyridine ring.⁶⁵ The result is that, at the concentrations typically used for luminescence and UV/Vis spectroscopic studies, partial dissociation of the dinuclear d-f complexes occurs, which complicates the luminescence analysis in solution. Given the relatively low basicity of pyrimidine compared to pyridine (*pK_a* values in water of 1.3 and 5.2 respectively for protonation), it was felt that this was likely to be an issue with these complexes, and accordingly UV/Vis and luminescence titrations on representative systems were carried out.



Scheme 4.3.1 Chemical structures of studied complexes

Addition of portions of [Ln(hfac)₃(H₂O)₂] (Ln = Gd, Yb) to a solution of (bpym)**PtCF₃** in dry CH₂Cl₂ resulted in a deepening of the orange colour of the Pt chromophore, which is associated with the MLCT transition being reduced in energy and shifted more into the visible region, from 415 nm to 425 nm [Fig. 4.3.1(a)]. A graph of absorbance at a selected wavelength vs. amount of [Ln(hfac)₃(H₂O)₂] added gave a smooth curve which fitted well to a 1:1 binding isotherm [Fig. 4.3.1(c)], from which the association constant for binding of the lanthanide fragment to the diimine site (equilibrium constant for *eq.* 4.3.1) could be determined; the values obtained were 3.5 (±0.3) × 10⁵ M⁻¹ for **Pt-Yb** and 1.2 (±0.2) × 10⁵ M⁻¹ for **Pt-Gd**. These are rather low compared to the values

obtained for other lanthanide-diimine adducts with ligands such as bipyridine and phenanthroline,^{113, 114} as a consequence of the poor basicity of bipyrimidine. The slightly higher K_a value for **Pt-Yb** compared to **Pt-Gd** presumably reflects the smaller ionic radius and higher charge density of Yb^{3+} . It is not appropriate to over-analyse these binding constants as we found that they are very sensitive to traces of moisture in the solvent; use of ordinary undried CH_2Cl_2 from a fresh bottle afforded binding constants two orders of magnitude lower; the important point is that with K_a values of *ca.* 10^5 M^{-1} , significant dissociation is to be expected at the concentrations typically used for luminescence measurements in solution ($\approx 10^{-5} \text{ M}$).

Luminescence spectra were also recorded during the titrations. With $\text{Ln} = \text{Yb}$, binding of the lanthanide fragment results in complete quenching of the luminescence of free (bpym)**PtCF₃** [Fig. 4.3.1(b)]. In contrast, when $\text{Ln} = \text{Gd}$, there is some quenching of the (bpym)**PtCF₃** luminescence but this is not complete and about 15% of the original luminescence intensity remains after addition of excess $[\text{Gd}(\text{hfac})_3(\text{H}_2\text{O})_2]$. This implies two things. Firstly, binding of a lanthanide fragment to the secondary site of (bpym)**PtCF₃** provides an additional pathway for quenching of the Pt-based luminescence, either by providing additional vibrational pathways for deactivation of the excited state, or by the heavy-atom effect. These effects alone do not result in complete quenching, as shown by the **Pt-Gd** system where there is residual luminescence; it is important to note that Gd(III) cannot act as an energy-acceptor because its first electronically excited state is far too high in energy. In contrast, in the **Pt-Yb** system, quenching is complete because of the ability of Yb(III) to act as an energy-acceptor through its low-lying $^2\text{F}_{5/2}$ level. The presence of incomplete quenching of the Pt-based luminescence for $\text{Ln} = \text{Gd}$ but complete quenching for $\text{Ln} = \text{Yb}$ indicates that Pt \rightarrow Yb photoinduced energy-transfer is taking place in the latter case and we should see sensitized luminescence from Yb(III) following excitation of the (bpym)**PtCF₃** centre.

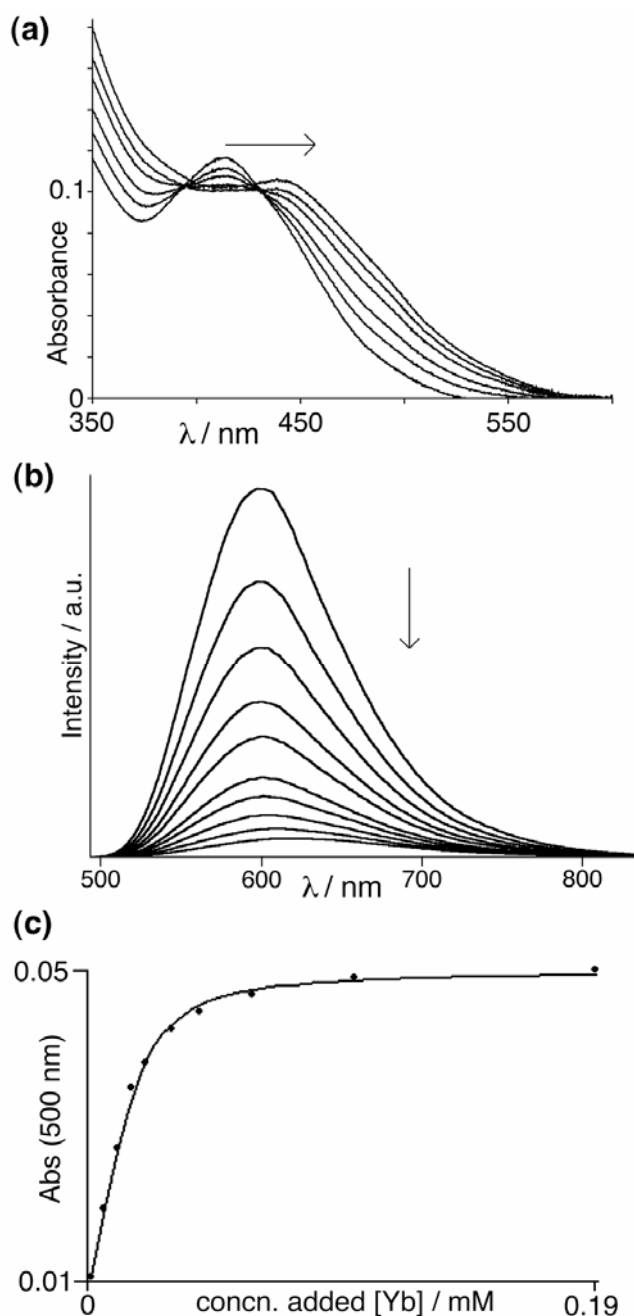


Fig. 4.3.1 Titration of $(bpym)PtCF_3$ with $Yb(hfac)_3(H_2O)_2$ in a CH_2Cl_2 solution: (a) red shift in the MLCT absorption maximum of $(bpym)PtCF_3$; (b) quenching of Pt-based luminescence; (c) absorbance values at 500 nm during titration (dots) fitted to a 1:1 binding isotherm (line) to give $K_a = 3.5 \times 10^5 M^{-1}$.

A similar titration experiments was performed on the $[Re(bpym)(CO)_3Cl]/ Yb(fod)_3$ system, with similar results. Binding of the $Yb(fod)_3$ fragment at the vacant diimine site results in a red-shift of the MLCT absorption in the UV/Vis spectrum, from which an association constant for lanthanide binding in **Re-Yb** of $1.9 (\pm 0.2) \times 10^5 M^{-1} cm^{-1}$ was determined, comparable to the values obtained for the **Pt-Ln** complexes. Photophysical properties of dinuclear **Re-Ln** ($Ln = Nd, Yb$ and Er) and **Pt-Nd** complexes were investigated in CH_2Cl_2 solution. For the sake of comparison, mononuclear compounds $[Re(bpym)(CO)_3Cl]$, $(bpym)PtCF_3$, $[Nd(tta)_3(H_2O)_2]$, $[Yb(fod)_3(H_2O)_2]$, and $[Er(fod)_3(H_2O)_2]$ have been also studied, the absorption spectra are depicted in Figure 4.3.2. For the Nd(III) complexes the light absorbing antenna unit is the diketonate ligand tta or hfac (to be used for **Re-Nd** and **Pt-Nd**, respectively), for Yb(III) and Er(III) analogues this role is played by fod. The

presence of different ligands is reflected in the different UV absorption profiles.

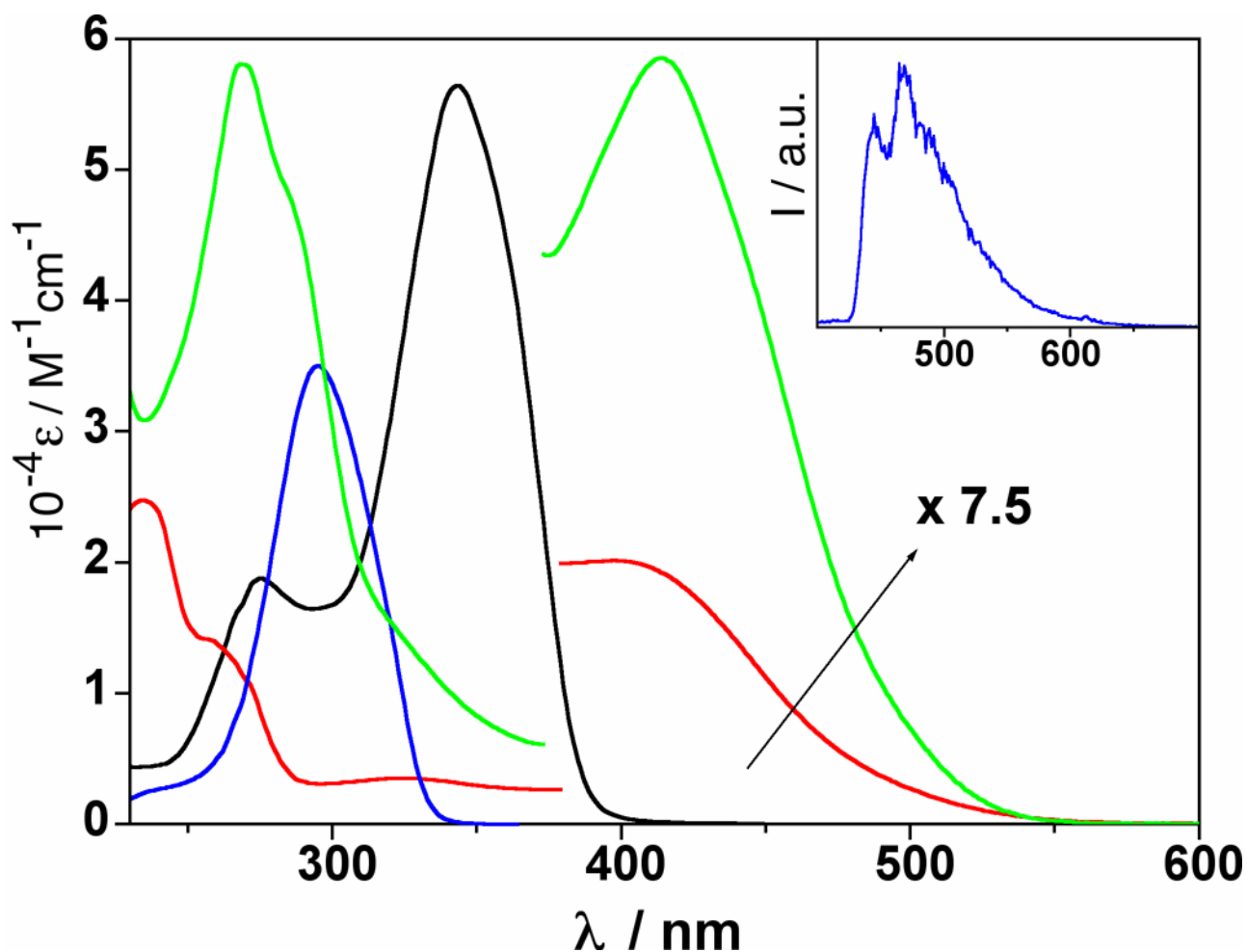
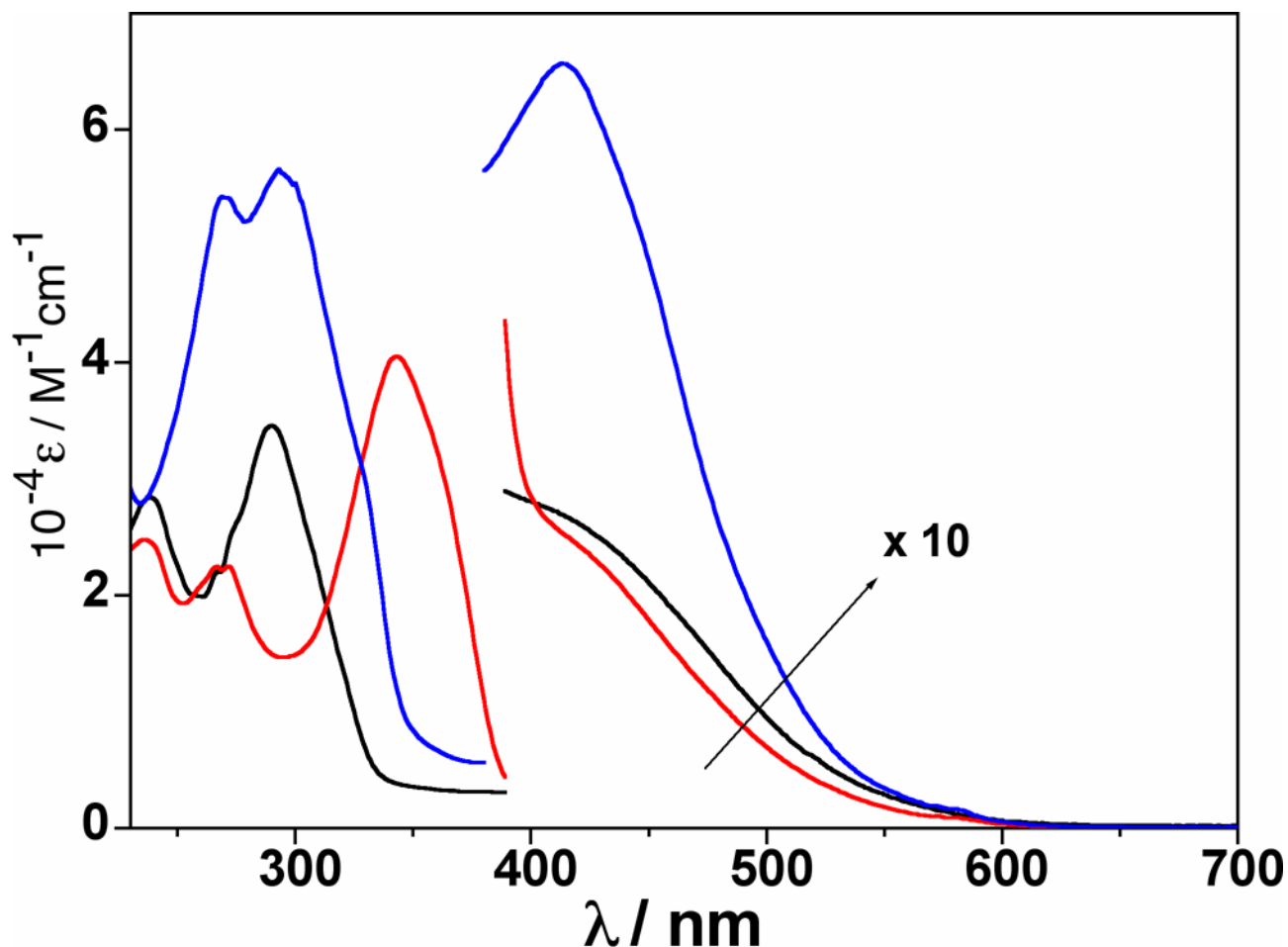


Fig. 4.3.2 Electronic absorption spectra of $[\text{Re}(\text{bpym})(\text{CO})_3\text{Cl}]$ (red), $(\text{bpym})\text{PtCF}_3$ (green), $[\text{Nd}(\text{tta})_3(\text{H}_2\text{O})_2]$ (black), and $[\text{Yb/Er}(\text{fod})_3(\text{H}_2\text{O})_2]$ (blue). Above 400 nm, the spectra are multiplied by a factor of 7.5. Inset: phosphorescence spectra of $[\text{Gd}(\text{fod})_3(\text{H}_2\text{O})_2]$ at 77 K in CH_2Cl_2 , $\lambda_{\text{exc}} = 294$ nm.

The lowest electronic excited states of $[\text{Re}(\text{bpym})(\text{CO})_3\text{Cl}]$ ^{115, 116} and $(\text{bpym})\text{PtCF}_3$ ¹¹⁷⁻¹²⁰ are of ³MLCT nature, their energy being about 2.19 and 2.39 eV, respectively, as estimated from 77 K emission spectra. For the mononuclear lanthanide complexes, UV excitation of the ligand-centred band, results in typical luminescence of the corresponding Ln(III) ion in the NIR spectral region, with energy levels below 1.4 eV. This is a consequence of an energy transfer process from the diketonate ligand to the corresponding metal ion. The sensitization process in lanthanide complexes occurs from the ligand triplet levels¹²¹ which, for fod/hfa and tta, are positioned at 2.80 and 2.57 eV, respectively, according to the phosphorescence spectra of the reference Gd(III) complexes.¹²¹

From this energy level description, the dinuclear complexes **Re-Ln** or **Pt-Ln** possess an energy gradient allowing energy transfer from the *d*-block to the *f*-block moiety. The absorption spectra of **Re-Ln** and **Pt-Nd** in CH₂Cl₂ solution are depicted in Figure 4.3.3.



*Fig. 4.3.3 Electronic absorption spectra of **Re-Yb/Er** (black), **Re-Nd** (red), and **Pt-Nd** (blue) in a CH₂Cl₂ solution. Above 400 nm, the spectra are multiplied by a factor of 10. The dinuclear complexes undergo partial dissociation; therefore, the spectra reflect a mixture of dissociated and undissociated samples (see text).*

The UV spectral range is characterized by ligand centred transitions. The contribution of the bpym chelating ligand is of minor importance and only observable in the peak/shoulders around 235 nm (see spectrum of [Re(bpym)(CO)₃Cl] in Figure 4.3.2). The remarkable differences observed in the various cases are related to the presence of the three different diketonate ligands (fod, tta, or hfa) which exhibit peculiar UV absorption profiles (Figure 4.3.2). For binuclear complexes, by inspecting the absorption spectra of mononuclear compounds in Figure 4.3.3, one can assign the

absorption features above 400 nm to MLCT transitions of the Re- or Pt-complexed moiety. The intensity of the Pt(II)→bpym MLCT absorption band is substantially stronger than that of the Re(I)→bpym absorption. Of course, in these conditions there will be some dissociation of the dinuclear complex, but the main features of the complexes [*viz.* the diketonate-centred transitions at 300 – 400 nm; the MLCT transition of the d-block fragment at $\lambda > 400$ nm] are only slightly affected by this and, apart from the shift in the MLCT absorption of the d-block unit in the dinuclear complexes, the spectra of the dinuclear complexes are approximately the sum of the spectra of the two chromophores.

Upon excitation of the MLCT band of the Re moiety at 460 nm, all the dinuclear **Re-Ln** complexes exhibit the NIR emission features of the lanthanide ion (Fig. 4.3.4). Since no direct excitation of the lanthanide moiety occurs at this wavelength, the observed NIR emission signals can only arise by sensitization of the lanthanide ions from the Re-complexed moiety, via energy transfer.^{104, 108-112, 122} As shown by Fig. 4.3.4, three emission bands were observed for Nd(III) one for Yb(III), and one for Er(III). Following the measurements of association constants described above, it is to be expected that partial dissociation of the **Re-Ln** complexes into their mononuclear complexes will occur. Indeed, weak ³MLCT luminescence from [Re(bpym)(CO)₃Cl] was observed, with a quantum yield corresponding to about 20% dissociation of the dinuclear **Re-Ln** complexes. The lifetime of this excited state (2.1 ns) is the same as that of free [Re(bpym)(CO)₃Cl]. No shorter-lived ³MLCT luminescence component was detected, indicating that in the intact **Re-Ln** complexes the Re-based luminescence is completely quenched (or is reduced to sub-nanosecond lifetime), because of fast Re→Ln energy-transfer (Ln = Yb, Nd, Er). The quenching is therefore stronger than observed in some other dinuclear lanthanide complexes with [Ru(bpy)_n]²⁺-type moieties, where residual ³MLCT luminescence from the d-block unit was also found.^{104, 108-110, 112, 122} In the present case the close proximity of the two metal centres allows a very fast energy transfer, which can compete successfully with the fast intrinsic ³MLCT deactivation. Fortunately, the weakness of the residual ³MLCT luminescence from free [Re(bpym)(CO)₃Cl] means that its

low-energy tail does not significantly interfere with the lanthanide luminescence measurements of the **Re-Ln** series in the NIR region (Fig. 4.3.4).

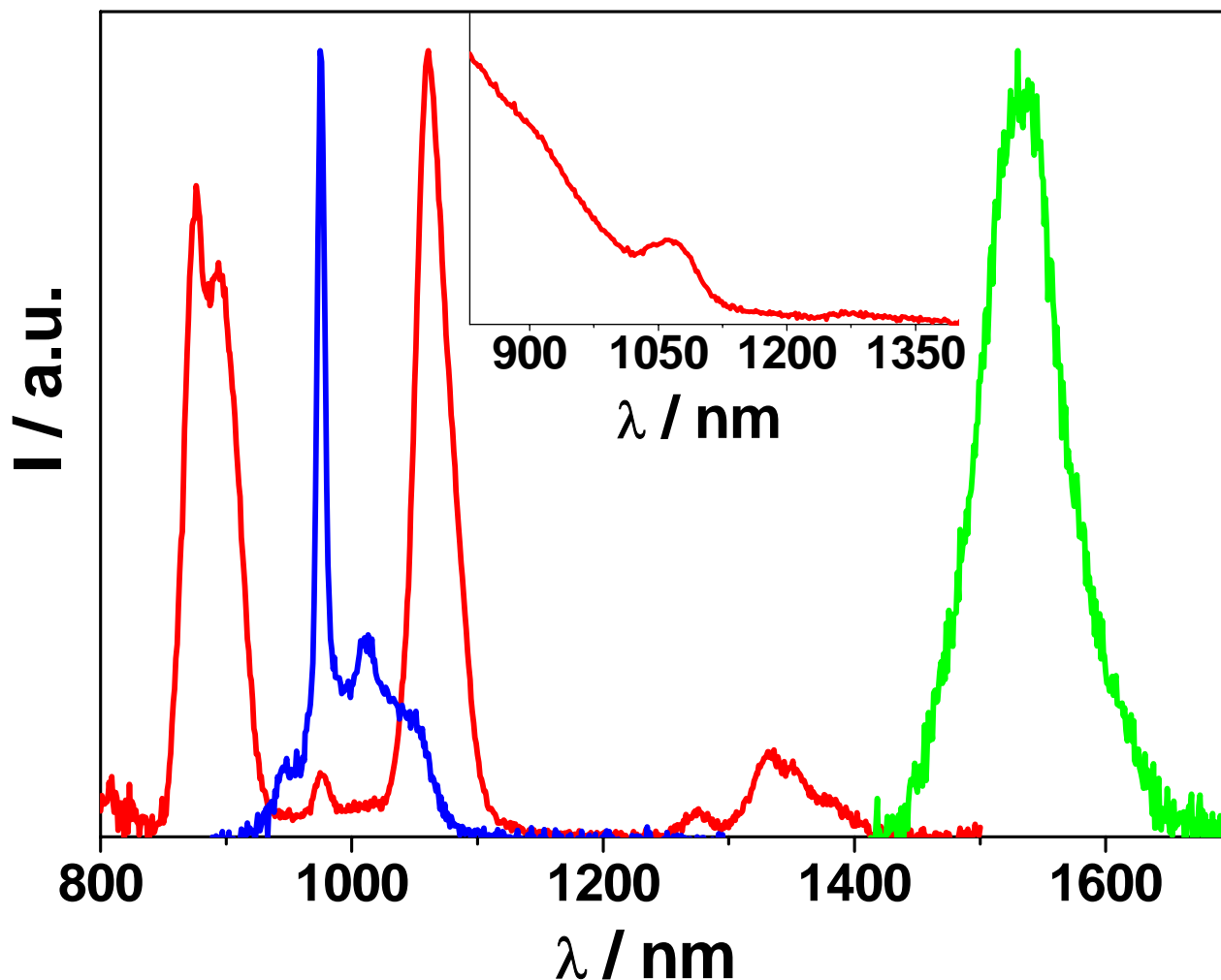


Fig. 4.3.4 Corrected and normalized emission spectra from **Re-Nd** (red), **Re-Yb** (blue), **Re-Er** (green), and **Pt-Nd** (red, inset) in CH_2Cl_2 solutions, $\lambda_{\text{exc}} = 460 \text{ nm}$, absorbance at excitation wavelength = 0.2.

In order to test whether any change of the emission yield of the Ln moiety occurs in the binuclear complexes, we compared the emission yields of the **Re-Ln** compounds with that of the corresponding mononuclear lanthanide complex, upon excitation in the UV region. A small increase of the NIR emission intensity in **Re-Nd** and **Re-Yb** was detected compared to the mononuclear species $[\text{Nd}(\text{tta})_3(\text{H}_2\text{O})_2]$ and $[\text{Yb}(\text{fod})_3(\text{H}_2\text{O})_2]$ (in the case of **Re-Er** the emission is so weak that quantitative considerations are prevented). This is probably related to the replacement of solvent

molecules by *N,N'*-bipyrimidine in the Ln(III) coordination sphere which could depress non-radiative deactivation pathways through vibrational quenching, as we have seen before when comparing [Ln(dik)₃(H₂O)₂] and [Ln(dik)₃(diimine)] luminophores.¹²³

Excitation of **Pt-Nd** into the MLCT Pt-based band (460 nm) in CH₂Cl₂, also gives rise to Nd(III) emission in the NIR region, confirming that Pt→Nd energy transfer occurs. However, a relatively intense MLCT emission band at $\lambda_{\text{max}} = 575$ nm is observed, whose low-energy tail partially overlaps the sharp emission features of the Nd(III) centre (inset of Figure 4.3.4). As mentioned above, residual ³MLCT luminescence has been observed in many cases^{104, 108-110, 112, 122} in dinuclear d-f complexes with Ru(II)-polypyridine type sensitizing units and, on the basis of lifetime measurements, this has been related to a slow Ru→Ln energy transfer process which undergoes competition from intrinsic deactivation of the ³MLCT level of the Ru-complexed moiety.¹⁰⁴ However, upon excitation at 460 nm, here we find identical ³MLCT lifetimes for (bpym)**PtCF₃** and **Pt-Nd** (107 ns), indicating that for the latter we are seeing luminescence from free (bpym)**PtCF₃** as a result of partial dissociation of the complex into its mononuclear components. For intact **Pt-Nd** the Pt-based luminescence should be completely quenched, as shown by the titration measurements and from the solid-state luminescence data. The inherently strong luminescence of free (bpym)**PtCF₃** accounts for the sensitized NIR luminescence from Nd(III) being partially obscured by the tail of the ³MLCT luminescence.

In order to avoid the dissociation process and get “clean” luminescence data in the NIR region, we measured also emission spectra ($\lambda_{\text{exc}} = 460$ nm) and lifetimes of the dinuclear complexes in the solid state as powders. In the solid state, no residual MLCT emission is observed for any complex, either of Re- or Pt-type, confirming that in the intact dinuclear complexes the energy transfer process from the *d*-block to the *f*-block metal centers is very efficient. On the basis of eq. 4.3.2, taking the measured values of solid samples (τ_{obs}) and the radiative (“natural”) lifetimes of Nd(III), Yb(III), and Er(III) ions (τ_{R}) as reported in the literature,⁸⁷ we obtain emission quantum

yield values of the lanthanide ion for dinuclear compounds.¹²⁴ Such values are comparable to those of previously reported for NIR emitting Ln(III) complexes in the solid state.¹²³

eq.4.3.2

$$\phi_{em} = \tau_{obs} / \tau^{\circ}$$

4.4 Ln(III) complexes doped Sol-gel glasses

Most of the mentioned application fields (Chapter 3) require the use of solid state samples. To this purpose, we extended the PL study of the Ln(III) complexes in several matrices such as polymer,¹²⁵⁻¹²⁷ sol-gel glasses¹²⁸⁻¹³² and carbon

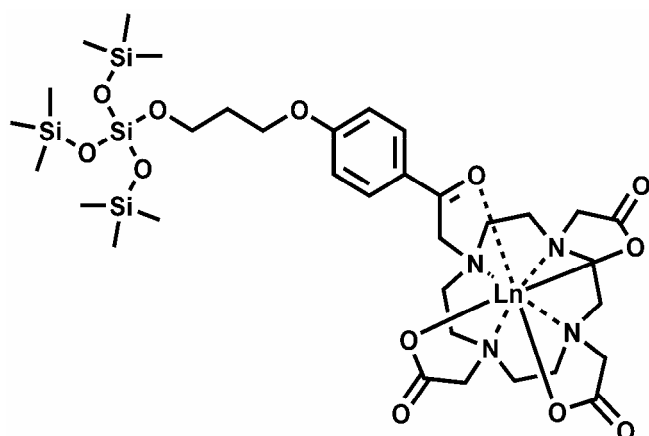


Chart 4.4.1 Chemical structure of generic **Ln•5** covalently linked to the silica (or polymer) matrix.

nanotubes.¹³³⁻¹³⁶ Within a solid matrix, the wished statistical distribution of the chromophores is not always observed; a variety of different aggregates may instead form.¹³⁷

Clearly, formation of aggregates can be a source of problems, because mutual interaction between spatially close luminescent centres may lead to self-quenching, a parasitic event pulling down luminescence efficiency. To this,

an highly stable Eu(III) centre has been anchored to a silica glass upon acidic hydrolysis by using tetraethylorthosilicate (TEOS) as a silica source. **Eu•5** has been also covalently anchored to a polymer matrix through an amine terminal group and showed similar PL properties ($\phi_{em} = 0.11$, $\tau = 1.20$ ms) to those of Sol-gel glasses.

The complex employed was obtained from bipartite ligand **5**, which features a DO3A macrocycle as a hosting unit for the Eu(III) centre, connected to a methoxy-acetophenone antenna unit. Within **Eu•5** and **Eu•6** (**6** is a ligand featuring the same hosting and antenna functionalities of

5, wherein the –OH residue is replaced by an unreactive group, a benzoylmethyl residue), all the coordination positions of the lanthanide centre are fulfilled but one (only one coordination site is available to solvent molecules, which is indicated by $q = 1$),⁹¹ and these complexes are highly stable, the 1:1 ligand:Ln association constant being $K_A > 10^{20} \text{ M}^{-1}$.¹³⁸

Eu•5 can be covalently linked to the forming silica glass through the –OH moieties, yielding highly homogeneous layers with luminophores tightly anchored to the host medium.

Physical and Optical Properties of films. The films were prepared as described elsewhere.¹³⁹ The europium distribution throughout their thickness was investigated by Secondary Ion Mass Spectrometry (SIMS) depth profiling on selected silica layers. Estimates of film thickness yielded values around 40 nm irrespective of the thermal treatment, that at our employed conditions correspond to *ca.* 4.8 nm^3 of film volume/luminophore.

While ligand **5** is non emissive upon irradiation at 305 nm, both **Eu•5** in water and the film incorporating this complex showed a strong red emission. Actually, within the chromophore/luminophore associate, the MAP (4'-methoxyacetophenone) unit plays as an *antenna* for sensitisation of the lanthanide-based luminescence. This occurs according to the following sequence of events:¹⁴⁰ (i) absorption of UV light at 305 nm ($\epsilon_{308} = 19300$ and $24300 \text{ M}^{-1} \text{ cm}^{-1}$ for **Eu•5** and **Eu•6**, respectively), (ii) highly efficient intersystem crossing (ISC) from the populated singlet level to the triplet level, lying at 25200 cm^{-1} ($\phi_{\text{ISC}} = 1$),^{92, 141} and (iii) transfer of excitation energy to the lanthanide cation. The last step, a MAP→Eu(III) energy transfer, occurs with an efficiency $\phi_{\text{en}} \sim 1$,⁹¹ as expected because the acetophenone triplet exhibits a slow decay ($k_T \sim 5 \times 10^6 \text{ s}^{-1}$)^{92, 142} and the energy gap between the donor and the acceptor levels is *ca.* 7300 cm^{-1} , i.e. so high to hamper any back-transfer process.^{12, 143} The absorption results indicate that inclusion of the lanthanide centre causes a shift of the absorption peak of the MAP unit from 282 (for the lanthanide-free ligand **5**) to 308 nm for both the **Eu•5** and the **Eu•6** complexes in water solution and to 310 nm for the **Eu•5** unit bound to the silica-glass. A similar perturbation effect of the electronic properties of the MAP ligand by the cationic Eu(III) centre was already noted for very similar

complexes that were found to exhibit practically identical luminescence properties in water solution.⁹¹ The lack of any emission for the lanthanide-free chromophore **5** is explained by the fact that the lowest-lying singlet level of **MAP** is of acetophenone origin and is depopulated with unit efficiency by the ISC step, leading to a non-emissive triplet.^{91, 92, 141}

The luminescence spectra observed in solution and in film are quite similar each other and appear finely resolved. The most intense peak occurs at 612 nm in solution (616 nm in the film), and corresponds to the $^5D_0 \rightarrow ^7F_2$ transition. This is the so called hypersensitive transition,^{91, 144, 145} and the ratio between its intensity and that for the lower energy transition ($^5D_0 \rightarrow ^7F_1$) is *ca.* 5 and 6 for the solution and the film, respectively. This suggests that the Eu-based luminophore is embedded in a similar environment for the two cases (solution and film), which in turn points to a high degree of homogeneity for the physical state of the film as pointed out by SIMS analysis.¹³⁹

Along this line, by employing the same coordinating ligand (**5**), also a green emitting Tb(III) complex has been synthesized and anchored in to a single SiO₂ transparent layer. Because of the high interest in gaining control over colour tunability,^{139, 146} we investigated a two-colour approach based on the use of different and controlled combinations of the Eu(III)- and Tb(III)-based complexes covalently linked to SiO₂ substrates. This fabrication approach is based on a statistical distribution of the different emitting centres within the same substrate and not on the tedious and time consuming multistrata arrangement technique largely used, for instance, in fabrication of white light emitting OLED devices.¹⁴⁷⁻¹⁵¹

The solutions containing the single lanthanide complex, were prepared employing a Eu/Si = Tb/Si = 1/400 molar ratio. The same procedure afforded the mixed systems reported here, with Tb/Eu molar ratio of 0.4, 1.0 and 2.2, yielding **(Eu•5)₂-(Tb•5)₁**, **(Eu•5)₁-(Tb•5)₁** and **(Eu•5)₁-(Tb•5)₂** films, respectively. Before film deposition, the transparent and clear solutions were aged at room temperature under stirring for 24h. The obtained layers were subsequently used in the luminescence experiments both as-prepared, and dried at 100 and 200 °C for 5 h. Since the thermal

treatment does not influence the photophysical properties of the different specimens, the following discussion will be focused on the samples annealed at 200 °C.

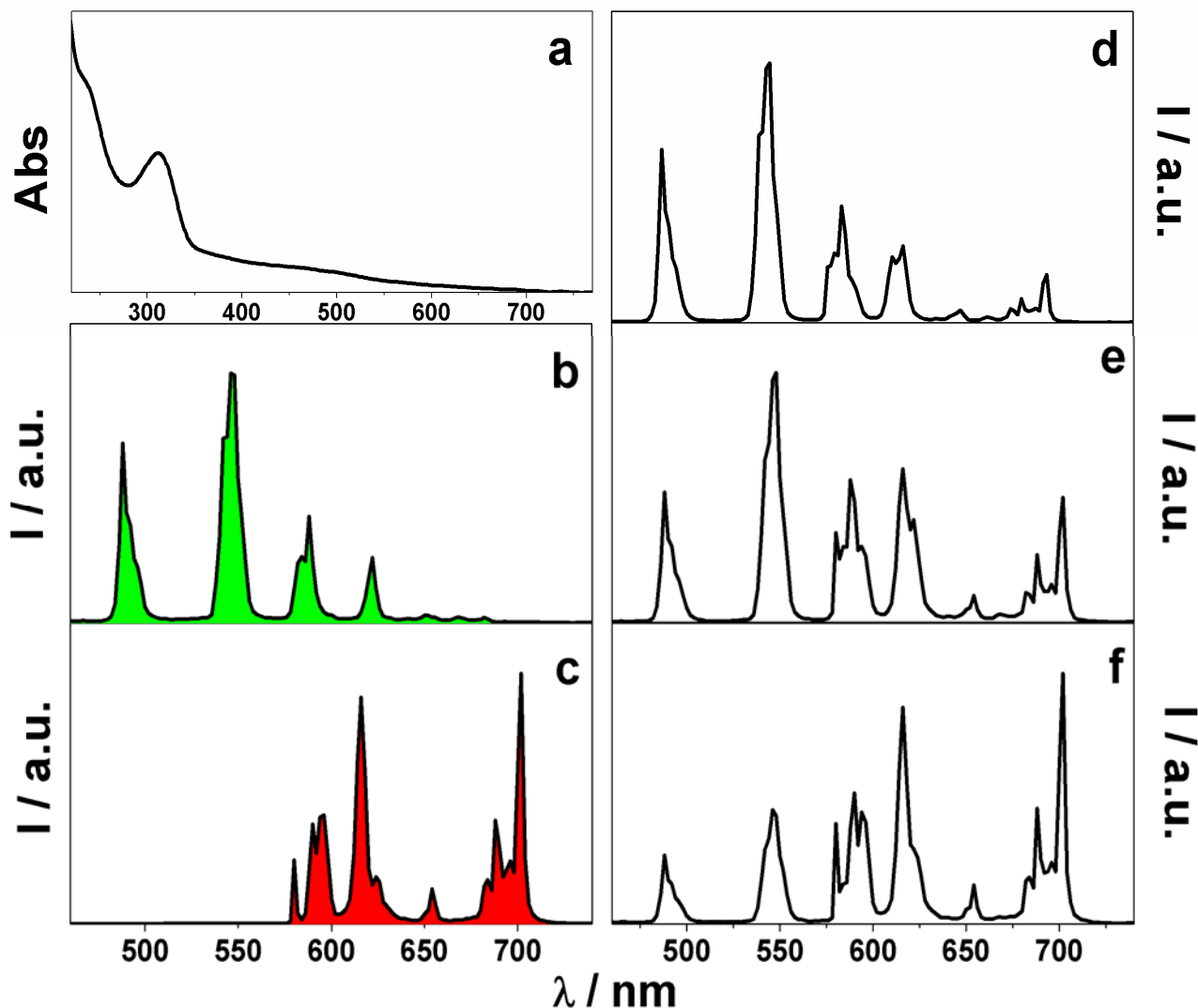


Fig. 4.4.1 Absorption a) $(\text{Eu}\cdot\mathbf{5})_1-(\text{Tb}\cdot\mathbf{5})_1$ and corrected emission spectra ($\lambda_{\text{exc}} = 300 \text{ nm}$) of b) Tb, c) Eu, d) $(\text{Eu}\cdot\mathbf{5})_1-(\text{Tb}\cdot\mathbf{5})_2$, e) $(\text{Eu}\cdot\mathbf{5})_1-(\text{Tb}\cdot\mathbf{5})_1$ and f) $(\text{Eu}\cdot\mathbf{5})_2-(\text{Tb}\cdot\mathbf{5})_1$ in SiO_2 matrix.

The absorption and emission (PL) spectra of the $(\text{Eu}\cdot\mathbf{5})_2-(\text{Tb}\cdot\mathbf{5})_1$, $(\text{Eu}\cdot\mathbf{5})_1-(\text{Tb}\cdot\mathbf{5})_1$ and $(\text{Eu}\cdot\mathbf{5})_1-(\text{Tb}\cdot\mathbf{5})_2$ films, as obtained at room temperature, are reported in Fig. 4.4.1. The absorption profile was identical for all samples and the peak, around 300 nm, is ascribed to the substituted acetophenone unit, as the sole light collector.¹⁵² Regarding the emission properties,^{41, 153} the change in relative intensities between Eu(III) and Tb(III) bands (Figure 4.4.1), appears related to the molar ratio of the metal complexes and, in turn, to the colour output as illustrated by Figure 4.4.2. The PL

efficiencies (ϕ_{se}) measured by an integrating sphere apparatus^{7, 154} upon excitation with an He-Cd laser source ($\lambda_{\text{exc}} = 325$ nm), revealed comparable values for the **Tb•5** and **Eu•5** films ($\phi_{\text{se}}^{\text{Tb}} = 0.09$ and $\phi_{\text{se}}^{\text{Eu}} = 0.10$, Table 4.4.1). This is consistent with the luminescent output of the mixed **(Eu•5)₂-(Tb•5)₁**, **(Eu•5)₁-(Tb•5)₁** and **(Eu•5)₁-(Tb•5)₂** layers, see inset of Fig. 4.4.2. Furthermore, the luminescence decays from the Eu(III) ($\tau = 0.7$ ms, as detected at $\lambda = 614$ nm) and Tb(III) ($\tau = 1.1$ ms at $\lambda = 544$ nm) centres are nearly the same, for all glassy samples, indicating that chromophore interactions do not take place significantly, Table 4.4.1. The soluble Eu(III)- and Tb(III)-based hydroxypropenyloxyacetophenone-DO3A complexes have also been studied in water solution and results are collected in Table 4.4.1. In the case of Eu(III) no remarkable differences between PL properties in solid and liquid phase ($\phi_{\text{se}} = 0.08$) were registered. In contrast, the Tb(III) complex showed notably higher PL quantum yield in solution than in film ($\phi_{\text{se}} = 0.31$ and 0.09 , respectively), a behaviour we cannot explain at the moment.

Table 4.4.1. Luminescence data in H_2O and SiO_2 matrix at room temperature.

	H_2O^a		SiO_2 matrix ^b	
	ϕ_{se}	τ / ms	ϕ_{se}	τ / ms
Eu•5	0.08	0.6	0.10	0.7
(Eu•5)₂-(Tb•5)₁	-	-	0.10	0.6^c 1.1^d
(Eu•5)₁-(Tb•5)₁	0.19	0.7^c 1.7^d	0.09	0.6^c 1.0^d
(Eu•5)₁-(Tb•5)₂	-	-	0.09	0.7^c 1.0^d
Tb•5	0.31	1.6	0.09	1.1

^a In all cases $[\text{Eu}] = [\text{Tb}] = 10^{-5}$ M. ^b See text for molar ratio details. ^c Eu(III)-centred emission. ^d Tb(III)-centred emission.

Predictably, the equimolar solution of both lanthanide complexes, $(\text{Eu}\cdot\mathbf{5})_1-(\text{Tb}\cdot\mathbf{5})_1$ showed

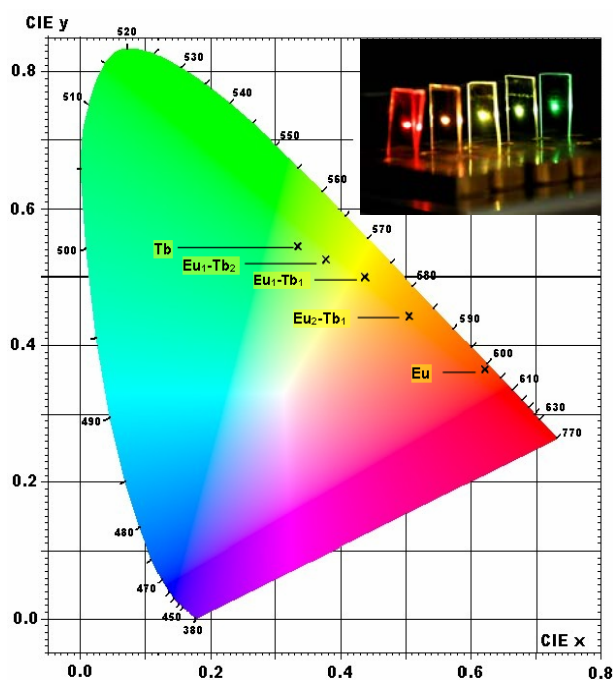


Fig.4.4.2 Main window: Commission Internationale de l'Eclairage (CIE) coordinates, of **Tb** (0.338, 0.544), $(\text{Eu}\cdot\mathbf{5})_1-(\text{Tb}\cdot\mathbf{5})_2$ (0.382, 0.525), $(\text{Eu}\cdot\mathbf{5})_1-(\text{Tb}\cdot\mathbf{5})_1$ (0.442, 0.498) $(\text{Eu}\cdot\mathbf{5})_2-(\text{Tb}\cdot\mathbf{5})_1$ (0.510, 0.441) and **Eu·5** (0.628, 0.363). Inset: emission behaviour (from left to right) of **Eu·5**, $(\text{Eu}\cdot\mathbf{5})_2-(\text{Tb}\cdot\mathbf{5})_1$, $(\text{Eu}\cdot\mathbf{5})_1-(\text{Tb}\cdot\mathbf{5})_1$, $(\text{Eu}\cdot\mathbf{5})_1-(\text{Tb}\cdot\mathbf{5})_2$ and **Tb·5** irradiated at 325 nm by a He-Cd continuum laser source.

an intermediate value of PL quantum yield, $\Phi_{se} = 0.19$. The obtained spectroscopic data are consistent with a homogeneous dispersion of the chromophores within the matrix, which likely results from the identical topology of the two Eu(III) and Tb(III)-based complexes, whose geometry is determined almost entirely by the ligand characteristics.¹⁵⁰ Consistent with this, upon changing the ratio between the metal complexes within the SiO_2 layer, the resulting colour changes from red, to intermediate colours and finally to green, without eye-appreciable colour heterogeneity, as shown in Figure 4.4.2 and inset.

4.5 Eu(III) complex adsorbed on single-walled carbon nanotubes sidewalls

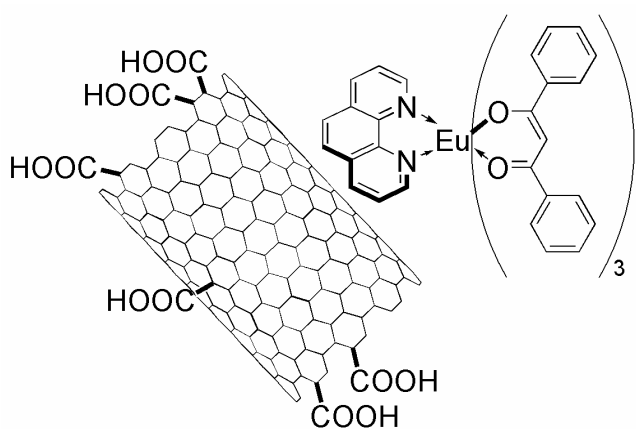
Introduction and applications. Since the discovery of new allotropic forms of carbon, carbon nanotubes (CNTs) have raised much interest in a number of different applications such as field-emission displays, nanoscale sensors, energy storages, molecular electronics, nanocomposite materials, biotechnology and many others.¹³³⁻¹³⁶ The tubular framework of CNTs is solely composed of carbon atoms arranged in rolled graphene-like structures.¹⁵⁵ There are two main varieties of CNTs: single-walled (SWNTs)¹⁵⁶ and multi-walled (MWNTs),¹⁵⁷ the latter being formed by several concentric layers of rolled graphite. In particular, SWNTs are characterized by

an elevated ratio of length over diameter. The lack of solubility and difficult manipulation both in solution and in the solid state are the main limitations toward the extensive use of such tubular carbon frameworks in real applications. Therefore, functionalization of CNTs with organic groups, which can enhance both the solubility in organic solvents and the number of reactive sites for post-integration into multi-component organic materials, revealed to be the best approach to render this material processable.¹⁵⁸⁻¹⁶¹ The main chemical approaches for the modification of CNTs are grouped into two categories:¹⁶² *i*) non-covalent (or supramolecular)¹⁶³⁻¹⁶⁷ and *ii*) covalent^{158, 168-170} functionalization. While the supramolecular approach does not lead to a structural modification of the carbon framework, the covalent derivatization often leads to profound structural (and consequently electronic) alterations as a consequence of the change in the carbon hybridization. Amongst the myriad of potential applications of CNTs, their use in the field of biotechnology have recently started to emerge, raising great expectations.¹⁷¹⁻¹⁷⁴ Surface functionalization enables CNTs to be easily employed as versatile molecular modules for the adsorption or attachment of various biological-active molecules or antigens, which subsequently can be targeted to the desired cell population for immune recognition or therapeutic effects.^{175, 176} Concerning the biomedical applications of CNTs, their use is becoming relevant in neuroscience research and tissue engineering.¹⁷⁷⁻¹⁸² For example, they have been employed as supports for neuronal and ligamentous tissue growth for regenerative interventions of the central nervous system (*e.g.*, brain and spinal cord).¹⁸⁰ Although safety issues have still to be thoroughly examined,^{179, 183-189} all these findings pave the way for the development of novel CNT-based materials which could lead to new insights into the biological and physical processes in which such carbon nanostructure are involved.^{171, 190, 191} In this perspective, for the first time, an Eu(III)-complex, tris-dibenzoylmethane mono-1,10-phenanthroline-europium(III) (**7**) (Fig.4.5.1), has been easily adsorbed *in-situ via* hydrophobic interactions to single-walled carbon nanotube (**SWNT**) surfaces from a methanol solution. *ca.* 5 mg of **SWNT**, was suspended in MeOH (5 mL) containing 25 mg of **7**. The suspension was sonicated for 1 hour and then stirred overnight at 298 K. The mixture was then

filtered through a classical filter paper, and extensively washed with MeOH, CHCl₃, CH₂Cl₂ (*ca.* 150 mL for each solvent) until no traces of red emission was detected in the filtrate and dried in the air. The resulting black precipitate **7•SWNT** was then transferred in a glass flask and dried under high vacuum for 18 hours. The Eu(III)-containing material has been comprehensively characterized via Thermogravimetric Analysis (TGA), UV-Vis-NIR absorption and luminescence spectroscopy, Raman spectroscopy, Atomic Force Microscopy (AFM), High-resolution Transmission Electron Microscopy (HR-TEM), Z-contrast Scanning Transmission Electron Microscopy (STEM) imaging and Energy Dispersive X-ray spectroscopy (EDS).¹⁹²

Luminescence. **7•SWNT** revealed interesting photoluminescence (PL) properties in different media. The electronic absorption profile of the hybrid material **7•SWNT** dispersed in MeOH solution (Fig.4.5.2) and trapped in polystyrene (PS) matrix (Fig. 4.5.3) clearly shows the presence of **7**. The absorption bands with maxima centered at 270 and 350 nm are indeed the typical signal for the 1,10-phenanthroline (Phen)^{22, 37, 124} and the dibenzoylmethane (DBM)^{193, 194} ligands, respectively. On the contrary, in the near infrared region (NIR), the detection of the typical nanotube-centered absorption tail^{102, 195} was not clearly observed due to the heterogeneity and opacity of the samples.

Intense metal-centered (MC) photoluminescence arising from both **7•SWNT** and **7** has been



detected in PS matrix (inset of Fig. 4.5.3). The coordinating ligands (DBM and Phen) act as sensitizers for Eu(III) emitting states, as confirmed by the **7•SWNT** excitation spectrum (Fig. 4.5.3, $\lambda_{em} = 614$ nm) which is largely overlapped with the absorption profile.

Fig. 4.5.1. Chemical structure of the hybrid **7•SWNT** complex.

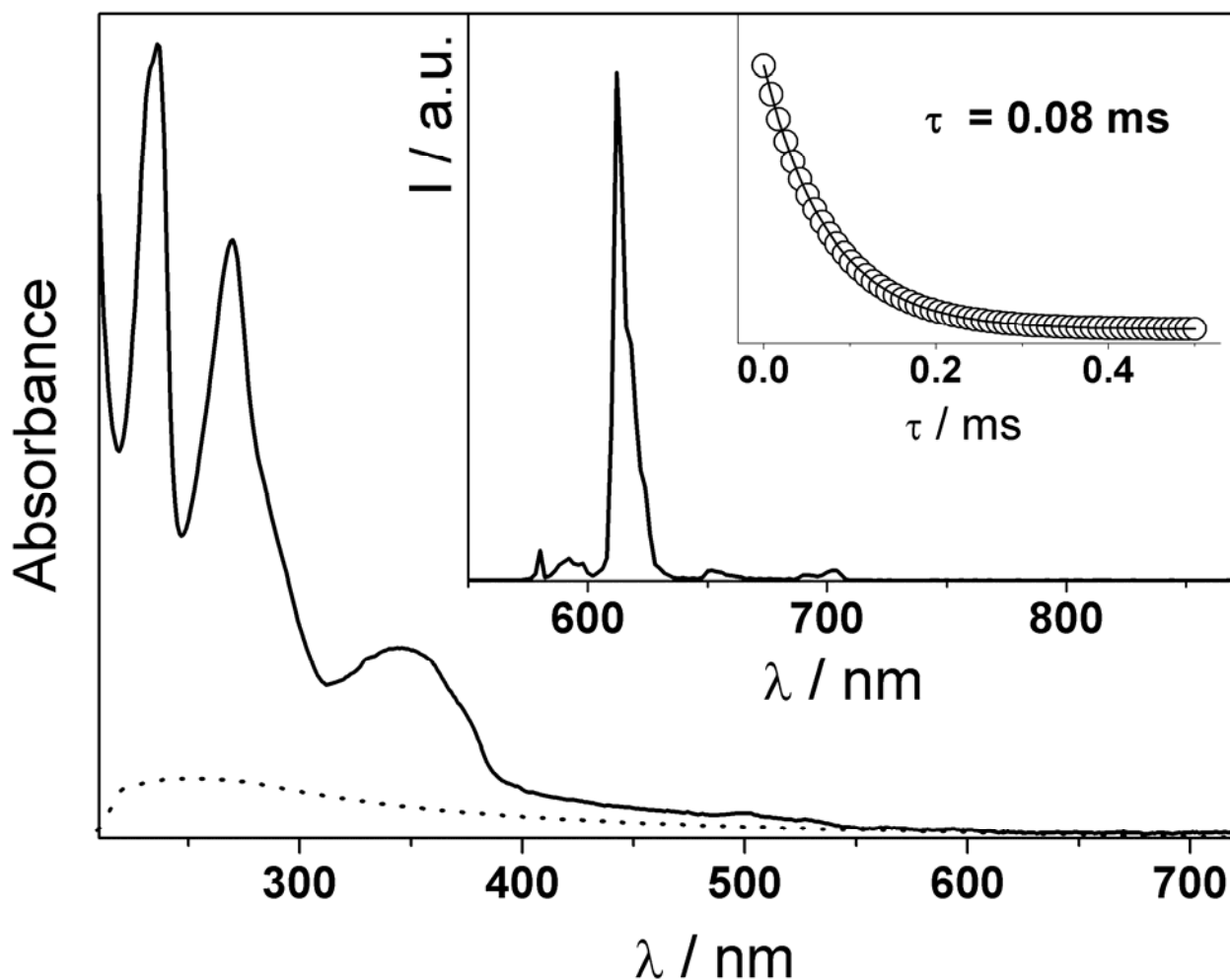


Fig. 4.5.2. Absorption (main window) and emission (inset, $\lambda_{exc} = 350$ nm, $O.D. = 0.4$) spectra of **7•SWNT** (full line) and **SWNT** (dotted line) in MeOH solution at room temperature. In the inset it is also shown the emission decay of **7•SWNT** in MeOH solution.

In rigid media the luminescence quantum yield is difficult to measure with acceptable accuracy, but the observed lifetimes ($\tau_{obs} = 0.5$ ms for both samples, consistent with values reported in literature for Eu(III) complexes in rigid media)^{100, 196} can provide some quantitative information. Indeed, an emission quantum yield of ≈ 0.1 has been calculated from radiative and measured lifetime. In MeOH solution (Fig. 4.5.2), the PL quantum yield of **7**, obtained by using a water solution containing $[Ru(bpy)_3Cl_2]$ as reference,^{140, 197} revealed to be remarkably lower ($\Phi_{em} = 2.5 \times 10^{-4}$) compared to that in PS matrix.

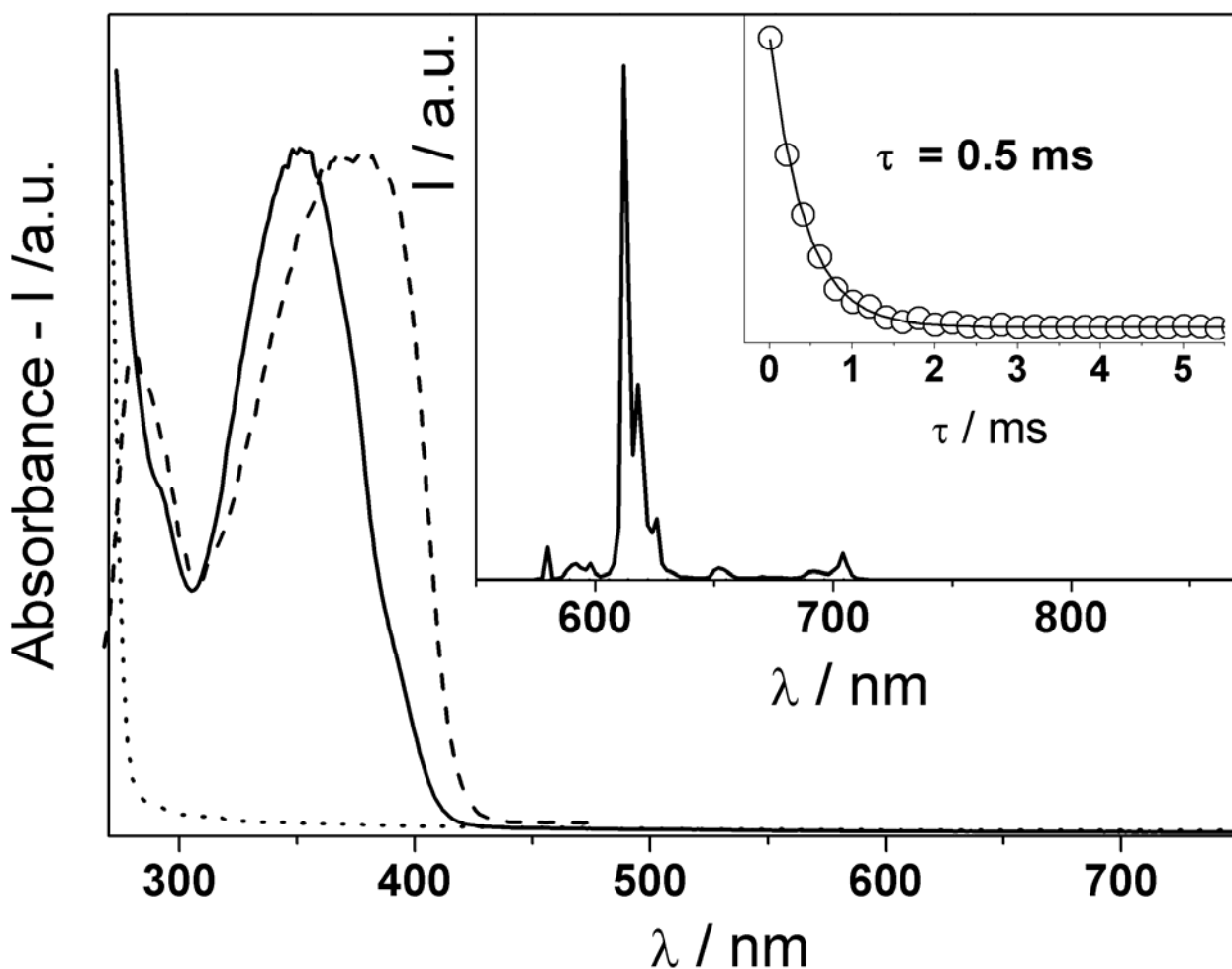


Fig. 4.5.3 Main window: absorption spectra of **7•SWNT** (full line) and **SWNT** carbon nanotube (dotted line) in polystyrene matrix at room temperature. Excitation profile of **7•SWNT** (dashed line, $\lambda_{em} = 614$ nm) is also depicted. Inset: emission spectra and lifetime decay of **7•SWNT** ($OD = 0.4$, $\lambda_{exc} = 350$ nm) in polystyrene matrix at room temperature.

Also the related lifetime decay (0.08 ms), which is known to be strictly correlated with the emission intensity, showed the same trend confirming that protonated solvents, such as MeOH, quench the Eu(III)-centered emitting states *via* vibronic coupling involving O–H or C–H oscillators.^{198, 199} In the case of **7•SWNT**, Φ_{em} has not been determined due to the unknown concentration of Eu(III) complex embedded in the nanotube skein, while the luminescence lifetime decay, within experimental uncertainties, resulted to be the same as that of **7**. Therefore, one can reasonably conclude that the presence of the nanotube framework, either in PS and MeOH, does not

affect the MC luminescence, thanks to the outstanding photoluminescence properties of trivalent lanthanide ions.

Microscopy. TEM and STEM observations were employed to reveal the morphology of the samples and to gain insights into the interactions of 7 with the SWNT. Sample preparation was carried out by suspending the 7•SWNT in MeOH and successively depositing a drop of the

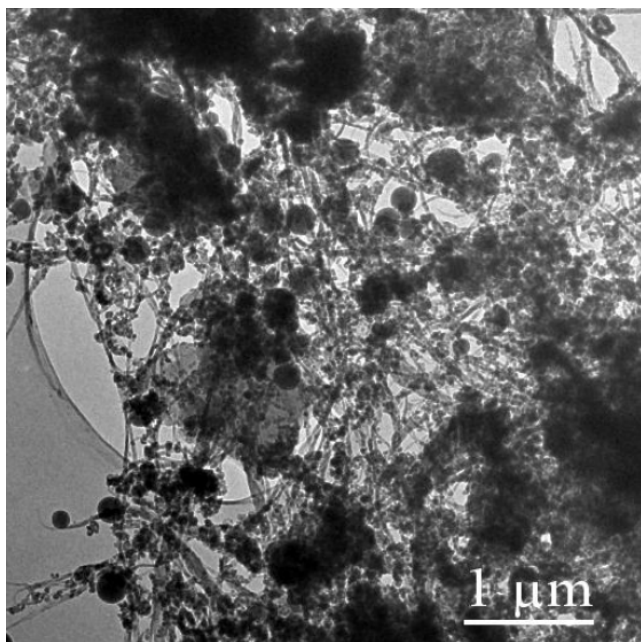


Fig. 4.5.4. BF-TEM micrograph of a typical deposit of 7•SWNT onto a holey C support film.

sonicated suspension onto a holey C support film on a Cu grid. In Fig. 4.5.4, a Bright Field (BF) TEM micrograph of a typical deposit, is reported. The “berried bush” appearance of this deposit evidences the presence of two main components, *i.e.* an ensemble of spherical particles dispersed throughout an entangled network of SWNT bundles. These particles have an average diameter of a few tenth of micron whereas the lateral width of the SWNT bundles ranges from a few nm to a few tens of

nm. The chemical composition of the spherical particles is revealed in the EDS spectrum reported in Fig. 4.5.5, relative to that visible in the inset of this figure. Besides the presence of Cu and some trace of Ni, arising from X-rays emitted from the TEM sample grid and from some residues of the catalyst employed for the nanotubes growth, respectively, the presence of Eu, C and O is clearly observed. This indicates that these particles are agglomerates containing Eu(III)-complexes. From Selected Area Electron Diffraction (SAED) observations (not shown here) they also appear to share a common amorphous structure.

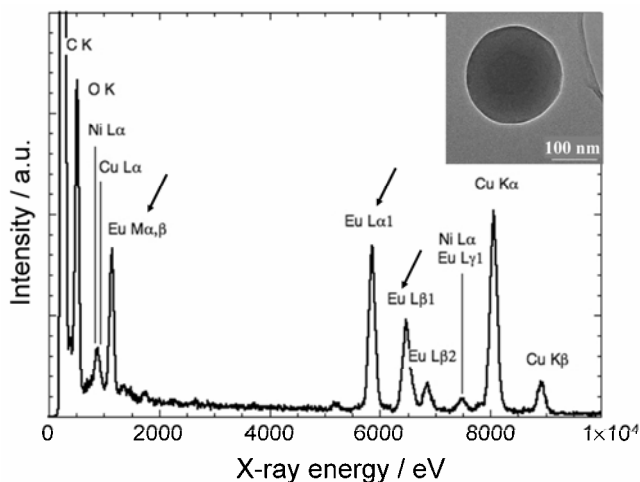


Fig.4.5.5. X-Ray spectrum relative to the particle visible in the BF-TEM micrograph reported in the inset. Peaks corresponding to Eu-M, Eu-K and Eu-L photons are marked by arrows.

The other deposit component, SWNT bundle, is observed in the HR-TEM micrographs reported in Fig. 4.5.6. This figure shows two micrographs of the same SWNT bundle portion, taken at different values of the microscope defocus. In Fig. 4.5.6a, taken close to the *Scherzer* defocus, the image contrast is dominated by the lateral walls of the SWNTs that are seen to run parallelly to the bundle axis.

In Fig. 4.5.6b, taken close to the so-called “minimum contrast” conditions, the wall contrast is minimised resulting in a better visibility of dark contrast regions, a few nm in size, that indicate the presence of very small agglomerates onto the bundle surface. As expected, given the very small dimension and irregular shape of these agglomerates, no evidence of crystalline features was

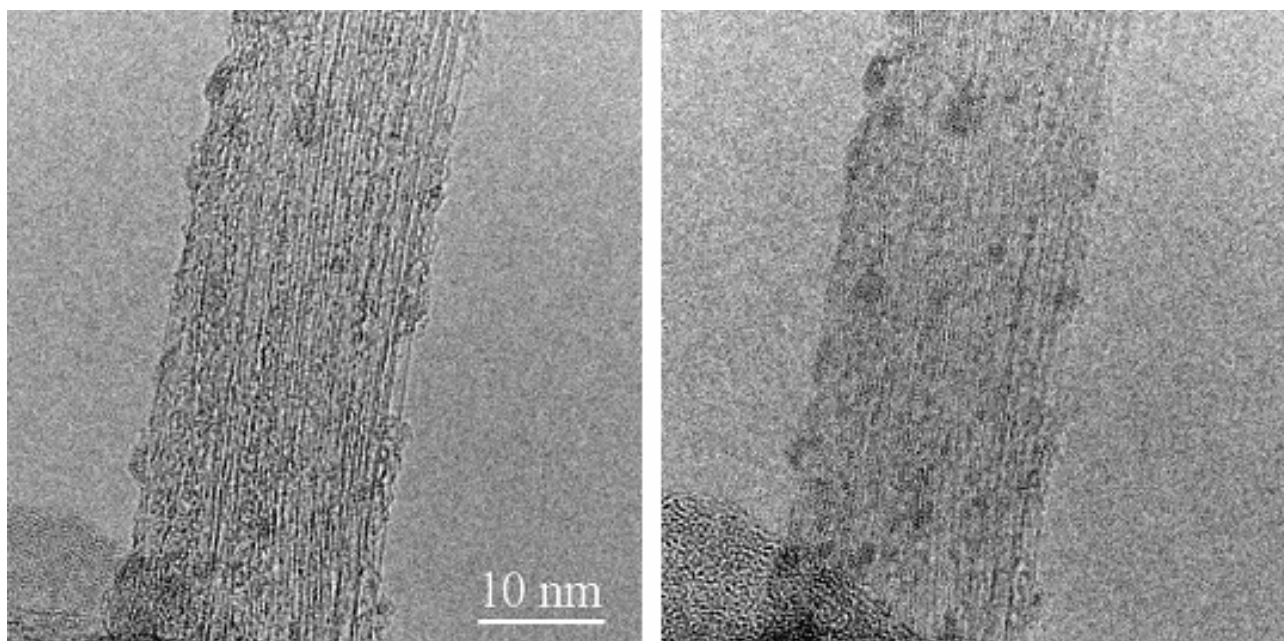


Fig. 4.5.6. HR-TEM micrographs of the same SWNT bundle portion taken under different defocus conditions. (a, left): *Scherzer* defocus, (b, right): minimum contrast condition.

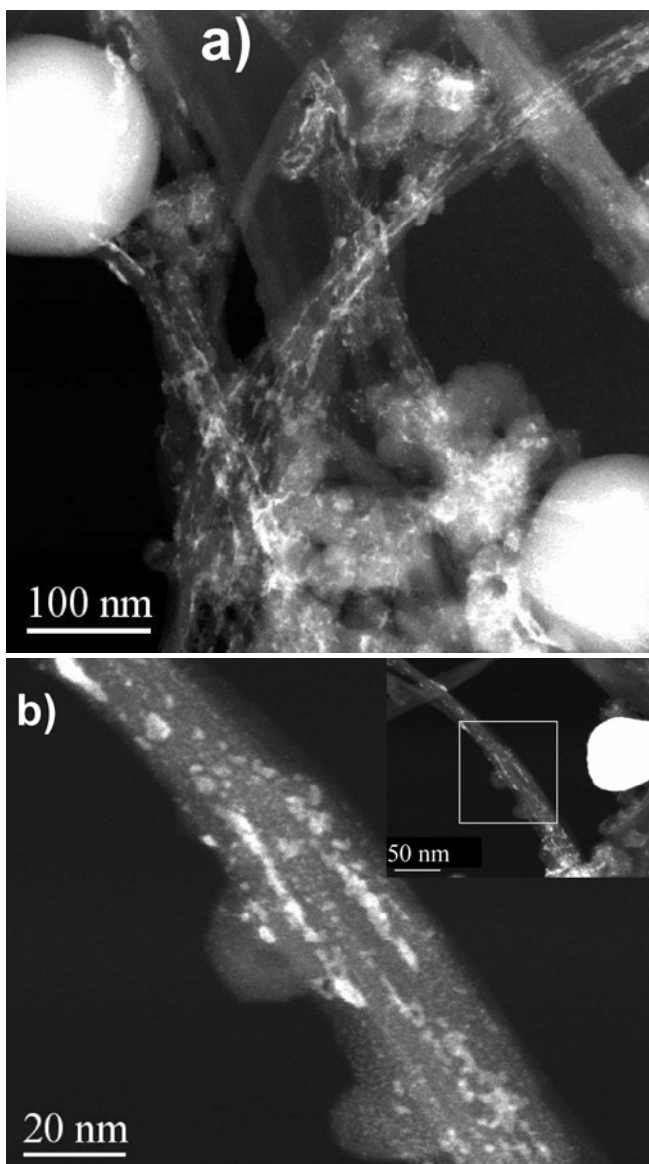


Fig. 4.5.7. Z-contrast ADF-STEM micrographs of a 7•SWNT deposit taken at different magnifications. Particles and agglomerates on the SWNT surfaces are visible with high intensity in the low magnification micrograph reported in (a). In (b), agglomerates on a SWNT bundle surface are observed at higher magnification.

obtained by HRTEM observations, as shown in Fig. 4.5.6. However, we want to caution the reader that at the high electron dose needed by this technique the structure of these small organic agglomerates could rapidly deteriorate by the electron beam induced damage. However, during our observations no phase transformations or agglomerate instability were observed. To investigate the presence of the Eu(III)-complex in the 7•SWNT hybrid material, Z-contrast STEM observations have been performed by using a high angle Annular Dark Field Detector (ADF). In Fig. 4.5.7, ADF-STEM micrographs taken at different magnifications, are reported.

In these dark-field micrographs a mass thickness contrast is operating, resulting in higher intensities in correspondence of thicker regions and/or heavier elements. In Fig. 4.5.7a, all the deposit components are finally visible,

i.e. spherical particles with the highest intensity, weakly contrasted SWNT bundles and high intensity streaks parallel to the bundles axis. The latter component is visible at higher magnification in Fig. 4.5.7b. From this micrograph, it is evident the presence of high Z element agglomerates onto the bundle surface. Very likely, the Eu(III)-containing agglomerates are adsorbed on the SWNT external surface and not confined inside the tubular framework. This can be deduced from the agglomerates width, which easily overcome 3 nm, a dimension not compatible with that of the

SWNT diameters, ranging from 1.3 to 1.7 nm, as obtained by HR-TEM observations of the thinnest bundles (not shown here). Finally, the results of an X-rays microanalysis investigation of the composition of the small agglomerates are reported in Fig. 4.5.8. In the ADF-STEM micrograph of Fig. 4.5.8a, the analysed regions are marked by circles: region 1 corresponding to a small agglomerate and region 2 to the SWNT bundle. A comparison of the corresponding X-rays spectra in Figure 4.5.8b and 4.5.8c clearly evidences that the agglomerates do contain the Eu(III)-complex. These findings show that in the 7•SWNT system, the Eu(III) complexes have a strong tendency to form agglomerates. This gives rise to two distinct forms, *i.e.* spherical particles with dimension of a few tenth of a micron remaining trapped in the SWNT network and nanometer sized agglomerates adsorbed onto the SWNT surfaces.

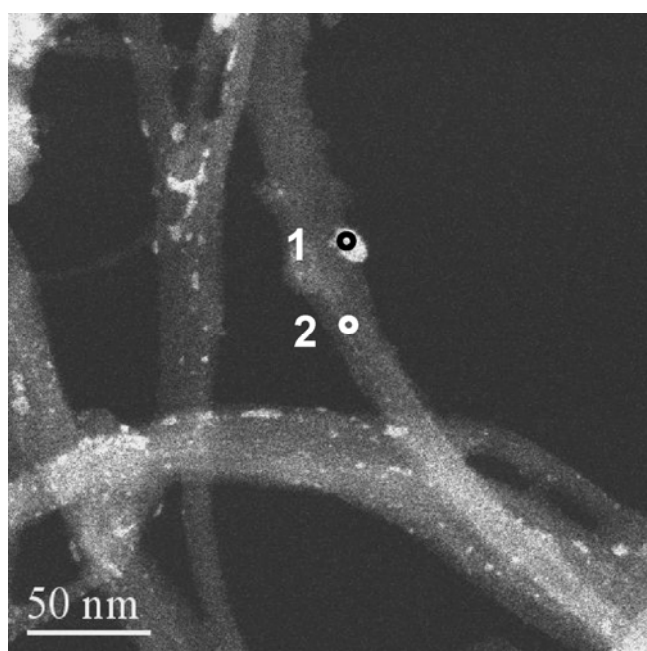
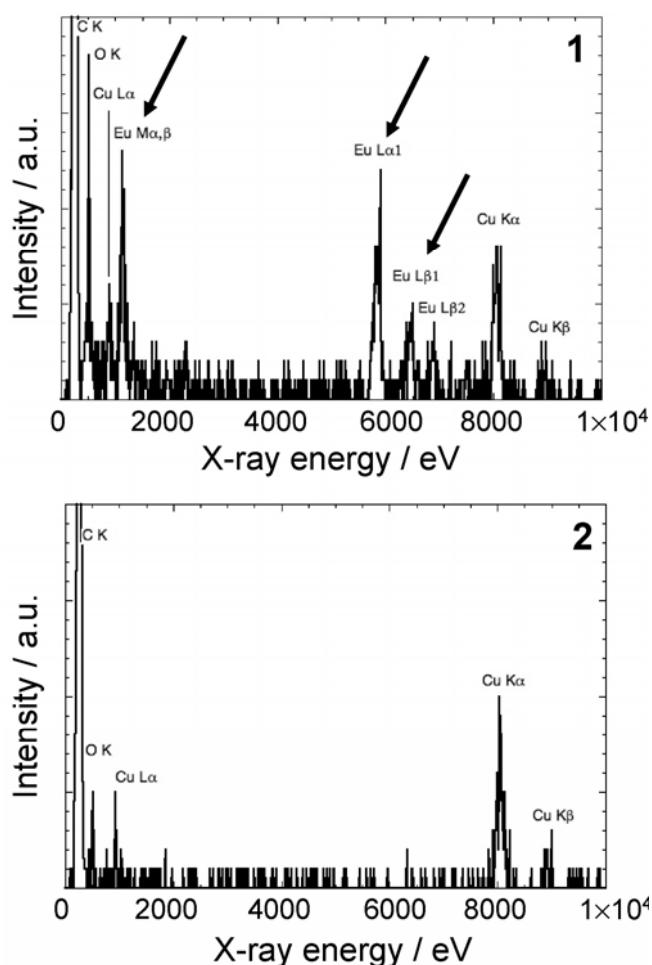


Fig. 4.5.8 Analyses of the composition of the agglomerates observed onto the SWNT bundle surface. The X-Ray spectra 1 and 2 have been recorded on the corresponding SWNT bundle positions marked with open circles in the ADF-STEM micrographs reported at the top of the figure. Peaks corresponding to Eu-M, Eu-K and Eu-L photons are marked by arrows.



5 EXPERIMENTAL SETUP

Absorption spectra were recorded with a Perkin-Elmer λ 40 spectrophotometer. For luminescence experiments, the samples were placed in fluorimetric 1-cm path cuvettes and, when necessary, purged from oxygen by bubbling with argon. Uncorrected emission spectra were obtained with an Edinburgh FLS920 spectrometer equipped with a peltier-cooled Hamamatsu R928



Edinburgh FLS920 spectrometer equipped with an integrating sphere-laser setup

photomultiplier tube (185-850 nm). The steady-state NIR luminescence spectra were obtained with an Edinburgh FLS920 spectrometer equipped with Hamamatsu R5509-72 supercooled photomultiplier tube (400-1700 nm) at 193 K and a TM300 emission monochromator with NIR grating blazed at 1000 nm. An Edinburgh Xe900 450 W Xenon arc lamp was used as exciting light

source. Corrected spectra were obtained *via* a calibration curve supplied with the instrument. Luminescence quantum yields (Φ_{em}) obtained from spectra on a wavelength scale (nm) were measured according to the approach described by Demas and Crosby²⁰⁰ using air-equilibrated $(Ru(bpy)_3Cl_2)$ in water solution, ($\Phi_{em} = 0.028$)¹⁹⁶ as standard. Emission lifetimes on the nanosecond time scale were determined with an IBH single photon counting spectrometer equipped with a thyatron gated nitrogen lamp working in the range 2–40 kHz ($\lambda_{exc} = 337$ nm, 0.5 ns time resolution); the detector was a red-sensitive (185–850 nm) Hamamatsu R-3237-01 photomultiplier tube. For the emission in the visible region, the luminescence lifetimes in the microsecond-millisecond scales were measured by using a Perkin-Elmer LS-50B spectrofluorometer equipped with a pulsed xenon lamp with variable repetition rate and elaborated with standard software fitting procedures (Origin 6.1). To record the 77 K luminescence spectra, the samples were put in glass



IBH single photon counting spectrometer

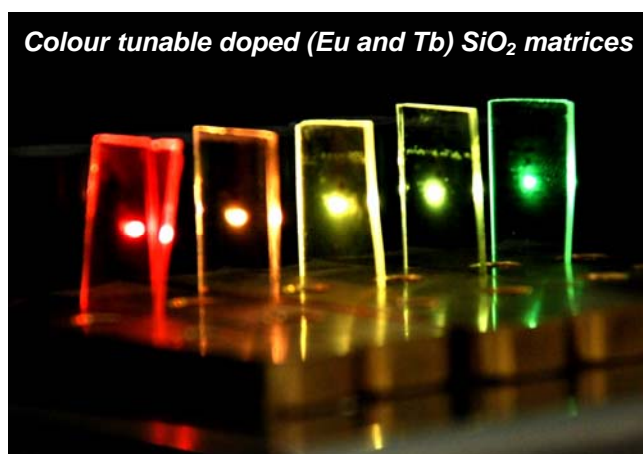
tubes (2 mm diameter) and inserted in a special quartz dewar, filled up with liquid nitrogen. For solid samples Φ_{em} have been calculated by corrected emission spectra obtained from an apparatus consisting of a barium sulphate coated integrating sphere (6 inches), an He-Cd laser (λ_{exc} : 325 nm, 5mW) as light source and a CCD AVA-Spec2048 as signal detector,

following the procedure described elsewhere.^{154, 201} Experimental uncertainties are estimated to be $\pm 8\%$ for lifetime determinations, $\pm 20\%$ for emission quantum yields, ± 2 nm and ± 5 nm for absorption and emission peaks respectively.

6 FINAL REMARKS

The present work has been motivated by the search for efficient emitting materials to be fruitfully employed in several application fields such as lighting, bioassay and telecommunication. In some cases, also the relaxometric properties of non-luminescent gadolinium samples have been investigated in order to test their suitability as contrast agents in MRI. The design and the synthesis of the various antenna units here presented were driven by the search for better and better ability to

protect the metal core and enhance the sensitization of the emitting states. Several organic ligands, including phenanthroline, naphthalene, quinoline and a variety of diketonate units have been employed leading to Ln luminescence efficiencies up to nearly 50% in the visible spectral window (Eu and



Tb, UV \rightarrow VIS down-conversion). Satisfactory results have been obtained also for NIR emitting Ln(III) ions when sensitized by *d*-block metal complexes (UV/Vis \rightarrow NIR down-conversion). For applicative reasons, doped solid matrices have been also investigated. Sol-gel glasses, polymer and more uncommon carbon nanotubes have been employed to link or trap the emitting species. Their PL properties, in most cases compared to that obtained in solution, have been studied. Intense, tunable (Eu and Tb, red \rightarrow green) and monochromatic (red, Eu) light resulted from doped SiO₂ and adsorbed SWNT matrices, respectively. The obtained results push to enhance their performances, for instance by adding a blue emitter (SiO₂ case) in order to get a complete control over colour tunability. Furthermore, the simple fabrication processes encourage their use for possible applications with potential benefits in energy-saving and environmentally sustainable technologies (e.g. OLED, Ln-based fibre-optics, *etc*). As discussed above (Chapter 3) lanthanides are advantageous because of their high performances in many hi-tech fields and relatively low toxicity (especially when compared to that of currently employed heavy metals). Finally, it must be pointed

out that this research work has been motivated also by the wish that new and more efficient materials could help to get a more sustainable development in affluent countries and reduce the impact of billions people living in rapidly developing countries (e.g. China, India), who are striving to attain higher standards of living.

BIBLIOGRAPHY

1. IUPAC: <http://www.chem.qmul.ac.uk/iupac/>.
2. Cotton and Simon., *Lanthanides and Actinides*, Oxford University Press, New York, 1991.
3. G. B. Haxel, J. B. Hedrick and G. J. Orris, *Rare Earth Elements—Critical Resources for High Technology*, US Geological Survey, <http://pubs.usgs.gov/fs/2002/fs087-02/>, 2002.
4. G. J. Orris and R. I. Grauch, *Rare Earth Element Mines, Deposits, and Occurrences. U.S. Geological Survey Open-File Report 02-189*, U.S. Geological Survey, <http://geopubs.wr.usgs.gov/open-file/of02-189>, Tucson (USA), 2002.
5. C. A. DiFrancesco and J. B. Hedrick, *Rare Earths Statistics: Survey Open-File Report 01-116*. U. S. Geological Survey. <http://minerals.usgs.gov/minerals/pubs/of01-006/>, Tucson, 2000.
6. J. B. Hedrick, *Metal Prices in the United States through 1998*. U. S. Geological Survey, http://minerals.usgs.gov/minerals/pubs/metal_prices/, 109-126, Tucson, 2000.
7. N. Sabbatini, M. Guardigli and I. Manet, *Handbook Phys. Chem. Rare Earths*, Elsevier, Amsterdam, 1996.
8. A. Dossing, *Eur. J. Inorg. Chem.*, 2005, 1425.
9. T. Christie, B. Brathwhite and A. Tullach, *Mineral Commodity Report 17: Rare Earths and Related Elements*, New Zealand Mining 24,7 1998.
10. Y. Hasegawa, Y. Wada and S. Yanagida, *J. Photochem. Photobiol. C-Photochem. Rev.*, 2004, **5**, 183.
11. S. Quici, M. Cavazzini, G. Marzanni, G. Accorsi, N. Armaroli, B. Ventura and F. Barigelletti, *Inorg. Chem.*, 2005, **44**, 529.
12. M. Latva, H. Takalo, V. Mikkala, C. Matachescu, J. C. Rodriguez-Ubis and J. Kankare, *J. Lumines.*, 1997, **75**, 149.

13. H. Takalo, V. M. Mukkala, L. Merio, J. C. RodriguezUbis, R. Sedano, O. Juanes and E. Brunet, *Helv. Chim. Acta*, 1997, **80**, 372.
14. N. Sabbatini, M. Guardigli and I. Manet, *Antenna Effect in Encapsulation Complexes of Lanthanide Ions*, Elsevier, Amsterdam, 1996.
15. B. Alpha, L. J.-M. and G. Mathis, *Angew. Chem.-Int. Edit. Engl.*, 1987, **26**, 266.
16. N. Sabbatini, M. Guardigli, A. Mecati, V. Balzani, R. Ungaro, E. Ghidini, A. Casnati and A. Pochini, *J. Chem. Soc.-Chem. Commun.*, 1990, 878.
17. N. Armaroli, G. Accorsi, P. Barigelletti, S. M. Couchman, J. S. Fleming, N. C. Harden, J. C. Jeffery, K. L. V. Mann, J. A. McCleverty, L. H. Rees, S. R. Starling and M. D. Ward, *Inorg. Chem.*, 1999, **38**, 5769.
18. V. Balzani, E. Berghmans, J. M. Lehn, N. Sabbatini, R. Terode and R. Ziessel, *Helv. Chim. Acta*, 1990, **73**, 2383.
19. J.-M. Lehn and R. Ziessel, *Chem. Commun.*, 1987, 1292.
20. J. J. Lessmann and W. D. Horrocks, *Inorg. Chem.*, 2000, **39**, 3114.
21. C. Piguet, J. C. G. Bunzli, G. Bernardinelli, C. G. Bochet and P. Froidevaux, *J. Chem. Soc.-Dalton Trans.*, 1995, 83.
22. S. Quici, G. Marzanni, M. Cavazzini, P. L. Anelli, M. Botta, E. Gianolio, G. Accorsi, N. Armaroli and F. Barigelletti, *Inorg. Chem.*, 2002, **41**, 2777.
23. S. Quici, G. Marzanni, A. Forni, G. Accorsi and F. Barigelletti, *Inorg. Chem.*, 2004, **43**, 1294.
24. L. F. Yang, Z. L. Gong, D. B. Nie, B. Lou, Z. Q. Bian, M. Guan, C. H. Huang, H. J. Lee and W. P. Baik, *New J. Chem.*, 2006, **30**, 791.
25. C. Yang, L. M. Fu, Y. Wang, J. P. Zhang, W. T. Wong, X. C. Ai, Y. F. Qiao, B. S. Zou and L. L. Gui, *Angew. Chem. Int. Edit*, 2004, **43**, 5010.
26. G. A. Hebbink, S. I. Klink, L. Grave, P. Alink and F. van Veggel, *ChemPhysChem*, 2002, **3**, 1014.

27. A. I. Voloshin, N. M. Shavaleev and V. P. Kazakov, *J. Lumines.*, 2000, **91**, 49.
28. A. I. Voloshin, N. M. Shavaleev and V. P. Kazakov, *J. Photochem. Photobiol. A-Chem.*, 2000, **131**, 61.
29. T. Förster, *Discuss. Faraday Soc.*, 1959, **27**, 7.
30. D. L. Dexter, *J. Chem. Phys.*, 1952, **21**, 836.
31. N. Armaroli, G. Accorsi, F. Barigelletti, S. M. Couchman, J. S. Fleming, N. C. Harden, J. C. Jeffery, K. L. V. Mann, J. A. McCleverty, L. H. Rees, S. R. Starling and M. D. Ward, *Inorg. Chem.*, 1999, **38**, 5769.
32. R. Englman and J. Jortner, *Mol. Phys.*, 1970, **18**, 145.
33. G. H. Dieke, *Spectra and Energy Levels of Rare Earth Ions in Crystals*, Wiley-Interscience, New York, 1968.
34. J. W. Verhoeven, M. H. V. Werts, J. W. Hofstraat and F. A. J. Geurts, *Chem. Phys. Lett.*, 1997, 196.
35. R. C. Evans, P. Douglas and C. J. Winscom, *Coord. Chem. Rev.*, 2006, **250**, 2093.
36. H. Maas, A. Currao and G. Calzaferri, *Angew. Chem. Int. Edit*, 2002, **41**, 2495.
37. S. Quici, M. Cavazzini, G. Marzanni, G. Accorsi, N. Armaroli, B. Ventura and F. Barigelletti, *Inorg. Chem.*, 2005, **44**, 529.
38. R. U. A. Khan, C. Hunziker and P. Gunter, *J. Mater. Sci.-Mater. Electron.*, 2006, **17**, 467.
39. J. P. Leonard and T. Gunnlaugsson, *J. Fluoresc.*, 2005, **15**, 585.
40. E. F. Schubert and J. K. Kim, *Science*, 2005, **308**, 1274.
41. B. W. D'Andrade and S. R. Forrest, *Adv. Mater.*, 2004, **16**, 1585.
42. T. X. Li, H. Fukuyama, Y. Yamagata, H. L. Lan and J. Kido, *Polym. Adv. Technol.*, 2004, **15**, 302.
43. M. A. Baldo, M. E. Thompson and S. R. Forrest, *Pure Appl. Chem.*, 1999, **71**, 2095.
44. Y. R. Sun, N. C. Giebink, H. Kanno, B. W. Ma, M. E. Thompson and S. R. Forrest, *Nature*, 2006, **440**, 908.

45. S. F. Li, G. Zhong, W. H. Zhu, F. Y. Li, J. F. Pan, W. Huang and H. Tian, *J. Mater. Chem.*, 2005, **15**, 3221.
46. S. F. Li, G. Y. Zhong, W. H. Zhu, F. Y. Li, J. F. Pan, W. Huang and H. Tian, *Chem. Lett.*, 2005, **34**, 688.
47. J. B. Yu, L. Zhou, H. J. Zhang, Y. X. Zheng, H. R. Li, R. P. Deng, Z. P. Peng and Z. F. Li, *Inorg. Chem.*, 2005, **44**, 1611.
48. D. L. Tao, Y. Z. Xu, J. Feng, T. Zhang, Z. H. Xu, H. Shen, J. G. Wu, Z. Xu, X. R. Xu and D. F. Xu, *J. Mater. Chem.*, 2004, **14**, 1252.
49. I. Hemmila and V. Laitala, *J. Fluoresc.*, 2005, **15**, 529.
50. J. L. Yuan and G. L. Wang, *J. Fluoresc.*, 2005, **15**, 559.
51. I. Hemmila and S. Webb, *Drug Discov. Today*, 1997, **2**, 373.
52. A. J. Kenyon, *Semicond. Sci. Technol.*, 2005, **20**, R65.
53. W. H. Wong, K. S. Chan and E. Y. B. Pun, *Appl. Phys. Lett.*, 2005, **87**.
54. L. N. Sun, H. J. Zhang, L. S. Fu, F. Y. Liu, Q. G. Meng, C. Y. Peng and J. B. Yu, *Adv. Funct. Mater.*, 2005, **15**, 1041.
55. L. H. Slooff, A. Polman, S. I. Klink, G. A. Hebbink, L. Grave, F. van Veggel, D. N. Reinhoudt and J. W. Hofstraat, *Opt. Mater.*, 2000, **14**, 101.
56. X. Orignac, D. Barbier, X. M. Du, R. M. Almeida, O. McCarthy and E. Yeatman, *Opt. Mater.*, 1999, **12**, 1.
57. J. K. R. Weber, J. J. Felten, B. Cho and P. C. Nordine, *Nature*, 1998, **393**, 769.
58. A. Tunnermann, T. Schreiber, F. Roser, A. Liem, S. Hofer, H. Zellmer, S. Nolte and J. Limpert, *J. Phys. B-At. Mol. Opt. Phys.*, 2005, **38**, S681.
59. W. J. Miniscalco, *J. Lightwave Technol.*, 1991, **9**, 234.
60. K. Kuriki, Y. Koike and Y. Okamoto, *Chem. Rev.*, 2002, **102**, 2347.
61. Y. Ohishi, T. Kanamori, T. Kitagawa, S. Takahashi, E. Snitzer and G. H. Sigel, *Opt. Lett.*, 1991, **16**, 1747.

62. P. Wang, J. M. Dawes, P. Dekker, D. S. Knowles, J. A. Piper and B. S. Lu, *J. Opt. Soc. Am. B-Opt. Phys.*, 1999, **16**, 63.
63. S. Kuck, *Appl. Phys. B*, 2001, **72**, 515.
64. N. Armaroli and V. Balzani, *Angew. Chem. Int. Edit*, 2007, **46**, 52.
65. N. M. Shavaleev, L. P. Moorcraft, S. J. A. Pope, Z. R. Bell, S. Faulkner and M. D. Ward, *Chem.-Eur. J.*, 2003, **9**, 5283.
66. S. Quici, M. Cavazzini, M. C. Raffo, M. Botta, G. Giovenzana, B. Ventura, G. Accorsi and F. Barigelletti, *Inorg. Chim. Acta*, 2007, **in press**.
67. G. M. Davies, R. J. Aarons, G. R. Motson, J. C. Jeffery, H. Adams, S. Faulkner and M. D. Ward, *Dalton Trans.*, 2004, 1136.
68. M. H. V. Werts, R. H. Woudenberg, P. G. Emmerink, R. van Gassel, J. W. Hofstraat and J. W. Verhoeven, *Angew. Chem. Int. Edit*, 2000, **39**, 4542.
69. S. Aime, M. Botta, S. G. Crich, G. Giovenzana, R. Pagliarin, M. Sisti and E. Terreno, *Magn. Reson. Chem.*, 1998, **36**, S200.
70. <http://www.radiology.co.uk/srs-x/cases/025/a.htm>.
71. P. Caravan, J. J. Ellison, T. J. McMurry and R. B. Lauffer, *Chem. Rev.*, 1999, **99**, 2293.
72. A. E. Merbach and E. Tóth, *The Chemistry of Contrast Agents in Medical Magnetic Resonance Imaging*, John Wiley & Sons: Chichester, 2001.
73. D. A. Galbi, *Telecommunications Policy*, 2001, **25**, 139.
74. W. A. Gambling, *Endavour*, 1992, **16**.
75. R. Scheps, *Progr. Quantum Electr.*, 1996, **20**, 271.
76. A. Braud, P. Y. Tigreat, J. L. Doualan and R. Moncorge, *Appl. Phys. B*, 2001, **72**, 909.
77. L. Esterowitz, J. Noonan and J. Bahler, *Appl. Phys. Lett*, 1967, **10**, 126.
78. E. Osiac, I. Sokolska and S. Kuck, *J. Alloy. Compd.*, 2001, **283**, 323.
79. E. Osiac, E. Heumann, S. Kuck, G. Huber, E. Sani, A. Toncelli and M. Tonelli, *Appl. Phys. Lett*, 2003, **82**, 3832.

80. E. Osiac, S. Kuck, E. Heumann, G. Huber, E. Sani, A. Toncelli and M. Tonelli, *Opt. Mater.*, 2003, **24**, 537.
81. E. Downing, L. Hesselink, J. Ralston and R. MacFarlane, *Science*, 1996, **273**, 1185.
82. G. Huber, E. W. Duczynski and K. Petermann, *J. Quantum Electron.*, 1988, **24**, 920.
83. K. Shimamura, H. Sato, A. Bensalah, V. Sudesh, H. Machida, N. Sarukura and T. Fukuda, *Cryst. Res. Technol.*, 2001, **36**, 801.
84. G. A. Hebbink, L. Grave, L. A. Woldering, D. N. Reinhoudt and F. van Veggel, *J. Phys. Chem. A*, 2003, **107**, 2483.
85. M. H. V. Werts, J. W. Verhoeven and J. W. Hofstraat, *J. Chem. Soc.-Perkin Trans. 2*, 2000, 433.
86. M. J. Weber, *Phys.Rev.*, 1968, **171**, 283.
87. M. H. V. Werts, J. W. Hofstraat, F. A. J. Geurts and J. W. Verhoeven, *Chem. Phys. Lett.*, 1997, **276**, 196.
88. F. Richardson, *Chem. Rev.*, 1982, **82**, 541.
89. J. Bourson, J. Pouget and B. Valeur, *J. Phys. Chem. A*, 1993, **97**, 4552.
90. C. S. Wilcox, *In Frontiers in Supramolecular Organic Chemistry and Photochemistry*, Schneider, H.-J. Dürr, H., Eds. VCH, Germany, 1991.
91. A. Beeby, L. M. Bushby, D. Maffeo and J. A. G. Williams, *J. Chem. Soc.-Dalton Trans.*, 2002, 48.
92. S. L. Murov, I. Carmichael and G. L. Hug, *Handbook of Photochemistry*, M. Dekker, New York, 1993.
93. A. Beeby, I. M. Clarkson, R. S. Dickins, S. Faulkner, D. Parker, L. Royle, A. S. De Sousa, W. J. A. G. and M. Woods, *J. Chem. Soc.-Perkin Trans. 2*, 1999, 493.
94. D. Parker, *Coord. Chem. Rev.*, 2000, **205**, 109.
95. J. W. Hofstraat, M. P. O. Wolbers, F. van Veggel, D. N. Reinhoudt, M. H. V. Werts and J. W. Verhoeven, *J. Fluoresc.*, 1998, **8**, 301.

96. M. Montalti, A. Credi, L. Prodi and M. T. Gandolfi, *Handbook of Photochemistry, 3rd Edition*, CRC Press, Taylor & Francis, Boca Raton, 2006.
97. A. J. Bard, *Standard Potentials in Aqueous Solution*, Marcel Dekker, New York, 1985.
98. R. A. Marcus and N. Sutin, *Biochimica Et Biophysica Acta*, 1985, **811**, 265.
99. M. A. El-Sayed, *J. Chem. Phys.*, 1963, **38**, 2834.
100. G. Stein and E. Wurzburg, *J. Chem. Phys.*, 1975, **62**, 208.
101. CS Chem3D 6.0 by CambridgeSoft, Cambridge, MA, USA
102. M. H. V. Werts, R. T. F. Jukes and J. W. Verhoeven, *Phys Chem Chem Phys*, 2002, **4**, 1542.
103. A. F. Kirby and F. S. Richardson, *J. Phys. Chem.*, 1983, **87**, 2544.
104. S. I. Klink, H. Keizer and F. van Veggel, *Angew. Chem. Int. Edit*, 2000, **39**, 4319.
105. A. Beeby, R. S. Dickins, S. FitzGerald, L. J. Govenlock, C. L. Maupin, D. Parker, J. P. Riehl, G. Siligardi and J. A. G. Williams, *Chem. Commun.*, 2000, 1183.
106. D. Imbert, M. Cantuel, J. C. G. Bunzli, G. Bernardinelli and C. Piguet, *J. Am. Chem. Soc.*, 2003, **125**, 15698.
107. M. A. Subhan, H. Nakata, T. Suzuki, J. H. Choi and S. Kaizaki, *J. Lumines.*, 2003, **101**, 307.
108. S. J. A. Pope, B. J. Coe and S. Faulkner, *Chem. Commun.*, 2004, 1550.
109. S. J. A. Pope, B. J. Coe, S. Faulkner, E. V. Bichenkova, X. Yu and K. T. Douglas, *J. Am. Chem. Soc.*, 2004, **126**, 9490.
110. D. Guo, C. Y. Duan, F. Lu, Y. Hasegawa, Q. J. Meng and S. Yanagida, *Chem. Commun.*, 2004, 1486.
111. P. B. Glover, P. R. Ashton, L. J. Childs, A. Rodger, M. Kercher, R. M. Williams, L. De Cola and Z. Pikramenou, *J. Am. Chem. Soc.*, 2003, **125**, 9918.
112. P. D. Beer, F. Szemes, P. Passaniti and M. Maestri, *Inorg. Chem.*, 2004, **43**, 3965.
113. G. Arena, G. Calogero, S. Campagna, L. M. Scolaro, V. Ricevuto and R. Romeo, *Inorg. Chem.*, 1998, **37**, 2763.

114. J. A. Bailey, M. G. Hill, R. E. Marsh, V. M. Miskowski, W. P. Schaefer and H. B. Gray, *Inorg. Chem.*, 1995, **34**, 4591.
115. N. M. Shavaleev, A. Barbieri, Z. R. Bell, M. D. Ward and F. Barigelletti, *New J. Chem.*, 2004, **28**, 398.
116. A. Vogler and J. Kisslinger, *Inorg. Chim. Acta*, 1986, **115**, 193.
117. S. C. Chan, M. C. W. Chan, Y. Wang, C. M. Che, K. K. Cheung and N. Y. Zhu, *Chem.-Eur. J.*, 2001, **7**, 4180.
118. M. Hissler, W. B. Connick, D. K. Geiger, J. E. McGarrah, D. Lipa, R. J. Lachicotte and R. Eisenberg, *Inorg. Chem.*, 2000, **39**, 447.
119. S. L. James, M. Younus, P. R. Raithby and J. Lewis, *J. Organomet. Chem.*, 1997, **543**, 233.
120. C. E. Whittle, J. A. Weinstein, M. W. George and K. S. Schanze, *Inorg. Chem.*, 2001, **40**, 4053.
121. N. Sabbatini, M. Guardigli and J.-M. Lehn, *Coord. Chem. Rev.*, 1993, **123**, 201.
122. T. A. Miller, J. C. Jeffery, M. D. Ward, H. Adams, S. J. A. Pope and S. Faulkner, *Dalton Trans.*, 2004, 1524.
123. N. Armaroli, G. Accorsi, D. Felder and J. F. Nierengarten, *Chem.-Eur. J.*, 2002, **8**, 2314.
124. N. M. Shavaleev, G. Accorsi, D. Virgili, D. R. Bell, T. Lazarides, G. Calogero, N. Armaroli and M. D. Ward, *Inorg. Chem.*, 2005, **44**, 61.
125. K. Kuriki, Y. Koike and Y. Okamoto, *Chem. Rev.*, 2002, **102**, 2347.
126. M. D. McGehee, T. Bergstedt, C. Zhang, A. P. Saab, M. B. O'Regan, G. C. Bazan, V. I. Srdanov and A. J. Heeger, *Adv. Mater.*, 1999, **11**, 1349.
127. C. Y. Yang, V. Srdanov, M. R. Robinson, G. C. Bazan and A. J. Heeger, *Adv. Mater.*, 2002, **14**, 980.
128. K. Binnemans, P. Lenaerts, K. Driesen and C. Görrler-Walrand, *J. Mater. Chem.*, 2004, **14**, 191.

129. A. M. Klonkowski, S. Lis, M. Pietraszkiewicz, Z. Hnatejko, K. Czarnobaj and M. Elbanowski, *Chem. Mat.*, 2003, **15**, 656.
130. P. Lenaerts, A. Storms, J. Mullens, J. D'Haen, C. Gorller-Walrand, K. Binnemans and K. Driesen, *Chem. Mat.*, 2005, **17**, 5194.
131. L. R. Matthews and E. T. Knobbe, *Chem. Mat.*, 1993, **5**, 1697.
132. B. T. Stone, V. C. Costa and K. L. Bray, *Chem. Mat.*, 1997, **9**, 2592.
133. C. M. Aguirre, S. Auvray, S. Pigeon, R. Izquierdo, P. Desjardins and R. Martel, *Appl. Phys. Lett.*, 2006, **88**.
134. D. M. Guldi, A. Rahman, V. Sgobba and C. Ehli, *Chem. Soc. Rev.*, 2006, **35**, 471.
135. Y.-P. Sun, K. Fu, Y. Lin and A. Y. Huang, *Acc. Chem. Res.*, 2002, **35**, 1096.
136. O. Zhou, H. Shimoda, B. Gao, S. J. Oh, L. Fleming and G. Z. Yue, *Acc. Chem. Res.*, 2002, **35**, 1045.
137. L. R. Matthews, X. J. Wang and E. T. Knobbe, *J. Non-Cryst Sol.*, 1994, **178**, 44.
138. D. E. Reichert, J. S. Lewis and C. J. Anderson, *Coord. Chem. Rev.*, 1999, **184**, 3.
139. S. Quici, M. Cavazzini, M. C. Raffo, L. Armelao, G. Bottaro, G. Accorsi, C. Sabatini and F. Barigelletti, *J. Mater. Chem.*, 2006, **16**, 741.
140. D. Parker and J. A. Williams, *J. Chem. Soc.-Dalton Trans.*, 1996, 3613.
141. S. K. Chattopadhyay, C. V. Kumar and P. K. Das, *J. Photochem.*, 1985, **30**, 81.
142. S. K. Ghoshal, S. K. Sarkar and G. S. Kastha, *Bull. Chem. Soc. Jpn.*, 1981, **54**, 3556.
143. D. Parker and J. A. Williams, *J. Chem. Soc.-Dalton Trans.*, 1996, 3613.
144. G. R. Choppin and D. R. Peterman, *Coord. Chem. Rev.*, 1998, **174**, 283.
145. S. T. Frey and W. D. Horrocks, *Inorg. Chim. Acta*, 1995, **229**, 383.
146. S. Kim, J. Seo, H. K. Jung, J. J. Kim and S. Y. Park, *Adv. Mater.*, 2005, **17**, 2077.
147. R. Shunmugam and G. N. Tew, *J. Am. Chem. Soc.*, 2005, **127**, 13567.
148. M. Mitsuishi, S. Kikuchi, T. Miyashita and Y. Amao, *J. Mater. Chem.*, 2003, **13**, 2875.
149. M. L. Rodriguez-Mendez, Y. Gorbunova and J. A. de Saja, *Langmuir*, 2002, **18**, 9560.

150. S. Blair, R. Katakya and D. Parker, *New J. Chem.*, 2002, **26**, 530.
151. S. Blair, M. P. Lowe, C. E. Mathieu, D. Parker, P. K. Senanayake and R. Katakya, *Inorg. Chem.*, 2001, **40**, 5860.
152. J. C. G. Bünzli and C. Piguet, *Chem. Rev.*, 2002, **102**, 1897.
153. W. Horrocks and S. D.R., *Acc. Chem. Res.*, 1981, **14**, 384.
154. J. C. deMello, H. F. Wittmann and R. H. Friend, *Adv. Mater.*, 1997, **9**, 230.
155. S. Iijima, *Nature*, 1991, **354**, 56.
156. S. Iijima and T. Ichihashi, *Nature*, 1993, **363**, 603.
157. C. N. R. Rao, B. C. Satishkumar, A. Govindaraj and M. Nath, *ChemPhysChem*, 2001, **2**, 78.
158. V. Georgakilas, K. Kordatos, M. Prato, D. K. Guldi, M. Holzinger and A. Hirsch, *J. Am. Chem. Soc.*, 2002, **124**, 760.
159. A. Hirsch, *Angew. Chem. Int. Edit*, 2002, **41**, 1853.
160. M. Holzinger, O. Vostrowsky, A. Hirsch, F. Hennrich, M. Kappes, R. Weiss and F. Jellen, *Angew. Chem. Int. Edit*, 2001, **40**, 4002.
161. D. Tasis, N. Tagmatarchis, V. Georgakilas and M. Prato, *Chem.-Eur. J.*, 2003, **9**, 4000.
162. D. Tasis, N. Tagmatarchis, A. Bianco and M. Prato, *Chem. Rev.*, 2006, **106**, 1105.
163. D. M. Guldi, H. Taieb, G. M. A. Rahman, N. Tagmatarchis and M. Prato, *Adv. Mater.*, 2005, **17**, 871.
164. C. Richard, F. Balavoine, P. Schultz, T. W. Ebbesen and C. Mioskowski, *Science*, 2003, **300**, 775.
165. O. Vostrowsky and A. Hirsch, *Angew. Chem. Int. Edit*, 2004, **43**, 2326.
166. Z. H. Wang, S. F. Xiao and Y. Chen, *Electroanal.*, 2005, **17**, 2057.
167. M. N. Zhang, L. Su and L. Q. Mao, *Carbon*, 2006, **44**, 276.
168. D. Bonifazi, C. Nacci, R. Marega, G. Ceballos, S. Modesti, M. Meneghetti and M. Prato, *Nano Lett.*, 2006, **7**, 1408.

169. M. A. Hamon, J. Chen, H. Hu, Y. Chen, M. E. Itkis, A. M. Rao, P. C. Eklund and R. C. Haddon, *Adv. Mater.*, 1999, **11**, 834.
170. K. A. Worseley, K. R. Moonosawmy and P. Kruse, *Nano Lett.*, 2004, **4**, 1541.
171. A. Bianco, K. Kostarelos, C. D. Partidos and M. Prato, *Chem. Commun.*, 2005, 571.
172. A. Bianco, K. Kostarelos and M. Prato, *Curr. Opin. Chem. Biol.*, 2005, **9**, 674.
173. A. Bianco and M. Prato, *Adv. Mater.*, 2003, **15**, 1765.
174. C. Klumpp, K. Kostarelos, M. Prato and A. Bianco, *Bba-Biomembranes*, 2006, **1758**, 404.
175. D. Pantarotto, R. Singh, D. McCarthy, M. Erhardt, J. P. Briand, M. Prato, K. Kostarelos and A. Bianco, *Angew. Chem. Int. Edit*, 2004, **43**, 5242.
176. G. Pastorin, W. Wu, S. Wieckowski, J. P. Briand, K. Kostarelos, M. Prato and A. Bianco, *Chem. Commun.*, 2006, 1182.
177. H. Hu, Y. Ni, V. Montana, R. C. Haddon and V. Parpura, *Nano Lett.*, 2004, **4**, 507.
178. H. Hu, Y. C. Ni, S. K. Mandal, V. Montana, N. Zhao, R. C. Haddon and V. Parpura, *J. Phys. Chem. B*, 2005, **109**, 4285.
179. A. V. Liopo, M. P. Stewart, J. Hudson, J. M. Tour and T. C. Pappas, *J. Nanosci. Nanotechno.*, 2006, **6**, 1365.
180. V. Lovat, D. Pantarotto, L. Lagostena, G. Spalluto, M. Prato, L. Ballerini, B. Cacciari, M. Grandolfo and M. Righi, *Nano Lett.*, 2005, **5**, 1107.
181. M. P. Mattson, R. C. Haddon and A. M. Rao, *J. Mol. Neurosci.*, 2000, **14**, 175.
182. Y. C. Ni, H. Hu, E. B. Malarkey, B. Zhao, V. Montana, R. C. Haddon and V. Parpura, *J. Nanosci. Nanotechno.*, 2005, **5**, 1707.
183. H. Dumortier, S. Lacotte, G. Pastorin, R. Marega, W. Wu, D. Bonifazi, J.-P. Briand, M. Prato, S. Muller and A. Bianco, *Nano Lett.*, 2006, **7**, 1522.
184. M. K. Gheith, V. A. Sinani, J. P. Wicksted, R. L. Matts and N. A. Kotov, *Adv. Mater.*, 2005, **17**, 2663.

185. G. Jia, H. F. Wang, L. Yan, X. Wang, R. J. Pei, T. Yan, Y. L. Zhao and X. B. Guo, *Environ. Sci. Technol.*, 2005, **39**, 1378.
186. K. Kostarelos, L. Lacerda, C. D. Partidos, M. Prato and A. Blanco, *J. Drug. Deliv. Sci. Tec.*, 2005, **15**, 41.
187. C. W. Lam, J. T. James, R. McCluskey, S. Arepalli and R. L. Hunter, *Crit. Rev. Toxicol.*, 2006, **36**, 189.
188. S. K. Manna, S. Sarkar, J. Barr, K. Wise, E. V. Barrera, O. Jejelowo, A. C. Rice-Ficht and G. T. Ramesh, *Nano Lett.*, 2005, **5**, 1676.
189. S. K. Smart, A. I. Cassady, G. Q. Lu and D. J. Martin, *Carbon*, 2006, **44**, 1034.
190. M. Shim, N. W. S. Kam, R. J. Chen, Y. Li and H. Dai, *Nano Lett.*, 2002, **2**, 285.
191. R. Singh, D. Pantarotto, L. Lacerda, G. Pastorin, C. Klumpp, M. Prato, A. Bianco and K. Kostarelos, *P Natl Acad Sci USA*, 2006, **103**, 3357.
192. G. Accorsi, N. Armaroli, A. Parisini, M. Meneghetti, R. Marega, M. Prato and D. Bonifazi, *Adv. Funct. Mater.*, 2007, *In press*.
193. J. Kido and Y. Okamoto, *Chem. Rev.*, 2002, **102**, 2357.
194. L. J. Li, A. N. Khlobystov, J. G. Wiltshire, G. A. D. Briggs and R. J. Nicholas, *Nat. Mater.*, 2005, **4**, 481.
195. M. J. O'Connell, S. M. Bachilo, C. B. Huffman, V. C. Moore, M. S. Strano, E. H. Haroz, K. L. Rialon, P. J. Boul, W. H. Noon, C. Kittrell, J. P. Ma, R. H. Hauge, R. B. Weisman and R. E. Smalley, *Science*, 2002, **297**, 593.
196. K. Nakamaru, *Bull. Chem. Soc. Jpn.*, 1982, **55**, 2967.
197. M. S. Dresselhaus, G. Dresselhaus and P. E. Avouris, *Carbon Nanotubes, Synthesis, Structure, Properties and Applications*, Springer-Verlag Berlin, Heidelberg, 2001.
198. J. Maultzsch, H. Telg, S. Reich and C. Thomsen, *Phys. Rev. B*, 2005, **72**, 205438.
199. E. Menna, F. Della Negra, M. Dalla Fontana and M. Meneghetti, *Phys. Rev. B*, 2003, 193412.

200. J. N. Demas and G. A. Crosby, *J. Phys. Chem.*, 1971, **75**, 991.
201. A. Barbieri and G. Accorsi, *EPA Newsletter*, 2006, **December**, 27.

ACKNOWLEDGMENTS

This work has been carried out during the years 2004 - 2006 at *Istituto per la Sintesi Organica e la Fotoreattività (ISOF), Consiglio Nazionale delle Ricerche (CNR), Bologna.*

I would like to express my sincere thanks to the staff of the Institute, particularly to Dr. Nicola Armaroli for giving me the opportunity and autonomy to attain the present work. Dr. Francesco Barigelletti and Dr. Andrea Barbieri are acknowledged for fruitful discussion on photophysical issues and advice on instrument. Many thanks to my co-workers Dr. Andrea Listorti, Dr. Barbara Ventura, Dr. Dalia Virgili, Dr. Cristiana Sabatini and Dr. Raffaella Amodio for helping me on experimental measurements and administrative management.

I appreciated the collaboration with Prof. Dr. Davide Bonifazi, FUNDP – Faculté des Sciences Département de Chimie, Namur, (Belgium); Prof. Dr. Maurizio Prato, Dipartimento di Scienze Farmaceutiche, University of Trieste (Italy); Dr. Silvio Quici, Istituto di Scienze e Tecnologie Molecolari, Milano (Italy) and Prof. M.D. Ward, University of Sheffield (UK). Thanks to Dr. Andrea Parisini and Dr. Lidia Armelao for microscopy investigations and Sol-gel film preparations, respectively.

I would like to express my gratitude to my supervisor Prof. Alberto Juris, Istituto G. Ciamician, Università di Bologna (Italy) who supported me at all stages of my work.

This work was financed by the EC through the Integrated Project OLLA (contract no. IST-2002-004607), CNR (Commessa PM.P04.010, MACOL: Materiali Avanzati per la Conversione di energia Luminosa) and MIUR (Contract FIRB RBNE019H9K).